Assessment of Clinical Contribution of Flattening Filter Free Beams

---

Dissertation

zur

Erlangerung der naturwissenschaftlichen Doktorwürde (Dr. sc. nat.)

vorgelegt der

Mathematisch-naturwissenschaftlichen Fakultät

der

Universität Zürich

von

Jan Hrbacek

aus der

Tschechischen Republik

Promotionskomitee

Prof. Dr. Martin Pruschy (Vorsitz)

Prof. Dr. Michael Hengartner

Prof. Dr. Antony Lomax

Dr. Stephan Klöck

Zürich, 2014

I would like to thank

Dr. Stephan Klöck
for his support and the proofreading of the thesis,

Prof. Dr. Martin Pruschy
for his support and for supervision of the thesis,

Prof. Tony Lomax
for his support, accepting to be co-examiner,
and the proofreading of the thesis,

Prof. Dr. Michael Hengartner
for his support and accepting to be co-examiner,

my friend Stephanie Lang
for the great cooperation,

University Hospital Zürich & Varian Medical Systems
for giving me the opportunity to work on this exciting project,

all colleagues I had the pleasure to work with,

my wife Sarah and my family.

Contents

List of Figures

List of Tables

To Sarah, for her support during these times...

Zusammenfassung

Seit Linearbeschleuniger für medizinische Zwecke verwendet werden, ist der Ausgleichfilter ein wichtiger Bestandteil des Beschleunigers. Er kompensiert den lateral nicht uniformen Teil, der durch Bremsstrahlung erzeugten Photonenfluenz und vereinfacht dadurch die Dosisberechnung vor allem, wenn mehrere Felder kombiniert werden. Mit der Einführung von modernen Planungstechniken, wie Intensitäts-modulierter Strahlentherapie (IMRT) und Volumen-modulierter Bogenbestrahlung (VMAT), die die Fluenzverteilung dynamisch anpassen, ist es nicht mehr unbedingt nötig, dass das initiale Fluenzprofil homogen ist. Basierend auf dieser Annahme wurden Ausgleichsfilter-freie (Flattening Filter Free: FFF) Strahlqualitäten interessant für die klinische Anwendung vor allem bei Therapieansätzen mit hoher Einzeldosis. Im Rahmen dieser Arbeit wurden verschiedene Aspekte untersucht, die den klinischen Nutzen von FFF Strahlqualitäten näher beleuchten.

Zunächst wurden die dosimetrischen Eigenschaften eines neuen Beschleunigertyps (TrueBeam, Varian Medical Systems), an dem sowohl FFF als auch konventionelle Strahlqualitäten mit Ausgleichsfilter (FF) verfügbar sind, untersucht. Für FF wie auch für FFF Strahlen mit nomineller Energie von 6 und 10 MV (X6, X6FFF, X10, X10FFF) wurden Tiefendosiskurven, Querprofile, Oberflächendosen, Halbschatten, Dosen ausserhalb des Feldes sowie Streufaktoren untersucht und verglichen. Es hat sich gezeigt, dass FFF Strahlen eine niedrigere mittlere Energie haben (Gewebe-Phantom Verhältnisse bei den Tiefen 20 cm und 10 cm (TPR 20/10): X6 0.667; X6FFF 0.631; X10 0.738; X10FFF: 0.692); das Dosismaximum näher an der Oberfläche liegt; und die Oberflächendosis um 10% erhöht ist. FFF Profile haben einen schmaleren Halbschatten nahe der Oberfläche der sich aber mit zunehmender Tiefe schneller verbreitert im Vergleich zu den FF Strahlen. Für kleine Feldgrössen und nahe der Oberfläche ist die Dosis ausserhalb des Feldes für FFF Strahlen reduziert, der Vorteil verschwindet jedoch aufgrund der

erhöhten Phantomstreuung mit zunehmender Feldgrösse und zunehmender Tiefe. Die maximale Dosisleistung im Zentrum erhöht sich um einen Faktor 2.26 für X6FFF und einen Faktor 4.03 für X10FFF. Ausserdem ist die Feldgrössenfaktor weniger von der Feldgrösse im Vergleich zu den FF Strahlen.

Die Genauigkeit der Strahlmodellierung mit dem anisotropischen analytischen Algorithmus (AAA, Varian Medical Systems) wurde untersucht, indem das Strahlmodell mit im Wasserphantom gemessenen Daten verglichen wurde. Obwohl die FFF Strahlen mit einem einfacheren AAA Modell modelliert werden, ist die Genauigkeit vergleichbar mit der der konventionellen Strahlen. Diese Ergebnisse stützen die Annahme, dass die Entfernung des Ausgleichfilters die Modellierung vereinfacht (weniger Änderung des Energiespektrums entlang des Feldnormalen, weniger gestreute Photonen, etc.). Mit Hilfe der γ-Analyse wurde gezeigt, dass alle Punkte das Kriterium von 2 mm Entfernung bis zur Übereinstimmung und 2 % Dosisdifferenz erfüllen.

Die γ-Analyse basiert auf einem modifizierten ein dimensionalen γ-Konzept. Der Algorithmus funktioniert folgendermassen: Erst wird ein lokaler Fit der Referenz- und der auszuwertenden Kurve gemacht. Für jeden Punkt auf der gefitteten auszuwertenden Kurve werden die γ-Werte ermittelt, als kürzester Abstand bis zur Übereinstimmung zwischen den Punkten auf der auszuwertenden Kurve und dem Fit der Referenz-Kurve. Diese Vorgehen vermeidet Abweichungen und Fehler des γ-Wertes aufgrund des diskreten Messpunkte und des Rauschens im Datensatz. Initial wurde diese Analysesoftware entwickelt, um zwei Datensätze von Kommissionierungsdaten zu vergleichen. Damit kann jedoch dank der Universalität der Methodik jede Art von ein-dimensionalen Dosisverteilungen verglichen werden.

Als Vorbereitung für die Kommissionierungsarbeiten mussten die dosimetrischen Eigenschaften der Ionisationskammern in den FFF Strahlen mit hohen Dosisraten (bis 25 Gy min^{-1}), untersucht werden. In den konventionellen FFF Strahlen war die Ionensammeleffizienz für alle luft-gefüllten Ionisationskammern über 0.995. In den FFF Strahlen war die Ionensammeleffizienz genügend hoch, um eine akkurate Relativdosimetrie zu garantieren, die Korrekturfaktoren für die Absolutdosimetrie waren unter 1% für beide FFF Strahlqualitäten. Jedoch war die Ionensammeleffizienz in den FFF Strahlen nicht ausreichend für eine Isooctan-gefüllte Ionisationskammer. Diese Kammer kann nicht für Relativdosimetrie empfohlen werden.

Radiobiologische Effekte im Zusammenhang mit FFF Strahlen wurden in zwei menschlichen Glioblastoma Zelllinien untersucht. Dosen bis zwanzig Gray wurden mit verschiedenen Dosisleistungen und Energien appliziert. Die Dosis wurde mit Hilfen von Filmen wie auch mit Ionisationskammern verifiziert und die Koloniebildungsfähigkeit wurde in Assays ausgewertet. Unsere Daten wurden gestützt von einer radiobiologischen Modellierung der Daten. Es zeigte sich, dass das klonogene Überleben statistisch signifikant reduziert wird, wenn die Gesamtdosis mit einer erhöhten Dosis pro Puls aber der gleichen Dosisleistung appliziert wird. Ausserdem wurde gezeigt, dass es keine Unterschiede zwischen dem Überleben gibt, wenn die Dosis mit X10FFF oder X10 bei der gleichen Dosis pro Puls appliziert wird. Daraus folgt, dass weder das unterschiedliche Spektrum noch die Pulsfrequenz einen Einfluss auf das Überleben hat.

Es wurden zwei Planungsstudien durchgeführt, die den Effekt von FFF Strahlen sowohl auf die Planqualität als auch auf die Behandlungseffizienz untersuchen. Die eine Studie fokussierte auf nicht-kleinzellige Lungentumore die andere auf lokalisierte Prostatakarzinome. Beide Studien haben gezeigt, dass mit konventionelle und FFF Strahlqualitäten vergleichbare dosimetrische Ergebnisse erreicht werden können; nur kleine Unterschiede wurden gefunden. Jedoch wurde die Behandlungseffizienz in beiden Studien deutlich gesteigert, wenn FFF Strahlen zur Behandlung benutzt wurden.

Im Rahmen der Lungenstudie erreichte man konformale Dosisverteilungen (Konformitätsindex: CI<1.17) und scharfe Dosisgradienten ausserhalb des Planungszielvolumens (PTV). Das Verhältnis der Monitoreinheiten zwischen FFF und FF Strahlqualitäten bewegte sich zwischen 0.95 bis 1.21 für X6FFF/X6FF und zwischen 0.93 bis 1.25 für X10FFF/X6FF. Der Vergleich des kumulierten Dosis-Volumen-Histogramms für das Zielvolumen und den Körper hat gezeigt, dass mit der X6FFF Strahlqualität eine bessere Konformität erreicht werden kann und das Volumen, das mehr als 50 % der verschriebenen Dosis bekommt, reduziert werden kann. Alle Parameter, die den Dosisgradienten beschreiben, zeigten eine statistisch signifikante Verbesserung. CI50%, CI60%, CI80%, und CI100% waren im Mittel reduziert um 4.6 % ($p<0.001$), 4.6 % ($p=0.002$), 3.1 % ($p=0.002$), und 1.2 % ($p=0.039$). Das Gradientenmass war im Mittel um 4.2 % ($p<0.001$) reduziert. Das führte zu einer Dosisreduktion im umliegenden Gewebe, die sich in einer Reduktion von V20Gy und V12.5Gy um 5.5 % ($p=0.002$) und 4.5 % ($p<0.001$) zeigte. Diese dosimetrischen Verbesserungen konnten für den X10FFF Strahl nicht beobachtet werden. Die Unterschiede in den Normalgewebsdosen waren für beide

FFF Strahlqualitäten statistisch nicht signifikant. Die mittlere Dauer der Bestrahlung (Strahlzeit) war 111 s (2 SD = 11 s) für X10FFF, 128 s (2 SD = 19 s) für X6FFF, und für X6FF Pläne im Mittel 269 s (2 SD = 71 s). Die mittlere Dosisleistung betrug 1555 ± 264 MU/min bzw 1368 ± 63 MU/min, für X10FFF und X6FFF. Pläne, die die konventionelle X6 Strahlqualität verwendeten, wurden immer mit maximaler Dosisrate von 600 MU/min bestrahlt.

Innerhalb der Prostata Studie fand man keine Unterschiede zwischen den vier verwendeten Strahlqualitäten in Bezug auf PTV Abdeckung, Konformität und Homogenität. Die mittlere Körperdosis und das Volumen des gesunden Gewebes, das mit 50% der verschriebenen Dosis bestrahlt wird nahm mit zunehmender Energie energy ab (r^2 = 0.8275, p <0.01). X6FFF deponierte 3.6% mehr Dosis im gesunden Gewebe im Vergleich zu X6 (p <0.01). X10FFF deponierte 3.0% (p <0.01), und X10 5.8% (p <0.01) weniger Dosis im gesunden Gewebe im Vergleich zu X6. Die mittlere Dosis zum Rektum nahm signifikant zu im Vergleich zu X6 (2.6%, p <0.01). Die mittlere Dosis zur Blase erhöhte sich für X6FFF um 1.3% und reduzierte sich um 2.3% für X10FFF. Die Benutzung eines einzelnen 360°Bestrahlungsbogen in Kombination mit FFF Strahlung erhöhte die Behandlungseffizienz um 35% (2 SD = 10%). Die X10FFF Strahlqualität war der beste Kompromiss zwischen einer niedrigen Gesamtkörperdosis und der Schonung der Risikoorgane Rektum und Blase.

Abstract

The flattening filter has been an inherent part of a clinical medical accelerator since the first application in 1953. It compensates the non-uniformity of the bremsstrahlung photon fluence across the field and thus simplifies dose calculations and prediction of dosimetric outcome when multiple fields are combined. With the introduction of modern treatment planning techniques, such as intensity modulated radiation therapy (IMRT) or volumetric modulated arc therapy (VMAT), that deliberately modify actual fluence distributions to produce optimal fluence maps for each treatment field, the need to flatten photon beams seems not to be absolutely necessary for these techniques. This led to introduction of so called Flattening Filter Free (FFF) beams. In the scope of this thesis, several specific areas have been investigated in order to asses the contribution of FFF beams to clinical radiation therapy.

Dosimetric characteristics of a new linear accelerator (TrueBeam, Varian Medical Systems), designed to deliver flattened and FFF beams, was investigated. Dosimetric data included depth dose curves, profiles, surface dose, penumbra, out-of-field dose, output, total and scatter factors and were examined for conventional as well as FFF beams of nominal energy 6 and 10 MV (X6, X6FFF, X10, and X10FFF). It was found that FFF beams have lower mean energy (tissue-phantom ratio at the depths of 20 and 10 cm (TPR 20/10): X6, 0.667; X6FFF, 0.631; X10, 0.738; X10FFF, 0.692); maximum dose is located closer to the surface; and surface dose increases by 10 %. FFF profiles have sharper but faster diverging penumbra. For small fields and shallow depths, dose outside a field is lower for FFF beams; however, the advantage fades with increasing phantom scatter. Output increases 2.26 times for X6FFF and 4.03 times for X10FFF and is less variable with field size; collimator exchange effect is reduced.

Accuracy of beam modelling under physical conditions using Anisotropic Analytical Algorithm (AAA, Varian Medical Systems) was evaluated by comparing beam model with measured dataset. Despite the fact that AAA has been simplified for FFF beams, it was shown that FFF beams are modelled with the accuracy comparable to the one known for conventional beams. These findings confirm the previous premise that the absence of flattening filter could make modelling of FFF beams more straightforward (less changes in the energy spectrum, reduction of extra-focal photons, etc.) Using γ-analysis, criteria of 2 % depth-dose and 2-mm distance-to-agreement were always met.

The γ-analysis utilised a modified 1D γ-concept. The algorithm first performs a "local" fit of the reference and the evaluated datasets. For a particular point on the fitted evaluated curve, the γ-value is derived as the shortest distance between the point and the fitted reference curve. This approach removes variations of the obtained γ-value related to the discrete character and noise in the original datasets. Originally, this tool has been developed to evaluate similarity of two sets of commissioning data. Thanks to its universal character, it can serve as well for comparison of any kind of one-dimensional dose distributions.

Commissioning measurements required a revision of dosimetric characteristics of ionisation chambers with respect to high dose rates of FFF beams (up to 24 Gy min^{-1}). For conventional beams, the ion collection efficiency of all air-vented ionization chambers was above 0.995. For FFF beams, the collection efficiency of all examined air-vented chambers was found sufficiently high to allow reliable assessment of relative dosimetry and correction factors for absolute dosimetry were less than 1 % in all cases. However, ion-collection efficiency was found to be insufficient for an iso-octane-filled ionisation chamber when utilised for FFF beams and this chamber cannot be recommended for relative dosimetry of these beams.

Radiobiological effects associated with FFF beams have been studied on two human glioblastoma cell lines treated with doses up to 20 Gy and using different dose rates. Dose verification was performed and colony formation assays were carried out. To compare the predictability of our data, radiobiological models were included. It was found that clonogenic survival was statistically reduced, if the total dose was delivered with a higher dose per pulse while keeping the mean dose rate constant. It was further demonstrated that X10FFF and X10 with the same dose per pulse do not exhibit difference in the

survival, hence the difference in the killing efficiency cannot be contributed to changes in energy spectrum. Pulse repetition frequency did not influence the survival.

Treatment planning studies assessing the contribution of FFF beams to stereotactic ablative radiotherapy of stage I non-small cell lung cancer and to localised prostate radiation therapy have been carried out. Both studies showed that conventional and FFF beams yield quantitatively comparable dose distributions and only minor dosimetric differences were found. However, significant improvement in treatment delivery efficiency was observed for FFF plans in both studies.

In case of the lung study, obtained dose distributions were conformal (CI<1.17) and exhibited a steep dose fall-off outside the PTV. The ratio of monitor units for FFF versus FF plans in the study ranged from 0.95 to 1.21 and from 0.93 to 1.25 for X6FFF/X6FF and X10FFF/X6FF comparisons, respectively. Comparison of cumulative dose volume histograms for a patient's body showed that X6FFF plans exhibited improved conformity and reduce the volume of tissue that received more than 50% of the prescription dose. Parameters related to dose gradient showed statistically significant improvement. CI50%, CI60%, CI80%, and CI100% were on average reduced by 4.6 % ($p<0.001$), 4.6 % ($p=0.002$), 3.1 % ($p=0.002$), and 1.2 % ($p=0.039$), respectively. Gradient measure was on average reduced by 4.2 % ($p<0.001$). Due to dose reduction in the surrounding lung tissue, the V20Gy and V12.5Gy were reduced by 5.5 % ($p=0.002$) and 4.5 % ($p<0.001$). These dosimetric improvements in the fall-off were not observed for the X10FFF plans. Differences in sparing of other normal tissues were not found to be statistically significant for either of the two FFF beams. Mean beam-on times were 111 s (2 SD = 11 s) for X10FFF, 128 s (2 SD = 19 s) for X6FFF, and X6FF plans required on average 269 s (2 SD = 71 s). While the mean dose rate was 1555 ± 264 MU/min, 1368 ± 63 MU/min, for X10FFF and X6FFF, plans using the conventional X6FF were delivered with the constant maximum dose rate of 600 MU/min.

In case of the prostate study, there were no difference detected between the four beams in PTV coverage, conformity, and homogeneity. Mean body dose and body volume receiving 50% of the prescribed dose decreased with increasing mean energy ($r^2 = 0.8275$, $p < 0.01$). X6FFF delivered 3.6% more dose compared with the X6 ($p < 0.01$). X10FFF delivered 3.0% ($p < 0.01$), and the X10 5.8% ($p < 0.01$) less mean body dose compared with X6. There was a significant increase in the mean dose to the rectum for the X10

compared with X6 (2.6%, p <0.01). Mean dose to the bladder increased by 1.3% for X6FFF and decreased by 2.3% for X10FFF. Using a single arc and FFF, treatment time was reduced by 35% (2 SD = 10%). X10FFF beam provided the best solution, sparing rectum and bladder and minimizing whole-body dose.

Chapter 1

Introduction

1.1 Cancer in Europe

Noncommunicable diseases - such as cardiovascular diseases, cancer, and chronic obstructive pulmonary disease - account for 80 % of deaths in the European region. Diseases of the circulatory system (ischaemic heart disease, stroke, etc.) are the most important cause of premature death (before the age of 65), accounting for nearly 50 % of the total. Cancer is the second leading cause, accounting for nearly 20 %. However, with the aging population, the risk of cancer is rising. Currently, cancer is the main cause of premature death in 28 of the 53 countries in the region, and is predicted to further increase by 2020 [3].

The latest provisional information for the 27 member countries of the European Community (EU-27) relating to causes of death shows that cancer was a major cause of death in the region - averaging 166.9 deaths per 100 000 inhabitants across the EU-27 in 2010 [4].

There were an estimated 3.45 million new cases of cancer (excluding non-melanoma skin cancer) and 1.75 million deaths from cancer in Europe in 2012. The most common cancer sites were cancers of the female breast, followed by colorectal, prostate and lung. These four cancers represent half of the overall burden of cancer in Europe. The most common causes of death from cancer were cancers of the lung, colorectal, breast and stomach [4].

1.2 Role of radiation therapy

The major treatment modalities for cancer are surgery, radiotherapy and systemic therapy (chemotherapy). Their selection is based on evidence of the best existing treatment given the resources available. They may be used alone or in a combination. Surgery alone is only likely to be highly successful when the tumour is localised and small in size. Chemotherapy alone can be effective for a small number of cancers, such as haematological neoplasms (leukaemias and lymphomas), which can generally be considered to be widespread from the outset. Combined modality therapy requires close collaboration among the entire cancer care team. Despite that radiotherapy utilisation rates for cancer may vary widely internationally, it is estimated that approximately 50 % of cancer patients should receive radiation [5].

1.3 Brief history of megavoltage radiation therapy

The generation and transmission of radiation in the clinical environment depends on very sophisticated technology. Up to the 1950's, most of the external beam radiotherapy was carried out with x-rays generated at voltages up to 300 kV. In the 1950's and 1960's, they were gradually replaced by development of high-energy machines and by the increasingly more popular cobalt-60 units. Radiotherapy utilising these machines is referred to as megavoltage radiation therapy despite the fact that strictly speaking the term megavoltage should be reserved only to x-ray beams of energy higher than 1 MV (hence excluding γ-rays). The shift from kilovoltage into megavoltage radiation therapy was accompanied by an improvement in overall five years survival from 39% in the 1960's to 50% in the 1980's took place [6]. Betatrons were used for radiotherapy in the early 1950's. They preceded the introduction of linear accelerators by several years. Operation of the betatron is based on the principle that an electron in a changing magnetic field experiences acceleration in a circular orbit. Although the betatrons can provide x-ray and electron therapy beams over a wide range of energies, from less than 6 MeV to more than 40 MeV, they have low electron current, and the x-ray dose rates and field size capabilities are low compared with linear accelerators or modern cobalt units. However, their beam current is adequate to provide a high dose rate for electron therapy mode. The reason for this difference is that the x-ray production via bremsstrahlung is relatively

inefficient and requires much higher primary electron beam current (about 1000 times). Linear accelerators (Linac) are technologically more advanced and their development evolved with the earlier advent of the microwave power tube such as the klystron that was developed during the World War II (source of microwave power for radars). Linacs use the high-frequency electromagnetic waves to accelerate charged electrons to high energies at they pass through a linear tube. Linac-based radiation therapy for cancer treatment began with treatment of the first patient in 1953 in London at Hammersmith Hospital, with an 8 MV machine built by Metropolitan-Vickers [1]. A short while later (1955), the first patient was treated with 6MV photons generated by a Linac in Stanford Hospital in San Francisco.

The earlier Linacs were limited by their inability to rotate around the patient. The first 360 degree isocentric Linac was developed in 1960 at Varian Medical Systems Inc (Palo Alto) and transported to University of California Los Angeles (UCLA). In the following years, further technological improvements made it possible to reduce Linac's complexity, reduce its cost, and to extend its versatility (electron/photon treatment mode, multiple energies, etc.) Linacs became gradually more popular and today they deliver the majority of radiation therapy in developed countries. In 2004, linear accelerators comprised 88 percent of treatment courses in the USA. [7]

The role of the Cobalt-60 unit has been largely taken over by the linear accelerator. The major limitations of the Cobalt-60 units are their low energy (1.17 and 1.33 MeV), lower output that further reduces with the decay of the source and necessitates replacement of the source every 5-7 years, and wider penumbra given by the finite size of the source. Also, disposal of spent source represents a problem. Meanwhile, whilst linear accelerator technology has experienced substantial developments over the intervening years, modernisation of the cobalt-60 units has been marginal. Despite these drawbacks, cobalt-60 units are still widespread especially in developing countries, since the machinery is relatively reliable and simple to maintain compared to the modern linear accelerator. However, the cobalt-60 plays useful role in specialised applications, such as the Leksell gamma knife.

1.4 Linac design

The general principle of operation of a typical medical linear accelerator can be summarised as follows (figure 1.1): a modulator provides high voltage pulses of microseconds duration. These pulses are delivered simultaneously to the electron gun and to magnetron or klystron - devices for producing microwaves. Pulsed microwaves are injected into the evacuated structure (tube) via a waveguide system. At the proper moment, electrons produced by an electron gun are also pulse injected into the accelerator structure. Injected electrons are accelerated either by stationary or travelling microwaves depending on the design of the accelerator's waveguide.

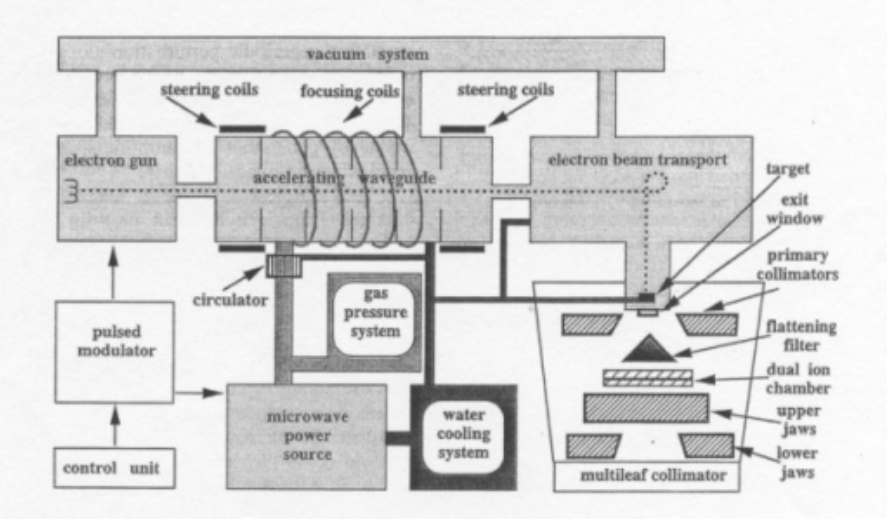

FIGURE 1.1: Schematic diagram of a medical accelerator (reproduced from [6]).

Magnetron functions as high-power oscillator, generating 3GHz microwave pulses of several microseconds duration and with repetition rate of several hundred pulses per second. Whereas the klystron acts as a microwave amplifier. It needs to be driven by a low-power microwave generator. Whereas magnetrons are less expensive, klystrons have longer time span, and are able of delivering higher power levels and are preferred for the beam energy above 20 MeV [8].

As high-energy electrons emerge from the exit window of the accelerator structure, they are in the form of a narrow pencil beam. Linacs providing energies up to 6 MeV have relatively short accelerator tubes, allowing electrons to proceed on a straight trajectory into the treatment head. In the higher energies Linacs, a longer accelerator tube is

typically placed perpendicularly to the treatment head axis and electrons are deflected by 90 (or 270) degrees using bending magnets.

The final part of a Linac is called treatment head. It consists of a target, scatter foil, primary and secondary collimating system, flattening filter, monitor ionisation chambers, and in some cases additional beam modifying devices.

Modern linear accelerators offer both x-ray and electron treatment modalities. Bremsstrahlung photons are produced when accelerated electrons impinge on a target of a high proton number material. The target is water-cooled and is thick enough to absorb most of the incident electrons. Bremsstrahlung photons are characterised by a continuous spectrum of energies with the maximum energy equal to the energy of incident electrons. The average energy of the photons is approximately one third of the maximum energy. For the electron treatment modality, accelerated electrons strike on a thin scattering foil. The foil ensures that most electrons are scattered instead of undergoing bremsstrahlung, hence a broad electron beam with uniform fluence is obtained from the original pencil beam.

The primary collimator is a shell around the treatment beam made of high-density shielding material such as lead-tungsten alloy. It provides sufficient shielding against leakage radiation and is the first definition layer for the therapeutic beam collimator.

Megavoltage bremsstrahlung has a strongly forward peaked distribution of intensity, i.e. most of the photons have a similar trajectory as the electrons impinging on the target. In order to make the beam intensity uniform (over a certain field width), the resultant bremsstrahlung beam passes through a flattening filter. The filter is conical in shape and is made of a combination of materials of different proton number. For each photon energy, a linac uses a dedicated flattening filter.

The flattened x-ray beam further passes through monitor ionisation chambers, typically transmission chambers, i.e. plan-parallel chambers with a diameter greater than the beam's cross-section. The main function of the monitor chambers is to control the instantaneous dose rate, accumulated dose, and beam's flatness and symmetry.

The secondary collimation consists of two pairs of movable jaws, made of lead or tungsten, which allow to collimate of the beam to rectangular fields of any size between 0 x

0 cm^2 and 400 x 400 cm^2. Finally, a photon beam can be additionally modified using devices such as multi-leaf collimator (MLC), wedges, blocks, compensators, etc.

1.5 Flattening filter

The flattening filter has been an inherent part of a clinical medical accelerator since the first application in 1953 [1, 2] (figure 1.2), and it used to compensate for the non-uniformity of the bremsstrahlung photon fluence across the field, which helped to simplify dose calculations. It should be noted that first computer-based treatment planning systems allowing a three-dimensional calculation of dose distribution appeared several decades later.

However, there are also trade-offs associated with the use of the flattening filter. Arguably the most important one is related to the reduction of output (dose rate) due to beam attenuation in the material of a flattening filter. One of the first references to the use of unflattened photon beams appears in 1991, reporting the properties of radiosurgical beams from a 6 MV Therac accelerator (Atomic Energy of Canada, Ltd) without the flattening filter [9]. The investigated application was limited to circular fields of size up to 3 cm in diameter, where the change in intensity across an unflattened beam is not pronounced. In this work, the authors were motivated by the need to reduce treatment delivery time of radiosurgery. In 1993, the concept of tomotherapy, a dedicated machine that delivers treatment in slices was introduced. This machine also utilises an unflattened beam and further beam modulation is achieved with a dedicated multileaf collimator [10].

Various Monte Carlo studies have shown that the flattening filter is responsible for the majority of scatter produced in the treatment head [11, 12], causes changes in beam quality away from the central axis [13] and acts as the main source of electron contamination [14–16]. Other Monte Carlo studies investigate various properties of flattening filter free (FFF) beams using commercially available Linacs, where a flattening filter was removed for the purposes of modelling [17–21]. There were also analogical dosimetric measurements performed with dedicated experimental machines or prototype linear accelerators without a flattening filter [22–25] and some preliminary treatment planning studies were performed for these prototypes [26].

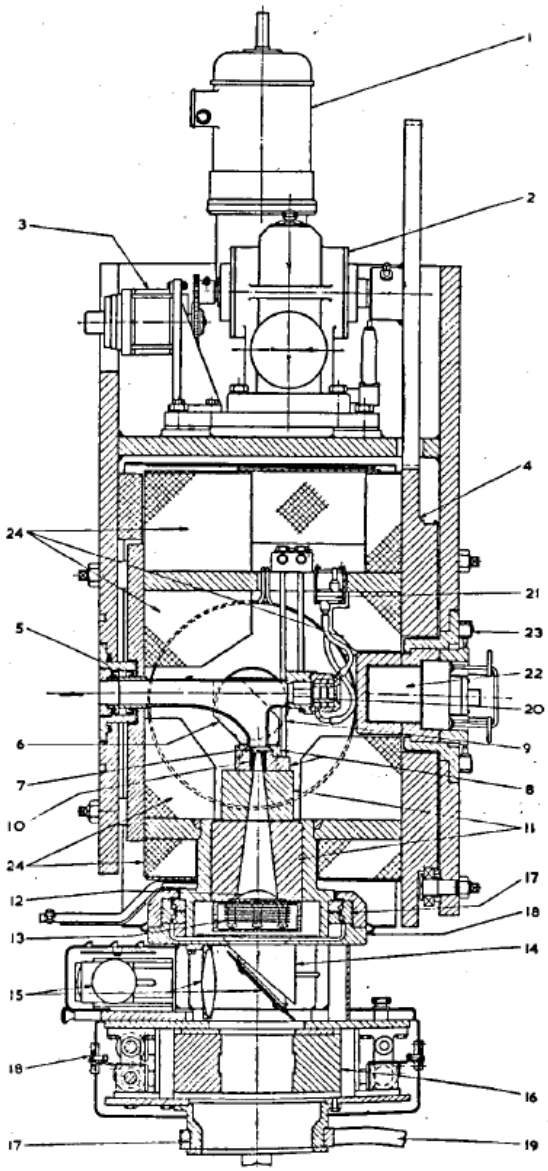

Fig. 11.—Cross-section of X-ray head.

(1) Driving motor for head rotation.
(2) Gearbox.
(3) Magslip resolver.
(4) Iron frame for magnet.
(5) Vacuum seal.
(6) Magnet pole.
(7) Gold target.
(8) Heavy-alloy flanges.
(9) Water cooling.
(10) Uranium collimator.
(11) Heavy alloy collimator.
(12) Beam-flattening filter.
(13) Ionization chambers.
(14) Removable wedge filter.
(15) Optical field illuminator.
(16) Adjustable diaphragms.
(17) Bearings for 360° rotation.
(18) Scales.
(19) Support for beam-defining pointers.
(20) Calorimeter.
(21) Thermocouple unit.
(22) Removable heavy-alloy plug.
(23) Plug interlock.
(24) Lead blocks.

FIGURE 1.2: Cross-section of x-ray head of historically first clinically used linear accelerator as depicted in [1]. Note the flattening filter (12).

In the last two decades, radiation therapy underwent substantial development in optimisation of treatment planning. Modern treatment planning techniques, such as intensity modulated radiation therapy (IMRT) or volumetric modulated arc therapy (VMAT), use multileaf collimators to deliberately modify actual fluence distributions to produce optimal fluence maps for each treatment field. Clinical experience shows that fluence maps can exhibit a high degree of complexity. In this context, the necessity to flatten photon beams seems not to be absolutely necessary for these techniques. Instead, the leaf sequences can be adjusted accordingly to take into account the non-flat profile of FFF beams.

1.6 Motivation

Vendors producing linear accelerators have reacted to these developments in radiation therapy. As an example, Varian Medical Systems introduced a dedicated C-arm Linac, TrueBeam, designed to deliver both flattened and FFF photon beams. The prototype of this accelerator was installed at University Hospital Zürich and Memorial Sloan-Kettering Cancer Centre. In the scope of this collaboration, the system was optimised and prepared for clinical application. Among other tasks, this mainly involved an assessment of basic dosimetric properties of FFF beams, investigating behaviour of available detectors, evaluation of radiobiological impact, and performing of comparative treatment planning studies in clinically relevant conditions.

University Hospital Zürich was the first clinic worldwide to use TrueBeam clinically utilising both conventional as well as FFF beams.

1.7 Outline of the thesis

In chapter 2, a modified concept for γ-analysis for a comparison of dose profiles is introduced. Originally, this tool has been developed to evaluate similarity of two sets of commissioning data. Thanks to its generality, it can serve as well for comparison of measured and modelled data as later demonstrated in chapter 3, and can be used for any kind of one-dimensional dose distribution. It has been even successfully applied for the verification of an agreement between measured and modelled depth dose curves

of proton beams (between energies 70 and 230 MeV). I developed the algorithm for the one-dimensional γ-analysis, acquired the necessary dosimetric data, performed the analysis, and have written the manuscript [27] presented in chapter 2.

Chapter 3 represents a dosimetric comparison of conventional and FFF beams from the TrueBeam linear accelerator and assesses the accuracy of beam modelling in a treatment planning system (Eclipse, Varian Medical Systems). Measurements were designed and led by myself. The execution of the measurements was done by myself and Stephanie Lang. The manuscript [28] was written by myself.

Chapter 4 deals with one of the dosimetric aspects encountered with FFF beams. These beams exhibit high dose rates which might influence the performance of some ionisation chambers (due to their lower ion collection efficiency). This study evaluates the suitability of several commercially available ionisation chambers for measurements in FFF beams. I have contributed to measurements and to the preparation of the manuscript [29].

The Clinic for Radiation Oncology of the University hospital Zürich has performed a radiobiological study examining the influence of high dose rates of FFF beams on cancer cell survival. I have contributed to address the dosimetric aspects of the study and supported the irradiation of samples. The published study [30] is presented in chapter 5.

Chapter 6 evaluates the utilisation of FFF beams for stereotactic ablative radiotherapy of stage I non-small cell lung cancer. The study was designed and the manuscript [31] has been written by myself. The manuscript was accepted for publication in *Medical Physics* and is currently prepared for publishing.

Another treatment planning study evaluating the contribution of FFF beams to localised prostate radiation therapy is presented in chapter 7. I have contributed to treatment planning and the data analysis. The study was published as a manuscript [32].

Chapter 2

Quantitative evaluation of a beam-matching procedure using one-dimensional γ-analysis[1]

2.1 Introduction

Many radiation therapy centres have more than one linear accelerator at their disposal. For these centers, vendors offer "beam matching" as a part of their contract. In this approach, treatment beams of the unit being installed are tuned in such a way that the dosimetric characteristics meet reference values within a specified interval. If all machines in the department have been tuned to these values, they are implicitly tuned to each other. When installing the reference unit, an extensive set of dosimetric data has to be gathered in order to properly commission it and to obtain all beam data needed for beam modelling in a treatment planning system. Beam matching significantly reduces the dosimetrical workload during commissioning. Instead of measuring the full set of dosimetric data, only a set of cross-check measurements is needed to investigate the agreement of subsequently installed units with the reference beams. If the reference and matched beams are shown to be identical within a certain level of tolerance, no further measurements need to be carried out. The beam data gathered for the reference unit

[1]This chapter has been published as a manuscript [27]: J. Hrbacek, T. Depuydt, A. Nulens, A. Swinnen, and F. Van den Heuvel, "Quantitative evaluation of a beam-matching procedure using one-dimensional gamma analysis," Medical physics, vol. 34, p. 2917, 2007.

can then be used to commission the other units. Moreover, having units with matched beams enables increased flexibility in clinical work. If one of the matched units is down, any of the others can take over its patient load without the necessity of re-planning. As early as in the 1990s, several scientific articles evaluating dosimetric performance of Varian's Clinacs 600C and 2100C (Varian Medical Systems, Inc., Palo Alto, CA) were published [33,34]. These articles confirm good agreement of photon beam characteristics of alike accelerators. Marshall and colleagues [34] showed satisfactory agreement of 6 MV beams of two dissimilar Varian machines after customisation of a flattening filter. To our knowledge, there is no recent study on this topic. Also, we have not found any evidence concerning the matching of electron beams. The published articles as well as comparison of dosimetric parameters in the beam matching acceptance procedure defined by the vendor is based on relative measurements at predefined points under specific geometry. In this article, we have implemented a one-dimensional (1D) γ-index that enables to evaluate the level of agreement of matched beams over entire profiles or depth dose curves.

2.2 Material and methods

Varian (Varian Medical Systems, Inc., Palo Alto, CA) offers two types of beam matching, a "basic" and a "fine" one. In this work we will solely concentrate on the matching termed as fine. The beam matching acceptance criteria are based on a depth ionisation curve as well as transverse, radial, and diagonal profiles measured at the vendor's prescribed geometry. The vendor does not use the entire curve to evaluate a quality of beam matching. Instead, only some points of a curve are used for this purpose. In case of a photon depth ionisation curve, the location of depth of maximum ionisation and relative ionisation at a depth of 10 cm is used. For electron depth ionisation curves, points of 90 %, 80 %, and 50 % relative ionisation are used. According to the vendor's procedure, for photon and electron profiles, the relative ionisation at any point within the central 80 % of a scan should meet prescribed criteria. However, only six points from this region are effectively investigated. A limited overview of the fine beam matching procedure as defined by the vendor is given later.

2.2.1 Beam matching criteria as defined by the vendor

For each measured parameter, an average value is calculated from the parameter's values of all matched units x_i. The vendor's acceptance criteria Δ are all related to the average $\bar{x}$ and define the interval around the average into which all x_i have to belong. This approach enables to match a group of more than two treatment units

$$|x_i - \bar{x}| < \Delta, \forall x_i \tag{2.1}$$

2.2.1.1 Depth profiles

The depth of maximum dose along the central axis shall be within ±1.5 mm of the average. The relative dose at 10 cm depth on the central axis shall be within ±10 % of the average for basic matching and ±0.5 % in the case of fine beam matching. For electron beams, a position of 90%, 80%, and 50% relative ionisation should be within ±1 mm of the reference value.

2.2.1.2 Transversal profiles (photons)

For photon profile measurements, the dose at any point within the central 80% of the radial and transverse axis, normalised to the central axis measured at a depth of 10 cm in water shall be within ±2% of the average of the measured values at that point. This test is performed for 40 x 40 cm^2 and 10 x 10 cm^2 field sizes. The maximum dose in the plane perpendicular to the beam axis at the depth of maximum dose in water shall be within ±1% of the average.

2.2.1.3 Transversal profiles (electrons)

For electron beams, the ionisation within 80% of the diagonal scans, normalised to the central axis, measured at the depth of maximum dose shall be within ±2% of the average of the measured values at that point. This test is performed for the applicators 25 x 25 cm^2 and 10 x 10 cm^2 with standard insets. If only a pair of treatment units is compared (the reference one and the tuned one as was the case in our department), it is more comprehensive to restate the criteria as the maximum allowable difference

in measurement of a dosimetrical parameter for the two units (x_R,x_T) rather than the difference between the value of a tuned unit and the average

$$\bar{x} = \frac{x_R + x_T}{2}, \tag{2.2}$$

$$|x_T - \bar{x}| = \frac{x_R + x_T}{2} < \Delta, \tag{2.3}$$

$$|x_T - x_R| < 2\Delta, \tag{2.4}$$

As seen from 2.4 the maximum allowable difference in the estimate of the parameter for the two compared units can be expressed as two times the vendor's criteria. For instance, if the vendor requires the depth of maximum dose along the central axis to be within ±1.5 mm of the average, the difference in the parameter's value between the reference and the tuned unit can be up to ±3 mm and still pass the match criterion. We consider the vendor's criteria rather loose and arbitrary to guarantee full interchangeability of beams in clinical practice. In the least favourable instance of beam matching, a significant systematical error would be introduced in the dosimetric chain. The borderline cases of beam matching are suitable for an emergency single fraction irradiation in a fractionated treatment, when an unexpected failure of a treatment unit occurs. However, we find it unacceptable to conceptually alternate units in this case without recalculating the dose distribution.

2.2.2 Measurements

As the evaluation of beam matching is performed during the acceptance test of a new unit with a set of measurements prescribed by the vendor, it was our concern to investigate the level of agreement of matched beams for commissioning measurements as they are more closely related to clinical dosimetry. Therapeutic beams of Varian Clinac 2100 C/D serial No. 3065 were compared with corresponding matched beams of Varian Clinac 2100 C/D serial No. 3170. Both accelerators have two photon beams of nominal energies of 6 and 10 MV and five electron beams with respective energies of 6, 9, 12, 16, and 20 MeV. The second unit was installed in our department approximately 6 months after the first one. The performed dosimetric measurements consist of point relative measurements and profile relative measurements. The same dosimetric equipment was used for the measurements of both treatment units. For point measurements, a CC13

chamber (Scanditronix-Wellhofer) has been utilised with Keithley 35040 electrometer. Profile measurements were carried out using the Scanditronix-Wellhofer Blue Phantom controlled by OmniPro Accept 6.1 software. A pair of CC13 ionisation chambers was connected to a dual processor based control unit CU 500-E (Scanditronix-Wellhofer). For electron depth ionisation curves, the field CC13 chamber was replaced with a NACP-02 ionisation chamber (Scanditronix-Wellhofer). The measured ionisation curves were converted to dose curves using the NACP formalism implemented in OmniPro software [35]. When scanning dose profiles, spacing between points of a profile is set by the software according to selected speed of the movement of the field detector. Due to the number of profiles needed, we chose a medium speed with a spacing of 0.4 mm.

2.2.2.1 Point measurements

- Output factors for 6 and 10 MV for selected field sizes including the smallest (3 x 3 cm^2), the largest (40 x 40 cm^2), and the most asymmetrical field size possible (3 x 40 cm^2),
- Quality index for 6 and 10 MV,
- MLC transmission for 6 and 10 MV,
- Block transmission for 6 and 10 MV,
- Tray transmission for 6 and 10 MV,
- Wedge factor for all hard wedges for 6 and 10 MV,
- Output factors for all hard wedges for 6 and 10 MV,
- Quality index for wedged fields 6 and 10 MV,
- Wedge factors for enhanced dynamic wedges for 6 and 10 MV were compared with a theoretical value calculated according to a formula provided by the vendor [36].

2.2.2.2 Profile measurements

- Depth dose curves for both photon beams with field sizes 3 x 3 cm^2,10 x 10 cm^2, and 40 x 40 cm^2,

- Depth dose curves for both photon beams and all hard wedges with field sizes 3 x 3 cm^2,10 x 10 cm^2, and 20(15) x 40 cm^2,
- Depth ionisation curves for all electron beams and all applicators (including no applicator option) with standard insets,
- Transversal/radial profiles for both photon beams with field sizes 3 x 3 cm^2,10 x 10 cm^2, and 40 x 40 cm^2, at depths of d_{max}, 5, 10, 20, and 30 cm,
- Transversal/radial profiles for both photon beams and all hard wedges with field sizes 3 x 3 cm^2 , 10 x 10 cm^2, and 40 x 40 cm^2, at depths of d_{max}, 10, and 30 cm,
- Transversal/radial profiles for all electron beams for applicator 25 x 25 at Varian recommended depth for all electron beams, and
- A profile in air for all electron beams required for commissioning of Varian's electron Monte Carlo algorithm [37, 38].

2.2.3 Algorithm for γ-index calculation

The γ-index is a mathematical concept that enables a quantitative comparison of two dose distributions. In principle, γ-evaluation can compare a pair of dose distributions of any number of dimensions. For instance, it has been employed in a verification of two-dimensional (2D) and three-dimensional dose distributions measured by gel dosimetry or for quality assurance of 2D fluence maps of intensity modulated radiation therapy (IMRT) fields [39]. A description of the γ-index may be found in an article by Low [40]. In the present work, we have used it to evaluate the agreement between dose profiles (i.e., of 1D distribution) of two treatment units with matched beams.

When performing the γ-evaluation, one distribution is referred to as the reference and the other as the evaluated. The γ-index is calculated independently for each data point of the reference distribution using the entire evaluated distribution. In general, the γ-evaluation is not symmetric with respect to the two distributions. If the two distributions are qualitatively different (for example a smooth analytically calculated dose distribution and a measured dose distribution with the presence of noise), care should be taken to decide which of the two distributions should be treated as reference and which as evaluated [41].

In our case, both distributions (dose profiles) are qualitatively the same. They represent

water phantom measurements for two different treatment units at different times. They were performed in the same manner, using the same equipment and the same setup. To us it seemed most natural to exchange the terms "evaluated" and "reference" distribution, so that for a particular point to be evaluated the closest of the points of the reference data set is sought. The new treatment unit profiles were chosen to be the evaluated and the profiles of the previously installed unit the reference.

A dose profile is a set of values that represent the ratio of the field-to-reference detector readings to a predetermined point at discrete (usually equidistantly spaced) points in a given scan direction. These measurements are subject to the introduction of stochastic noise. As Low has demonstrated, the discrete character of data perturbs the γ-evaluation [41]. Low concludes that the pixel spacing of the evaluated distribution needs to be sufficiently small to provide an accurate calculation of γ in regions of steep dose gradient. By histogram analysis he also demonstrates significant perturbations in the presence of noise. Introduction of noise in the evaluated distribution reduces the average value of γ. On the other hand, if the reference distribution is noisy, the average value of γ is accurately calculated, but there are great point to point variations in the γ-distribution. As a one-dimensional γ-evaluation does not require an extensive calculation time, we have decided to use a more sophisticated approach to calculate γ to overcome both limitations.

In the case of 1D γ-evaluation, the γ-index is the shortest distance between a reference point and any point of the evaluated dataset in a position-to-dose graph which has the axes normalised to distance-to-agreement (DTA) and dose difference (DD) criteria. Here, rather strict criteria of 1 mm DTA and 1% DD have been set for the evaluation of matched beams.

Our algorithm first performs a "local" a fit of both datasets. Points of each dataset that occur in the proximity of the reference point are fitted using a second order polynomial. This way two polynomials are obtained, each locally describing one of the profiles.Local in this sense means that only points of a profile within a certain region around the reference point are taken into account for the fit.

For this purpose a radial magnitude of 3 around the reference point in the normalised distance-to-dose space has been chosen. As changes in dose easily reach 10% per mm or more in some parts of a profile (such as the penumbra), the dose normalised to DD was reduced by a factor of 10. The proximity region shall be therefore considered to be an ellipse around the reference point having the major axes parallel with the dose axes.

The size of the proximity region was determined using the most complex profiles (profiles of the largest hard wedge in the direction of the gradient). The proximity region was gradually increased and after each increase, all fits on a profile were graphically visualised allowing us to make sure that data points were fit adequately. The chosen size of proximity region ensures good conditioning of the fitted polynomials as well as suitability of the chosen fitting function. Of course, if the region of proximity is enlarged, more data points are used to define the fitted polynomial and the resulting γ-profile gets smoother.

However, the size of the region cannot be enlarged arbitrarily. If the region is too large, some deformations of γ-profile occur due to the fact that the second order polynomial is not an adequate fit for some parts of the profile.

We have observed that it would be possible to further enlarge the proximity region and still obtain a suitable fit of the data points. Nevertheless, this did not improve the γ-profiles significantly. If the proximity region is too small, there might not be enough points within the region of proximity for the polynomial fit and the γ-value cannot be determined. It might also occur that the closest point to the evaluated point lies outside of the region. In this situation the γ-value will be overestimated. The higher the dissimilarity between the compared profiles, the larger the proximity region needs to be. For the chosen size of the proximity region used in this analysis, these effects would occur for $\gamma > 3$ and therefore are not disturbing this analysis.

The reference point with coordinates (x_R, y_R) is projected onto the reference polynomial curve. Instead of calculating γ for the point itself, γ is calculated for the projected value (x_R, y_{RP}). This way, noise in the reference profile is reduced.

As a final step, the γ-value is obtained by finding the minimal distance between the projected value (x_R, y_{RP}) and the polynomial fit of the evaluated dataset (described by the quadratic equation $y = a_0 + a_1x + a_2x^2$). Expressing the square of distance and substituting the polynomial fit formula, the coordinates of the point (x , y) with the minimum distance from (x_R, y_{RP}) is sought using

$$\frac{\partial r^2}{\partial x} = 2(x - x_0) + 1(a_0 + a_1x + a_2x^2 - y_0)(a_1 + 2a_2x) = 0. \tag{2.5}$$

This approach supresses perturbations related to the discrete character of the original dataset. By using the polynomial fit, the noise in the evaluated dataset is also reduced. The algorithm is graphically interpreted in figure 2.1.

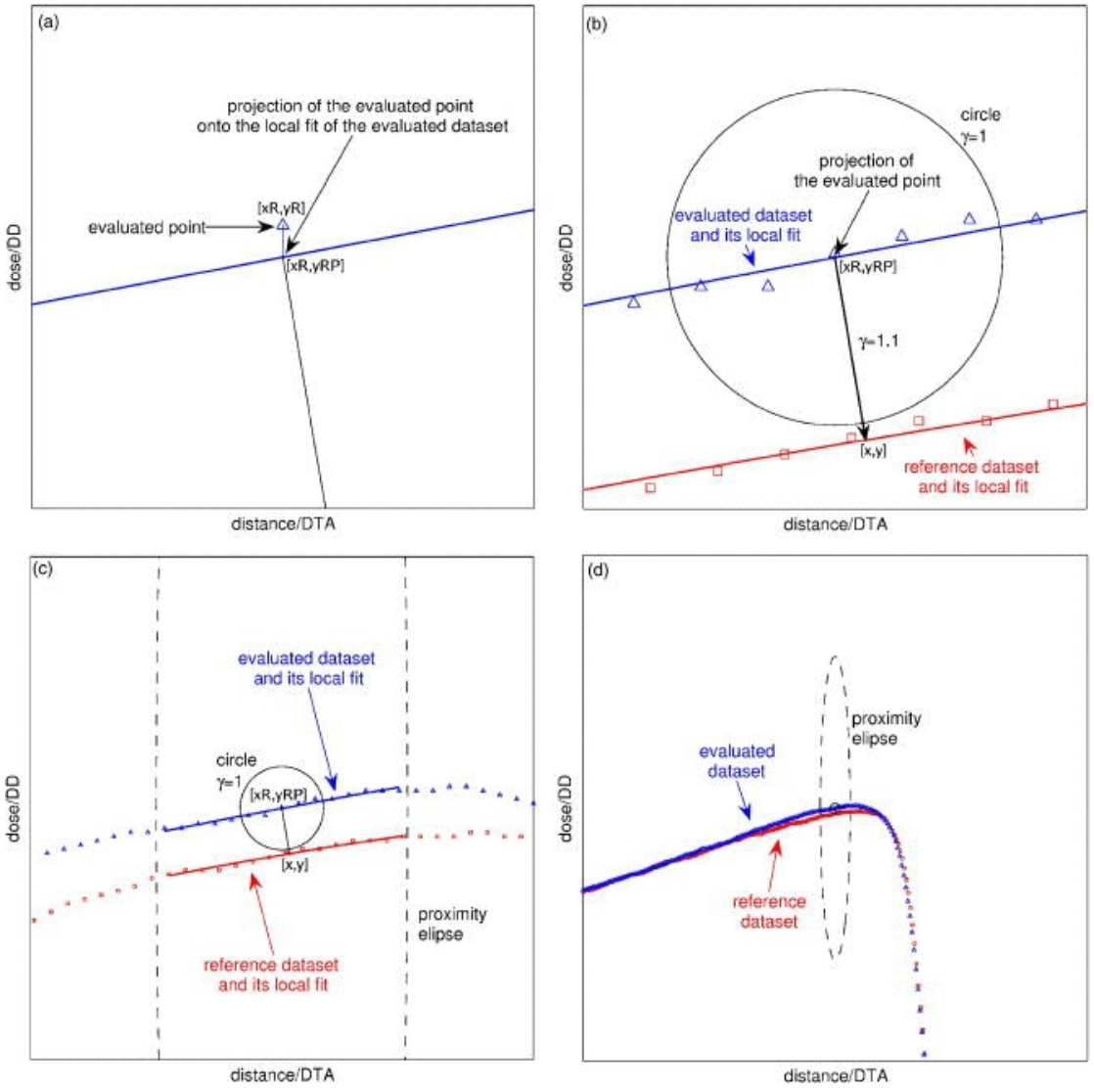

FIGURE 2.1: Graphical representation of the γ-evaluation algorithm. For a point of the evaluated dataset, the ellipse defines the proximity of the point (d). All points inside the proximity ellipse are used to construct polynomial fit of both datasets (c). The evaluated point is projected onto the local fit of the evaluated dataset (a). For the projection of the evaluated point, the closest point on the local fit of the reference dataset is sought (b). The γ-vector represents the shortest distance between the point and the curve. In this case, $\gamma = 1.1$ is demonstrated. The black circle represents the boundary of $\gamma \leqslant 1$.

2.2.4 Processing of the scanned profiles

The acquired relative dose profiles need to be normalised prior to their further evaluation. Dose profiles were arbitrarily normalised to the central axis, while the depth ionisation curves are normalised to their maximum. The γ is calculated for all pixels of the evaluated profile. The resulting set of γ-values is referred to as the γ-profile. We also define γ_{max} as the maximum value of the γ-profile.

To reduce inaccuracies in the positioning of the detector, all measured profiles were re-centered based on the position of 50% isodose using the OmniPro software. However, we have observed that this approach does not always provide the best alignment of profiles. Therefore, a new strategy was implemented to center the profiles.

After precentering using the OmniPro software function, one of the paired profiles was shifted -1.2, -0.9, -0.6, -0.3, 0, 0.3, 0.6, 0.9, and 1.2 mm relative to the other. (The magnitude of the positioning correction roughly corresponds with the precision of detector positioning in a water phantom.) For every new position, the displaced profile was renormalized to the new point corresponding to the central axis. For every cross-position of the profiles, we calculated γ-profiles, yielding nine profiles, from which the smallest γ_{max} was selected.

However, we did not apply this approach to (photon and electron) depth dose curves as the real discrepancies between profiles caused due to the difference of the mean energy of the two beams could undesirably be compensated.

2.3 Results

2.3.1 Point measurements

Relative point measurements are summarised in tables 2.1,2.2,2.3. For 6 MV all differences between the point parameters of the two units are within -0.62 % and +0.56 %. Similarly, for 10 MV the differences are within -0.29 % and +0.43 %.

2.3.2 Dose profile measurements

Out of the total of 170 profiles the 65 depth dose profiles were not subjected to the cross-positioning procedure as described earlier. In 38 of the 105 remaining cases, the

correction did not improve the γ-evaluation. A shift of 0.3, 0.6, 0.9, and 1.2 mm was needed for, respectively, 38, 17, 7, and 5 profiles. 119 (or 70%) of the profiles had a $\gamma_{max} < 1$. These profiles met the chosen criteria of 1 mm DTA and 1% DD of local dose in all pixels of a profile. The remaining 51 profiles include some pixels that fail these criteria. The median of γ_{max} was 0.86, a value of 80% and 90% percentile is 1.14 and 1.26, respectively. The greatest obtained value of γ_{max} was 1.70.

2.4 Discussion

2.4.1 Detailed analysis

2.4.1.1 Depth dose curves in the proximity of the water level

In case of 13 profiles, we have observed a weak transgression (e.g., $1 < \gamma < 1.3$) of our criterion in the first few pixels of a depth dose curve and agreement in the rest of the profile. These discrepancies are related to difficulties of dose measurement in the buildup region rather than the beam characteristics.

2.4.1.2 Low signal

In five profiles, a discrepancy in the low dose region was observed when measuring at the largest depth (figure 2.2). This effect is likely caused by variations in the base level (zeroing the detector). During the commissioning of the reference treatment unit an extensive number of scans was performed (including scans necessary for other treatment planning systems) and it is very likely that despite careful handling of the measurements, there are a few that were measured with the detector operating in a non-optimal range. In the higher dose region the agreement is very good.

2.4.1.3 Electron profiles

Crossline or inline profiles of electron fields (ten in total) exhibit the same characteristics. These scans were performed for the largest applicator (25 x 25 cm^2) using the standard insert. The level of agreement of the beams in the high dose region is very good, however,

the new treatment unit exhibits a slightly sharper penumbra (figure 2.3). This effect could be related to a small size discrepancy of the electron insets as well as a slightly different level of scatter. From a practical point of view, these discrepancies do not seem to be significant.

2.4.1.4 Wedged profiles

For seven wedged profiles, the infringement of $\gamma = 1$ criterion was found at the wedge's toe, i.e., around the point of highest dose of a wedged profile (figure 2.4). The dose profile in this region is rather complex especially for larger wedges. An additional set of measurements was performed to eliminate physical differences between the hard wedges of the same nominal angle used in both machines. Profiles for the different wedges placed in the same beam were compared. A very good agreement was observed and the hard wedges can be considered identical.

We have observed that this type of profile is sensitive to cross-positioning of profiles. As such, a significant increase of γ in this region is observed if the profiles are not properly aligned. As the failure of γ analysis occurs randomly (i.e., not related to certain wedge angle, field size, or depth of measurement), we consider that this effect is linked to the measurement uncertainty rather than to a difference in the beam characteristics.

2.4.1.5 Photon depth dose curves

In the depth dose curves for 10MV photons using hard wedges, nominal angles of 45°and 60°and the smallest field size (e.g., 3 x 3 cm^2), a consistent increase of γ is observed with enlarging depth (figure 2.5). This effect is more pronounced for the latter hard wedge. The discrepancies likely originate from a difference in the low energetic part of a spectrum (different level of beam hardening). For thinner wedges and for any wedge with a larger field size, this effect diminishes, whilst all other depth ionisation curves completely pass the chosen γ-evaluation criteria. An additional factor is the possible loss of electronic equilibrium in the measurement of this particular depth dose.

2.4.1.6 Solitary peaks

The remaining 12 profiles cannot be systematically classified. They exhibit solitary small peaks (with γ_{max} up to 1.20) that occur at random locations in a profile. The peaks have a local character and affect only several subsequent pixels of the profile. The excesses are attributed to residual noise in both profiles not fully suppressed by our analytical γ-evaluation algorithm.

2.4.2 General discussion

The results show that the beam matching procedure can attain the chosen criteria of 1 % DD and 1 mm DTA. Out of all profiles, 70 % pass the criteria. The analysis of remaining 30 % of profiles demonstrates that it is mainly the imperfections of measurement that are the limiting factor better correlations. It is only the ten inplane and crossplane profiles of electron beams and three photon depth dose curve profiles where a $\gamma > 1$ has been shown conclusively. On the level of gamma analysis there is no difference between comparing depth dose curves or profiles. Indeed, the gamma analysis just provides a number. However, the way the outcome is analysed does depend on the type of curve. Transversal curves have five specific parts (high dose region, two penumbras, and two scattered dose regions), whereas depth dose curves essentially consist of two parts: buildup and tail. For electrons a third part is of importance which is the bremsstrahlung tail. Each part of the profile includes a different number of points and has its local specifics. For example, depth dose curves will typically fail the criteria of the gamma evaluation in the proximity of the water level, whereas the rest of the curve exhibits good agreement.

The handling of the acquired profiles as demonstrated in this article goes beyond the common practice in most radiation therapy departments. Our results show a slight degradation of the γ-evaluation when cross-positioning optimisation is omitted. Despite this all profiles have $\gamma_{max} < 2$. As pointed out in the results section only five profiles out of 107 needed a shift of 1.2 mm. This is of the order of the accuracy with which the measurements were taken, using a 3 mm radius sized cylindrical chambers positioned with 1 mm thick positioning lasers.

TABLE 2.1: Point measurements

	Reference	Measured	Difference (%)	Reference	Measured	Difference (%)
MLC transmission	0.0119	0.0112	-0.07	0.0146	0.0137	-0.09
Block transmission	0.0283	0.0262	-0.21	0.0332	0.0303	-0.29
Tray transmission	0.9729	0.9725	-0.04	0.9834	0.9819	-0.15
Wedge factor W15	0.7719	0.7775	+0.56	0.8087	0.8130	+0.43
Wedge factor W30	0.6211	0.6233	+0.22	0.6742	0.6732	-0.10
Wedge factor W45	0.4916	0.4924	+0.08	0.5265	0.5277	+0.12
Wedge factor W60	0.4084	0.4060	-0.24	0.4412	0.4388	-0.24
Wedge factor EDW10	0.9492	0.9513	+0.22	0.9577	0.9574	-0.03
Wedge factor EDW15	0.9248	0.9247	-0.01	0.9371	0.9373	+0.02
Wedge factor EDW20	0.9005	0.9016	+0.12	0.9164	0.9164	0.00
Wedge factor EDW25	0.8760	0.8797	+0.42	0.8954	0.8959	+0.06
Wedge factor EDW30	0.8508	0.8529	+0.25	0.8736	0.8747	+0.13
Wedge factor EDW45	0.7671	0.7704	+0.43	0.7996	0.7997	+0.01
Wedge factor EDW60	0.6553	0.6575	+0.34	0.6973	0.6983	+0.14
Quality index open field	0.6660	0.6663	+0.45	0.7360	0.7350	+0.14
Quality index W15	0.6752	0.6767	+0.22	0.7410	0.7423	+0.30
Quality index W30	0.6804	0.6818	+0.21	0.7453	0.7479	+0.35
Quality index W45	0.6893	0.6937	+0.64	0.7462	0.7468	+0.01
Quality index W60	0.6925	0.6933	+0.12	0.7467	0.7481	+0.19

TABLE 2.2: Percentage deviation of output factors 6 MV

Field size (cm)	3	5	10	20	40
3	+0.51	+0.37	+0.29	+0.23	+0.55
5	+0.23	+0.24	+0.08	+0.31	+0.14
10	-0.62	-0.05	0.00	+0.06	0.00
20	+0.07	+0.35	+0.27	-0.04	-0.16
40	+0.30	-0.05	+0.32	-0.13	-0.42

TABLE 2.3: Percentage deviation of output factors 10 MV

Field size (cm)	3	5	10	20	40
3	+0.17	+0.14	+0.12	+0.04	+0.32
5	+0.20	+0.13	0.10	+0.10	+0.11
10	-0.02	-0.18	0.00	-0.05	-0.08
20	-0.05	+0.05	-0.18	-0.14	-0.12
40	+0.04	+0.06	-0.19	-0.29	-0.30

The sample used for further commissioning of other machines was chosen in such a way that for all modalities and energies the curves compared represented the reference conditions and the extrema. For example, a 6 MV depth dose curve was compared for field sizes 3 x 3,10 x 10, and 40 x 40 cm^2. A profile for the same beam was measured at the depth of maximal dose, 10 and 30 cm (the limit of our water tank). We do, however, want to stress that when finding good accordance and when using the same model in the planning system for the two machines, it is still necessary to perform spot checks to ensure the correct behaviour of the planning system. All absolute values (output, tray transmission, etc.) were always measured separately and entered in the planning system for each machine.

2.5 Conclusion

Relative point and profile measurements have been performed to cross-check the validity of Varian's beam matching procedure. Matched beams, both photon and electron, show very good level of agreement. 70% of profiles completely passes γ-evaluation with the chosen criteria 1% DD and 1 mm DTA, 90% of profiles have their maximal γ-value smaller than 1.26 (the highest γ_{max} is 1.70).

In this particular case, the quality of the beam matching was very high and allowed us to treat paired beams of both treatment units as identical and to use the beam model of the reference treatment unit for the new unit. Nevertheless, it should be

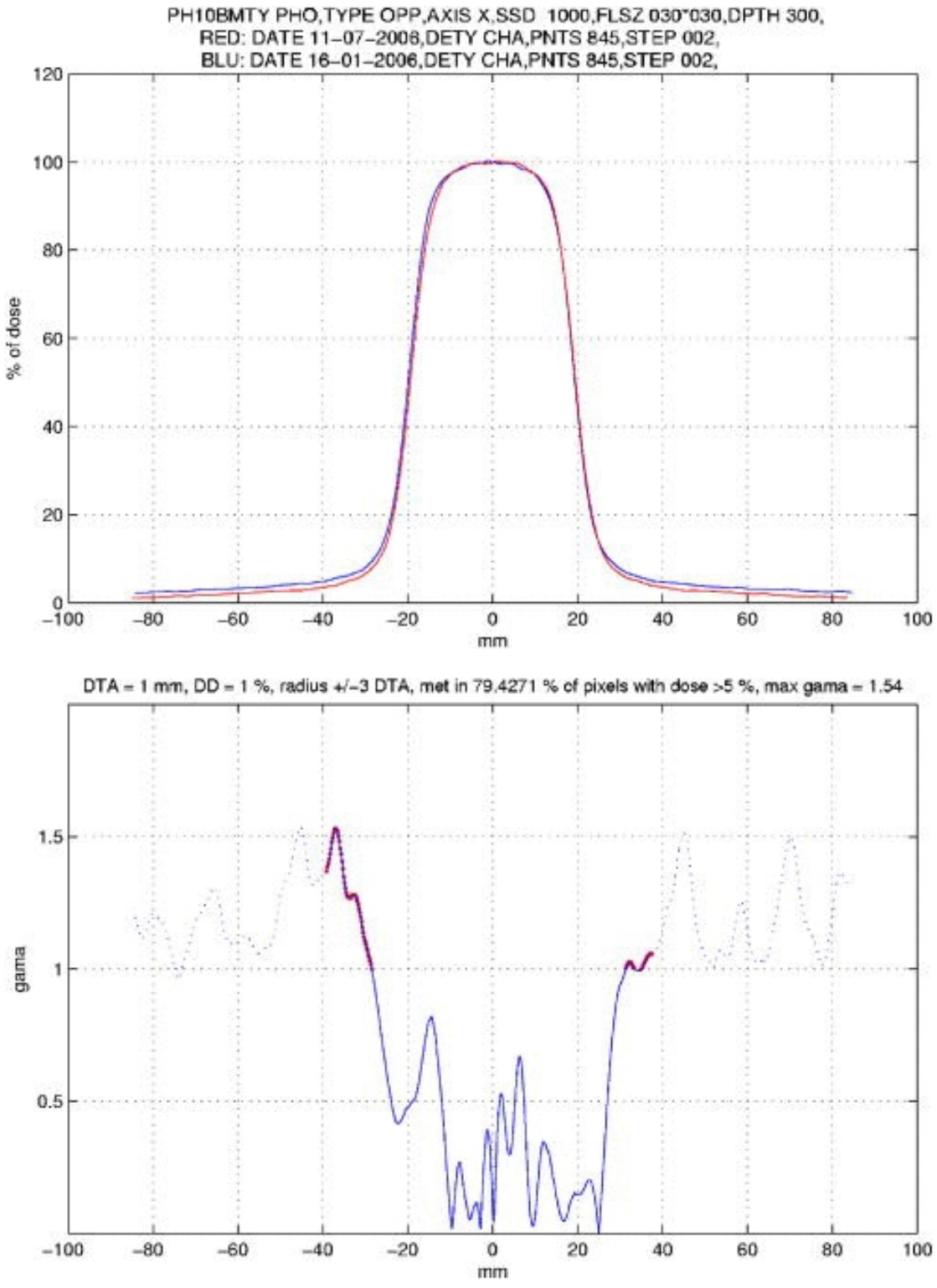

FIGURE 2.2: Example of a disagreement in the low dose region. The upper graph shows reference and evaluated profile. The lower graph exhibits the γ-profile.

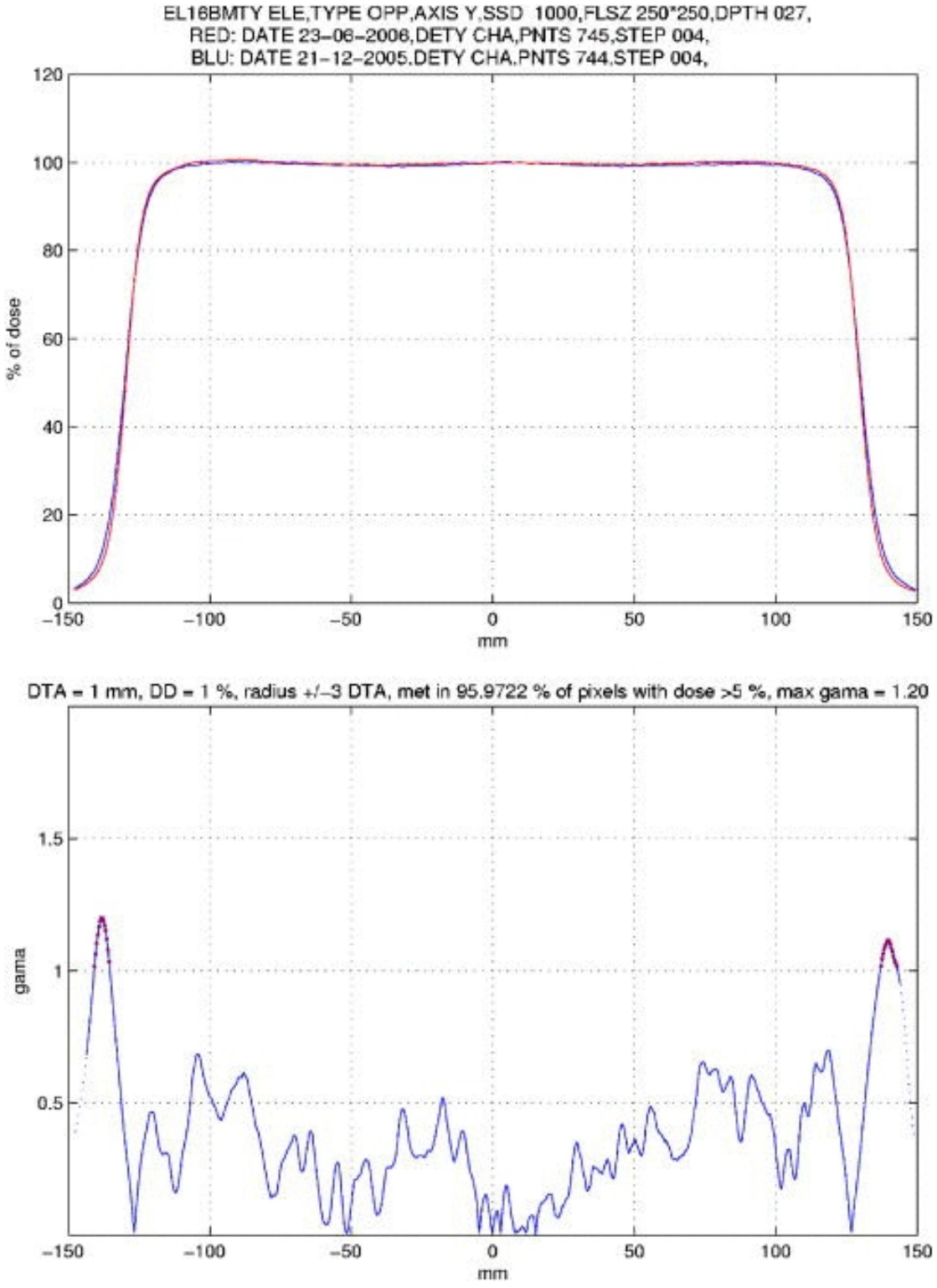

FIGURE 2.3: Discrepancies in the penumbra region for electron fields. The upper graph shows reference and evaluated profile. The lower graph exhibits the γ-profile.

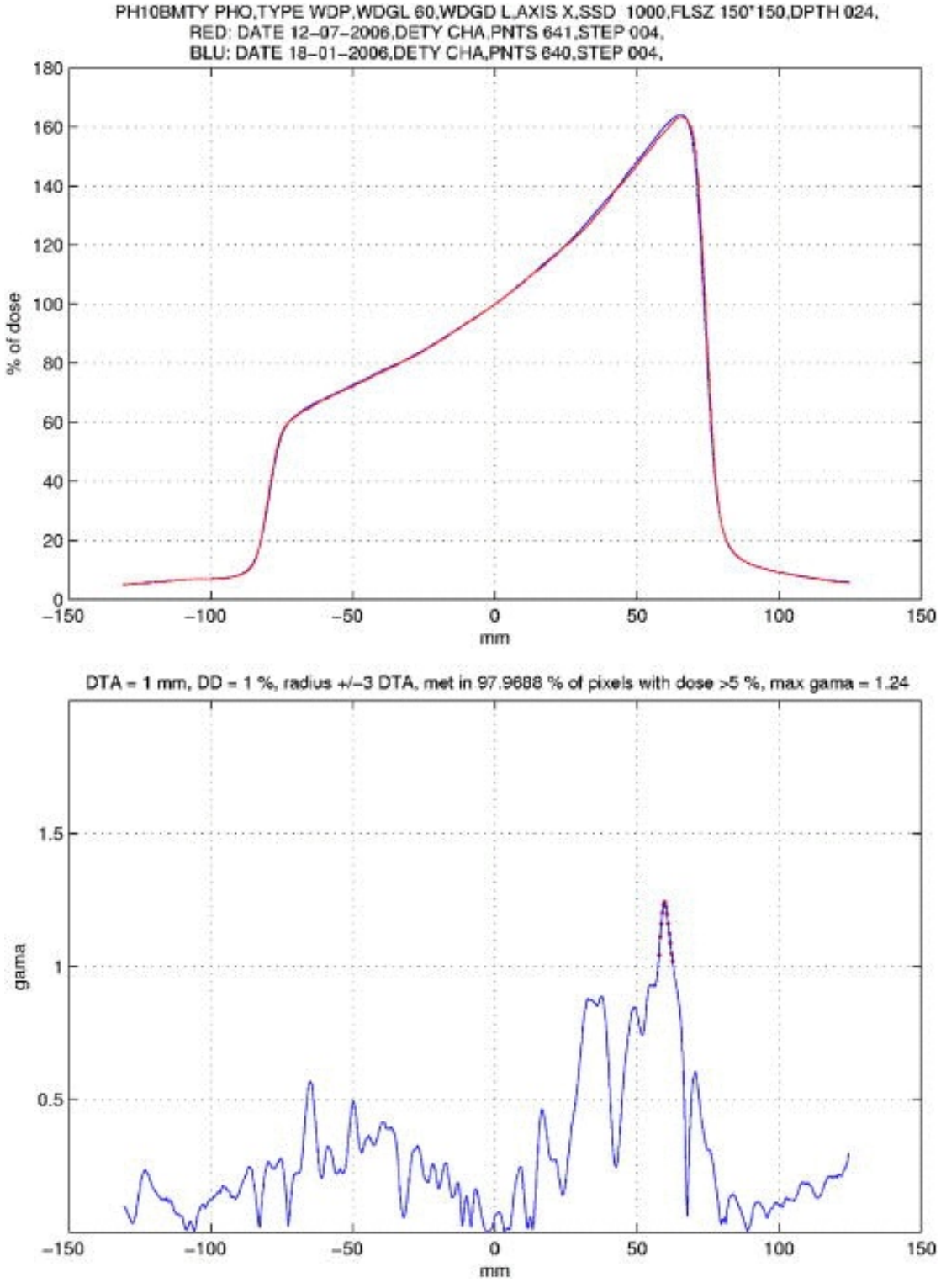

FIGURE 2.4: Discrepancies in the high dose region for wedged photon fields. The upper graph shows reference and evaluated profile. The lower graph exhibits the γ-profile.

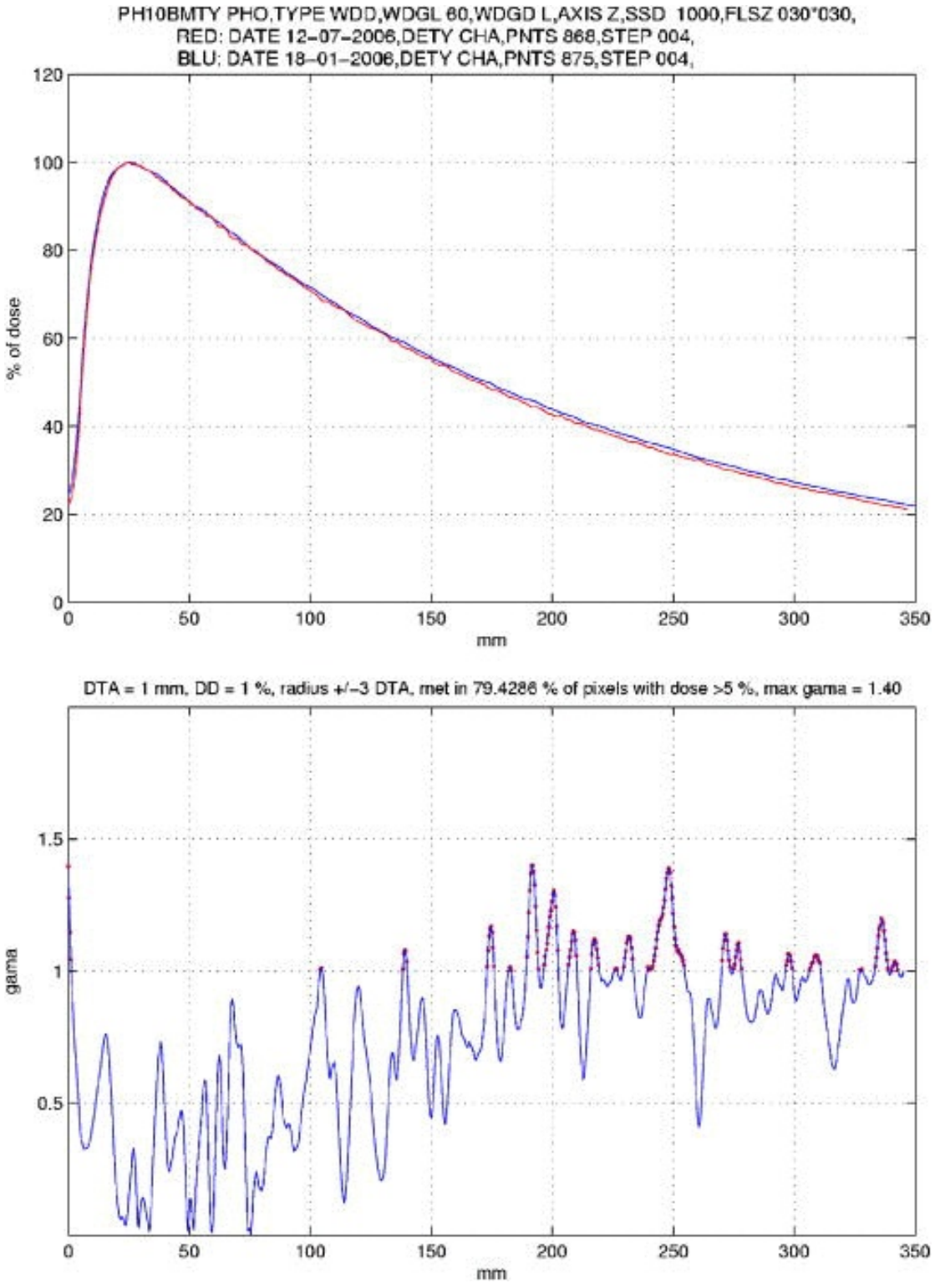

FIGURE 2.5: Depth dose curves for very small wedged photon fields at 10 MV. The upper graph shows reference and evaluated profile. The lower graph exhibits the γ-profile.

noted that acceptance criteria of beam matching defined by the vendor are much more benevolent. Therefore, although the acceptance criteria are met, the resulting quality of beam matching does not allow full interchangeability of beams in the clinical practice.
For all practical purposes, based on the presented results, we suggest 2 mm DTA and 2% DD as a convenient criteria for γ-analysis to be met when evaluating the agreement of profiles scanned in common dosimetrical conditions. Better results are attainable by employing different strategies coping with the imperfections of measurements.
It is our opinion that matched beams which do not meet the earlier suggested criteria should not be treated as clinically interchangeable.

Chapter 3

Commissioning of photon beams of a flattening filter-free linear accelerator and the accuracy of beam modeling using an anisotropic analytical algorithm[1]

3.1 Introduction

TrueBeam STx (Varian Medical Systems) is a new linear accelerator designed to deliver flattened, as well as flattening filter free (FFF), beams. It represents a new platform of Varian linear accelerators where many key elements, including the waveguide system, carousel assembly, beam generation and monitoring control system, differ from the preceding Clinac series. Based on our experience of commissioning the first clinically used TrueBeam linear accelerator, we present a framework that summarizes dosimetric characteristics of the new accelerator and compares our results with currently available evidence on FFF technology.

[1]This chapter has been published as a manuscript [42]: J. Hrbacek, S. Lang, and S. Klöck, "Commissioning of photon beams of a flattening filter-free linear accelerator and the accuracy of beam modeling using an anisotropic analytical algorithm," International Journal of Radiation Oncology* Biology* Physics, vol. 80, no. 4, pp. 1228-1237, 2011.

The interest in FFF technology results from the expectation that it will allow faster treatment with reduced out-of-field dose as the flattening filter removal leads to an increase of dose rate and a reduction of head scatter and leakage. FFF application is foreseen primarily in stereotactic radiotherapy or hypofractionated treatments with an escalation of dose per fraction. High dose rate could be advantageous for respiratory gated or breath-hold treatments where delivery time is limited.

There are several articles summarizing the properties of FFF beams of various linear accelerators, based on Monte Carlo simulations or dosimetric measurements. In all cases, however, linear accelerators under investigation are FFF prototypes only, created by mechanically removing a flattening filter from a standard clinical accelerator. A Monte Carlo evaluation of 6 MV FFF [19] and 18 MV FFF [20] of Varian Clinac 2100 was reported by MD Anderson Cancer Center. The same group of authors later performed measurements for 6 MV and 18 MV FFF beams for a Varian Clinac 21EX FFF prototype [23]. Similarly, dosimetric properties of 6 MV and 10 MV FFF beams of two Elekta Precise FFF prototypes can be found [24, 25]. A Monte Carlo simulation of 6 MV and 10 MV FFF beams for Elekta SL25 model is reported by Parsai et al [21].

FFF beams are already utilized clinically in helical tomotherapy [10, 43], where a 6 MV FFF beam is narrowly collimated, typically to a width of 2.5 cm. TrueBeam initiates the clinical use of FFF bundles for C-arm linear accelerators, enabling the generation of FFF beams of any field size, being constrained solely by the physical limits of the accelerator's collimator.

In this chapter, we report on the accuracy of modeling TrueBeam's photon beams in the Eclipse treatment planning system (Varian Medical Systems) using an anisotropic analytical algorithm (AAA, Varian Medical Systems) [44, 45]. There is existing evidence regarding the performance of the algorithm in homogeneous [46–50] as well as heterogeneous media [47–50]. We extend the spectrum of these publications by evaluating an agreement of the AAA model with measurements for FFF beams. This study is limited to the verification of the algorithm performance in physics conditions, i.e. in a water phantom.

3.2 Materials and methods

3.2.1 Linear accelerator

Photon beams of two nominal energies (6 & 10 MV) of TrueBeam were commissioned. TrueBeam allows delivery of both nominal energies, with a flattening filter in place or using so called open port - a carousel position where a thin foil is used instead of a flattening filter. We further refer to the four photon beams as X6, X6FFF, X10, and X10FFF. These bundles are available in the following dose rates:

- X6 & X10: 100, 200, 300, 400, 500 & 600 MU/min,
- X6FFF: 400, 600, 800, 1000, 1200 & 1400 MU/min,
- X10FFF: 400, 800, 1200, 1600, 2000 & 2400 MU/min.

TrueBeam handles beam generation and steering as well as dose calibration for each bundle separately. This approach is different from the practice reported for prototype machines [19,23], where the absolute calibration was done for a flattened beam, and after the removal of flattening filter, the machine output was not further adjusted. Beams were calibrated following the AAPM TG-51 formalism [51]; 100 MU corresponds to 1 Gy at the depth of maximum dose (d_{max}) for SSD 100 cm and the field size of 10x10 cm^2.

3.2.2 Multi-leaf collimator

TrueBeam STx is equipped with a high definition multi leaf collimator (HDMLC, Varian Medical Systems). This tungsten 120-leaf collimator has 32 leaf pairs of 2.5 mm leaf projection width in the isocenter, surrounded by 28 leaf pairs of 5.0 mm leaf projection width. The total length across leaves of HDMLC is 22 cm at the isocentric plane.

3.2.3 Depth dose curves & profiles

All measurements were acquired in a large water phantom (PTW Freiburg, Germany) at SSD 90 cm. Percentage depth dose curves (PDDs) were acquired for 12 different field sizes:

- 1x1 cm^2, 2x2 cm^2, 3x3 cm^2, 4x4 cm^2, 6x6 cm^2, 8x8 cm^2, 10x10 cm^2, 12x12 cm^2, 15x15 cm^2, 20x20 cm^2, 30x30 cm^2, 40x40 cm^2

PDDs for field sizes above 3x3 cm^2 were measured with a 0.125 cm^3 cylindrical chamber (PTW31010); for small field sizes a pinpoint chamber (PTW31016) was used to avoid the partial volume irradiation effect obvious for the larger chamber. Error introduced by the ion collection inefficiency of both chambers is smaller than 1.3 % (based on the measurement in the least favorable circumstances - X10FFF, 40x40 cm^2, SSD 90 cm, d_{max}). Radial and transversal profiles of symmetric fields were measured for the following set of previously specified field sizes and depths of d_{max}, 5 cm, 10 cm, 20 cm, and 30 cm. Transverse profiles of asymmetric fields were measured at the depth of 10 cm for the following rectangular fields:

- X x (10 + Y2) and X x (Y1 + 10), where X $\in$ {10, 20} cm, Y1 $\in$ {-5, 0, 5, 10} cm, Y2 $\in$ {-5, 0, 5, 10} cm

Profiles up to a field size of 15x15 cm^2 were measured with a shielded diode detector (PTW60008), and above this field size, a liquid ionization chamber (microlion, PTW31018) was used. The shielded diode provides high spatial resolution, but it could not be used for profiles of larger field sizes as this non-tissue equivalent detector overresponds to scattered radiation [52]. The difference in profiles between the liquid chamber and the 0.125 cm^3 cylindrical chamber was within 1 %, yet profiles measured with the liquid chamber benefited from sharper penumbra and the elimination of cabling effects.

3.2.4 Surface dose

A Markus chamber (PTW34045) in a solid water phantom was used to estimate the surface doses. We have measured the response of the chamber for no build-up (an entrance window of 0.025 mm of water equivalent material) and for 1 mm solid water build-up and related these to measurements at the depth of maximum dose.

3.2.5 Penumbra evaluation

The definition of penumbra width - a difference in position between 80% and 20% relative dose point of a profile - cannot be applied to FFF beams normalised to the central axis, as dose inside a field can be as low as 30 % depending on the beam's energy and field size (figure 3.1). To overcome this limitation, Pönisch et al [53] proposed for FFF beams normalization to the inflection point of a profile's penumbra. The same normalization is used in our study.

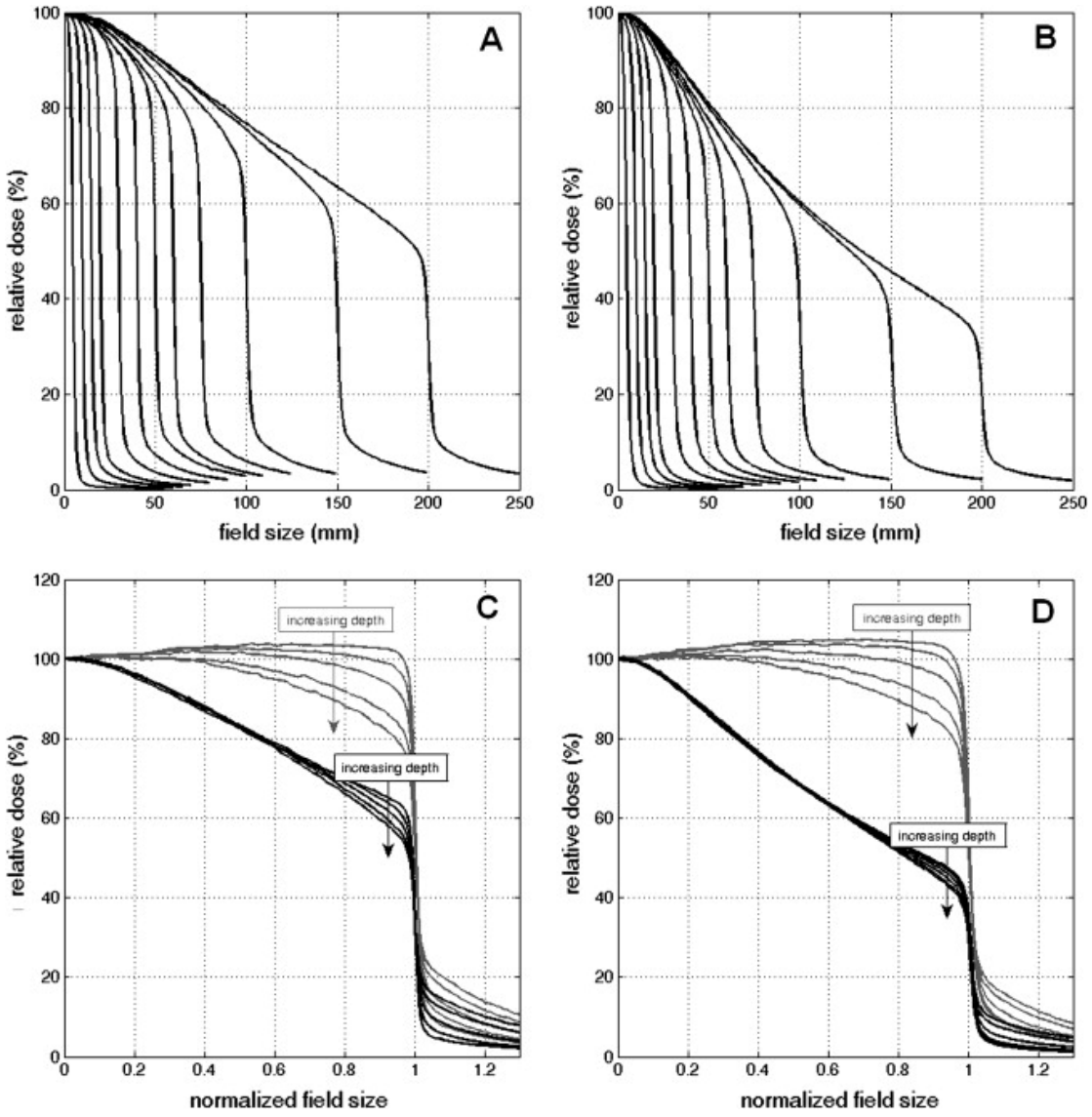

FIGURE 3.1: Measured profiles for all field sizes at 10 cm depth for X6FFF (A) and X10FFF (B) and for the 30 x 30 cm^2 field at all measured depths for X6 and X6FFF (C) and X10 and X10FFF (D). FFF profiles are represented by black lines; flattened profiles are indicated by gray lines.

3.2.6 Out of field dose

To evaluate out-of-field dose, a half-profile of a dose up to 40 cm off the central axis was measured for X6, X6FFF, X10, X10FFF for the following depths and field sizes:

- field size: 4x4 cm^2, 10x10 cm^2
- depth: 2 cm, 10 cm, 20 cm

A large water phantom was placed asymmetrically so that the beam's central axis was aligned close to a phantom wall, yet ensuring that the entire field remains inside the water phantom at any depth. The solid water phantom was aligned to the wall of the water phantom to ensure full scatter conditions. The measurement was performed with the 0.125 cm^3 cylindrical chamber. The previously mentioned normalization to the inflection point was used.

3.2.7 Changes in the output

To evaluate the delivery efficiency achieved by the removal of the flattening filter, the dose measured in the reference conditions for 100 MU was related to the charge on the target. Total scatter factors (S_{cp}) were measured in a large water phantom at SSD 90 cm and the depth of 10 cm for all rectangular field sizes created using the following jaw positions:

- 1 cm, 2 cm, 3 cm, 4 cm, 6 cm, 8 cm, 10 cm, 12 cm, 15 cm, 20 cm, 30 cm, and 40 cm.

For field sizes down to 3x3 cm^2, a 0.125 cm^3 cylindrical chamber (PTW31010) was used. Field sizes below 3x3 cm^2 were measured with a shielded (PTW60008) and unshielded diode (PTW60012) following the recommendation of Schwedas et al [54].

3.2.8 HDMLC transmission and dosimetric leaf gap

HDMLC leaf transmission was determined by a measurement with a Roos chamber (PTW34001) in a large water phantom at SSD 90 cm for three different depths (5 cm,

10 cm, and 20 cm). A jaw collimated 8x22 cm^2 field, with HDMLC leaves of one carriage completely blocking the field, was used to acquire transmission profiles across HDMLC with a liquid ionization chamber (PTW31018). For the determination of the dosimetric leaf gap (DLG), the sweeping gap method was used [55, 56]. Dose measured by the Farmer ionization chamber (PTW300013) for a sweeping gap of 1, 10, 20, and 30 mm was corrected for the HDMLC transmission and the corrected dose was plotted against the field size. The interpolation of this dataset to zero field size was used as an estimator of the DLG.

3.2.9 Beam modeling and evaluation of the model

The measured depth dose curves, transverse profiles, diagonal profiles, and output factors were imported into Eclipse in order to calculate the beam data for the anisotropic analytical algorithm (AAA 8.9.08, Varian Medical Systems) [44, 45]. Profiles and depth dose curves were modeled by the configured AAA with a calculation grid of 1.5 mm and exported.

The agreement of the modeled profiles with the measured dataset was evaluated using an in-house implementation of a one-dimensional gamma [27] approach. The criteria of 1 % dose difference (DD) and 1 mm distance to agreement (DTA) have been selected. Each measured - modeled profile pair was individually reviewed and additionally, histograms were generated from the obtained gamma profiles to quantify the overall agreement for each bundle and its sub-regions (inside-field, penumbra, out-of-field for profiles and build-up and fall-off for depth dose curves).

3.3 Results

3.3.1 Depth dose curves

Mean energy of FFF beams is lower than the one of corresponding flattened beams (see quality indexes in table 3.1). For field sizes between 1x1 cm^2 and 30x30 cm^2, FFF beams have the d_{max} located closer to the surface than the flattened beams (up to approximately 2 mm for X6FFF and 4 mm for X10FFF). Generally, with increasing field size, the d_{max} shifts closer to the surface; this effect is less pronounced for FFF

TABLE 3.1: Depth dose curve parameters (2 standard deviations in brackets)

	d_{max} (mm)	%dd (0.025 mm)	%dd (1 mm)	%dd (100 mm)	$TPR_{20/10}$
X6	14.3 (0.44)	18.9 (0.4)	47.3 (0.4)	66.0 (0.4)	0.667 (0.004)
X6FFF	12.1 (0.17)	24.3 (0.4)	56.1 (0.4)	63.2 (0.2)	0.631 (0.004)
X10	22.3 (0.60)	14.0 (1.0)	32.3 (1.0)	73.5 (0.5)	0.738 (0.004)
X10FFF	21.0 (1.2)	19.1 (1.6)	43.6 (1.0)	69.1 (1.0)	0.692 (0.012)

%dd = percentage depth dose
$TPR_{20/10}$ = tissue-phantom ratio at the depths of 20 and 10 cm

TABLE 3.2: Ratios of maximum and minimum dose inside the field (within 80 % of the field size) for different field sizes measured at 10 cm depth (SSD 90 cm)

Square field size (cm^2)	1	2	4	10	20	40
X6	1.41	1.15	1.05	1.05	1.04	1.04
X6FFF	1.39	1.14	1.07	1.13	1.28	1.65
X10	1.45	1.23	1.09	1.04	1.03	1.04
X10FFF	1.45	1.21	1.12	1.25	1.54	2.23

beams however, and therefore the difference in the d_{max} of flattened and FFF depth dose curves gradually diminishes and eventually results in deeper located d_{max} for both FFF beams for the 40x40 cm^2 field size. The surface dose for the field size 10x10 cm^2 increases by approximately 10 % (table 3.1).

3.3.2 Profiles

FFF profiles have the maximum dose on the central axis and decrease gradually towards the field edge. This non-flattened shape becomes more pronounced with increasing field size and beam energy (figure 3.1, table 3.2). Up to a field size of 3x3 cm^2, the in-field part of a profile is practically the same for X6 & X6FFF, as well as X10 & X10FFF beams. Smaller profile variations with depth are observed for FFF beams (figure 3.1).

3.3.3 Penumbras

X6FFF penumbra is approximately 0.3 mm sharper than the penumbra of X6 at d_{max}. With increasing depth, the difference gradually diminishes and at a depth of 12 cm, penumbras of X6 and X6FFF are practically identical. Beyond this range, the flattened beam creates sharper penumbra. For X10FFF, sharper penumbra than for X10 was measured for all investigated depths, the difference between penumbras reaches up to 0.6 mm at the d_{max} and slowly decreases with depth. A slight widening of penumbra with increasing field size was observed for all beams. This widening occurs at a slightly faster rate for FFF beams. Table 3.3 summarizes penumbra width for selected conditions

TABLE 3.3: Measured transverse/radial penumbras (mm) for selected field sizes and depths

field (mm^2)	depth (mm)	X6	X6FFF	X10	X10FFF
10x10	d_{max}	2.01/2.79	1.77/2.59	2.66/3.19	2.29/2.84
100x100	100	4.09/4.83	3.71/4.93	4.63/5.65	4.25/4.77
150x150	200	6.38/6.30	7.26/8.85	7.20/7.75	6.98/7.60

in the transverse and radial direction. Figure 3.2 summarizes penumbral width for the highest (X10) and the lowest (X6FFF) energy bundle under investigation as a function of field size and depth.

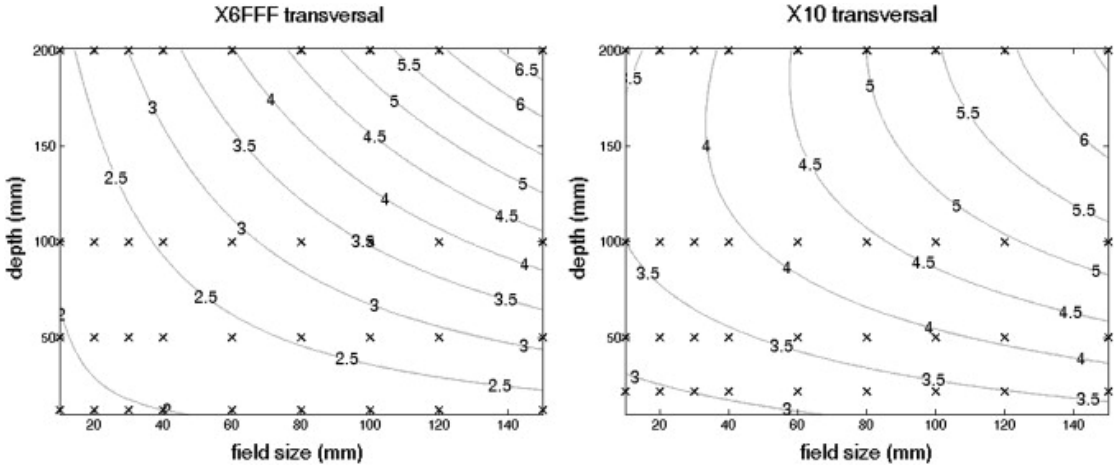

FIGURE 3.2: Penumbra width (in mm) are shown in a transverse direction as functions of field size and depth for X6FFF (A) and X10 (B). Isolines of penumbra width were obtained as quadratic least square fit of measured points (presented as crosses). A root-mean-square deviation of the fit and measurement is 0.13 mm for X6FFF and 0.14 mm for X10.

3.3.4 Out of field dose

Figure 3.3 represents a ratio of (half) dose profiles of a FFF and a flattened beam for different field sizes and depths. Out-of-field dose deposited by FFF beams is, under most conditions, lower than for flattened beams. There is a noticeable dose reduction effect at the edge of a field and at further distances from the edge. At interim region, the FFF/flattened dose ratio reaches its maximum and under some circumstances, a FFF beam can deposit more dose than a flattened one in this region. At a distance of around 20 cm from the central axis, an increment on the dose ratio curve is visible. With increasing field size and depth, the dose reduction effect of a FFF beam gradually decreases.

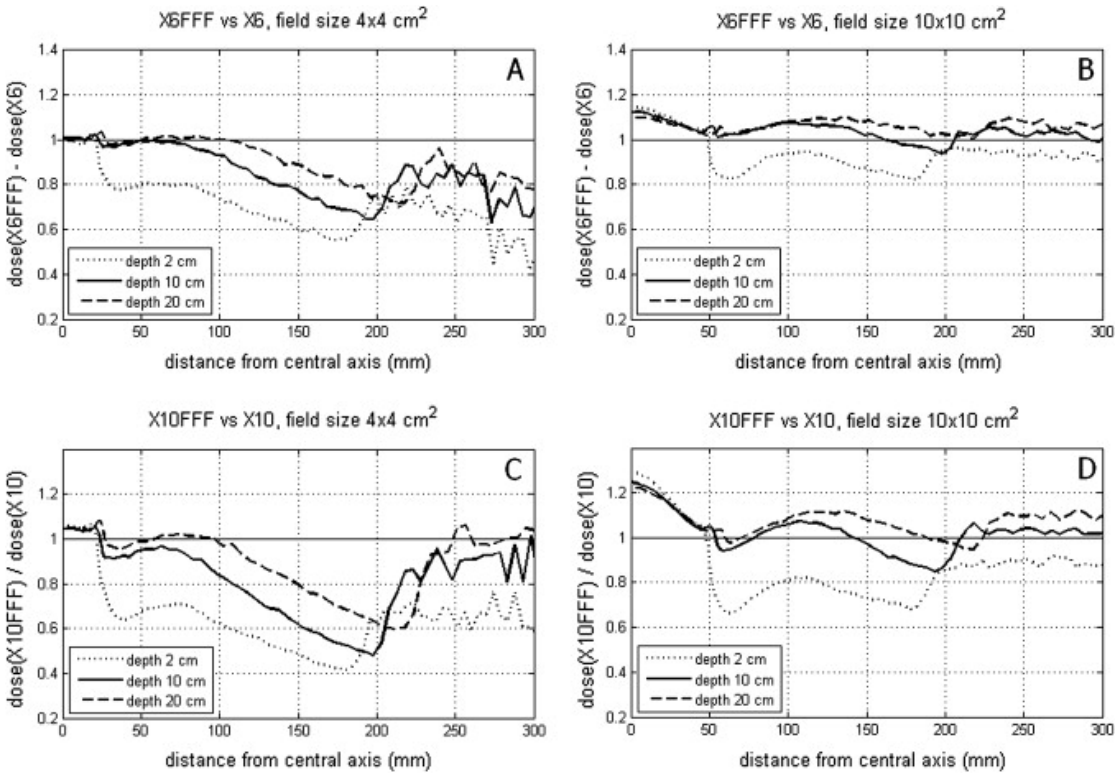

FIGURE 3.3: Out-of-field dose ratios for X6FFF/X6 (A, B) and X10FFF/X10 (C, D) are shown for two selected field sizes.

3.3.5 Changes in the output

Under reference conditions, the dose in the reference point on the central axis produced by the same charge on the target is 2.26 times higher for X6FFF than for X6; this ratio is 4.03 for X10FFF. Total scatter factors (S_{cp}) for symmetric fields are plotted in figure 3.4. FFF beams exhibit smaller output variations with field size and the collimator exchange effect is reduced - the change in S_{cp} for 2x40 cm^2 and 40x2 cm^2 rectangular field is 1.2 % for X6FFF, 1.8 % for X6, 1.5 % for X10FFF and 2.4 % for X10.

3.3.6 HDMLC transmission and dosimetric leaf gap

Both FFF beams have lower transmission than the corresponding flattened beams (table 3.4). Transmission increases with depth for all beams and this effect is most pronounced for X6FFF. Radial changes in the transmission of FFF beams are smaller (difference in transmission on the central axis and 10 cm off-axis is 0.16 % for X6FFF, 0.23 % for X6,

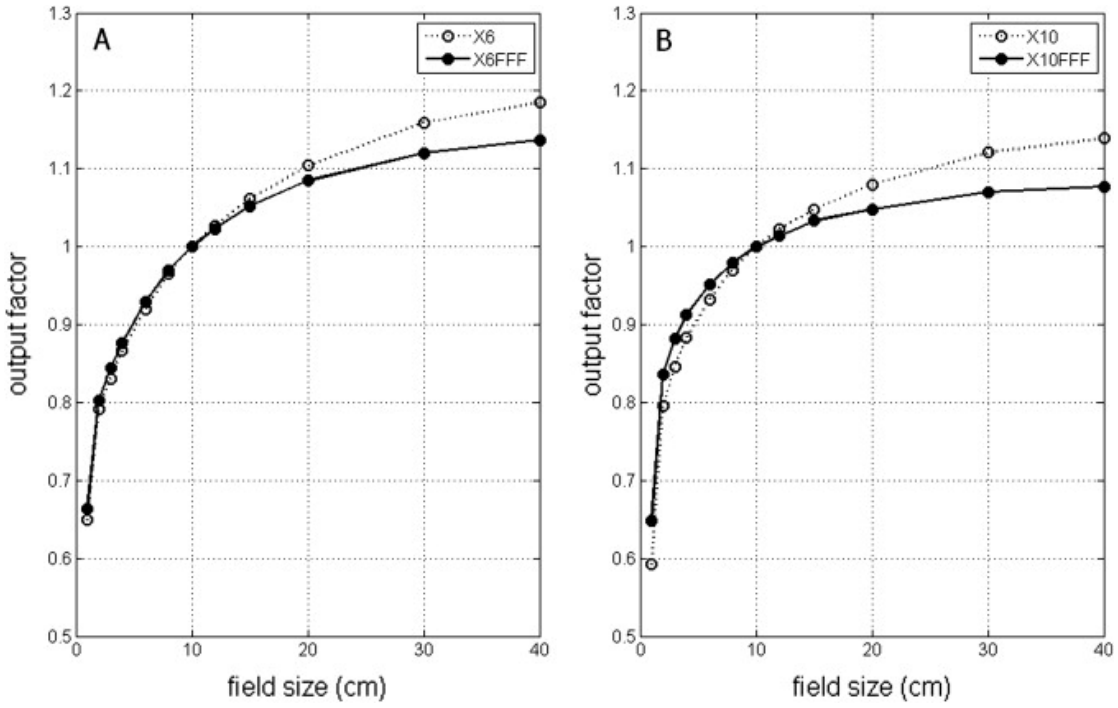

FIGURE 3.4: Total scatter factors for symmetric fields are shown for X6 and X6FFF (A), X10 and X10FFF (B).

TABLE 3.4: Dosimetric leaf gap and transmission of HDMLC (2 standard deviations in brackets)

DLG (mm)		MLC transmission		
		depth 5 cm	depth 10 cm	depth 20 cm
X6	0.93 (±0.08)	1.19 %	1.21 %	1.30 %
X10	1.03 (±0.08)	1.38 %	1.39 %	1.41 %
X6FFF	0.91 (±0.07)	0.98 %	1.02 %	1.13 %
X10FFF	1.04 (±0.08)	1.17 %	1.20 %	1.27 %

0.18 % for X10FFF, 0.25 % for X10). A dosimetric leaf gap of approximately 1 mm was determined for all bundles (table 3.4).

3.3.7 Modeling in Eclipse

In general, a good agreement between the modeled and measured data is observed for all beams under investigation. Whilst the high dose region of profiles is well modeled for all bundles, it is obvious that the accuracy of penumbra modeling is limited. The modeled penumbras are on average 0.7 mm ± 0.4 mm wider than the measured ones. The impact of less accurate penumbra modeling is accentuated for small field sizes (below

TABLE 3.5: Gamma score (GS) and values of different percentiles of γ-histograms for symmetric and asymmetric profiles and depth dose curves

	GS (%)	50 %	75 %	80 %	90 %	95 %	100 %
Profiles (symmetric fields)							
X6	96.9	0.24	0.47	0.53	0.73	0.90	1.73
X6FFF	98.1	0.19	0.38	0.44	0.62	0.78	1.77
X10	95.3	0.28	0.53	0.61	0.82	0.99	1.83
X10FFF	94.2	0.18	0.37	0.44	0.71	1.07	2.02
Depth dose curves (symmetric fields)							
X6	99.2	0.15	0.29	0.35	0.54	0.70	2.00
X6FFF	99.5	0.15	0.31	0.36	0.47	0.58	1.17
X10	98.3	0.19	0.33	0.36	0.49	0.68	1.87
X10FFF	99.7	0.13	0.25	0.30	0.44	0.66	1.07
Profiles and depth dose curves (asymmetric fields)							
X6	96.4	0.35	0.56	0.62	0.78	0.95	1.48
X6FFF	99.2	0.25	0.43	0.48	0.62	0.73	1.43
X10	87.4	0.34	0.68	0.79	1.10	1.37	1.94
X10FFF	91.0	0.22	0.47	0.58	0.95	1.18	1.54

approximately 4x4 cm^2) where penumbra creates a proportionally larger part of a profile (figure 3.5).

The largest discrepancies are observed at the foot - the boundary between the penumbra and the out-of-field part - of a profile. The discrepancy in this region increases with depth and is more obvious for X10 and X10FFF bundles. Dose of a measured profile is lower then the one modeled in this region for all beams. Depth dose curves are well modeled for all four energies. Good agreement is observed inside the build-up region as well as beyond the d_{max} for all field sizes including 1x1 cm^2 (figure 3.6).

Parameters of gamma histograms quantifying the agreement between measured and modeled curves are summarized in table 3.5. The majority of evaluated points complies with the selected agreement criteria (1% DD, 1 mm DTA) and the value of gamma is always smaller than 2. In the out-of-field region of X10 and X10FFF where agreement was poor, approximately 10 % of the points fail the criteria.

A similar evaluation made for the modeling of asymmetric fields shows a similar level of agreement, with both FFF beams attaining a slightly better gamma score than the flattened ones (table 3.5).

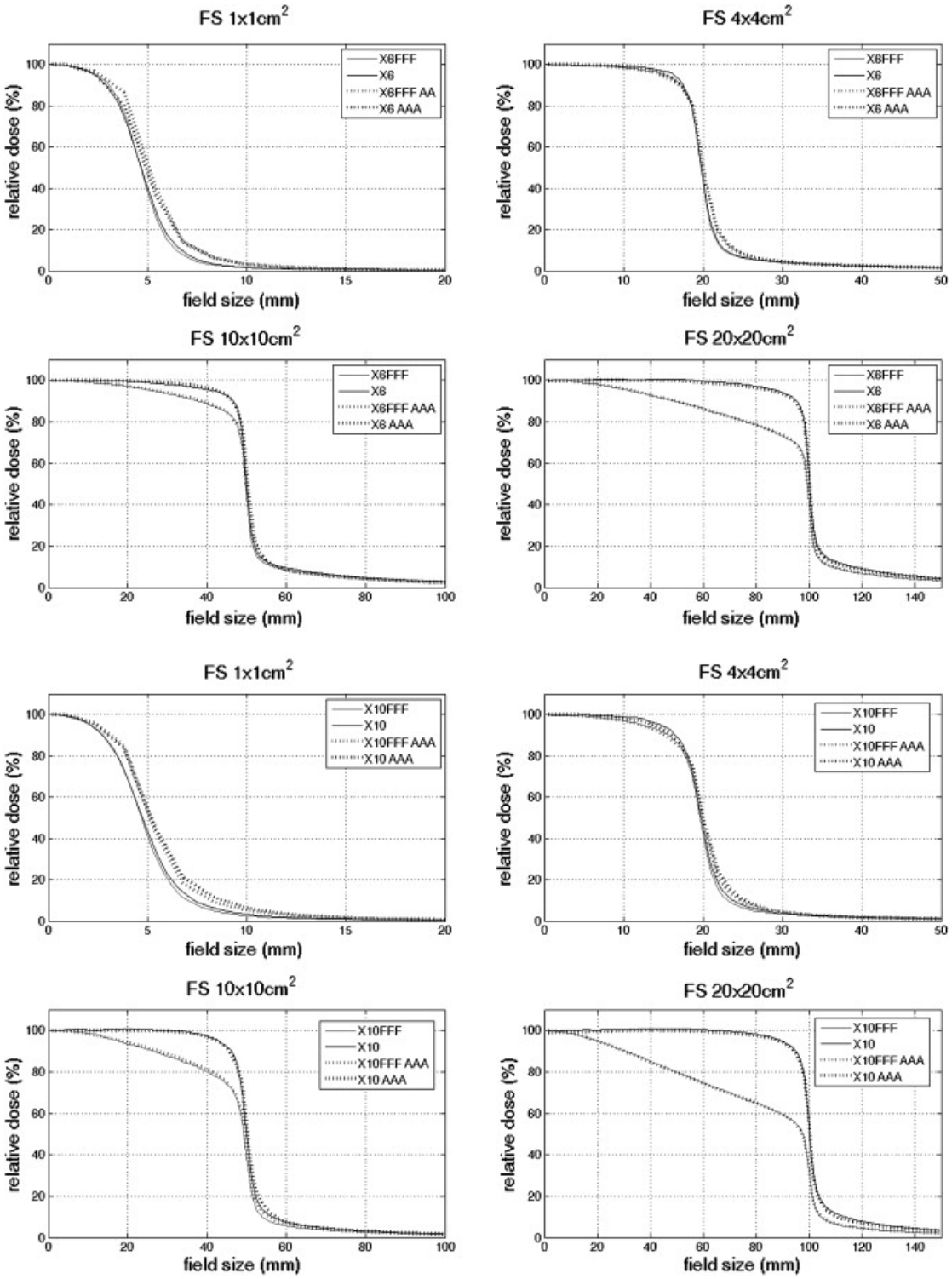

FIGURE 3.5: Comparison of measured and modeled profiles for X6FFF and X6 and for X10FFF and X10 at four selected field sizes.

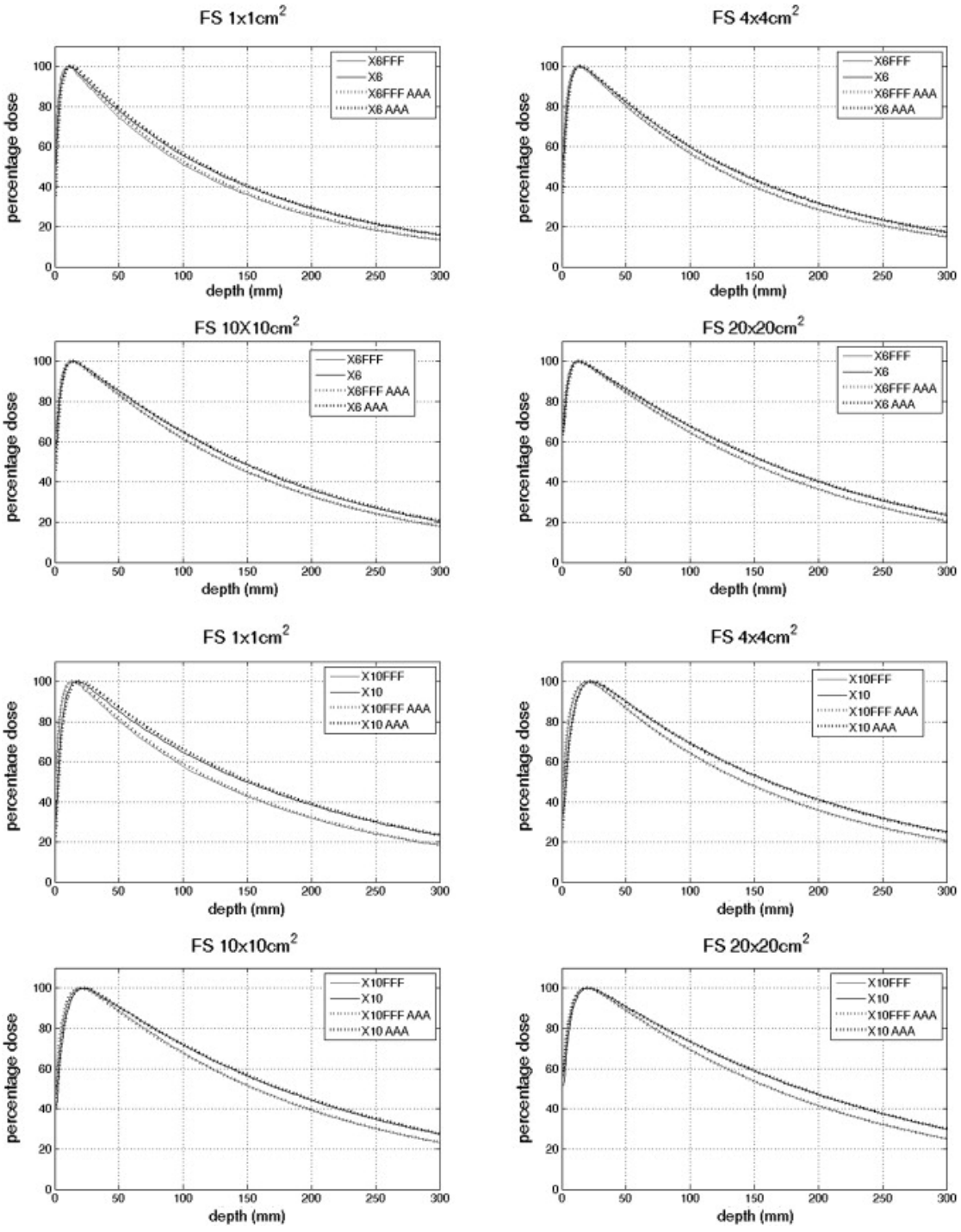

FIGURE 3.6: Comparison of measured and modeled depth dose curves are shown for X6FFF & X6 and for X10 FFF & X10 at four selected field sizes.

3.4 Discussion

3.4.1 Depth dose curves & profiles

From a qualitative point of view, changes of depth dose curves and profiles induced by the removal of a flattening filter are consistent with other studies dealing with this topic [19–21, 23–25, 57]. As beam hardening does not occur for FFF beams, their mean energy is lower due to the presence of low energy photons and FFF depth dose curves have more rapid fall-off. Low energetic photons contribute to the increase of superficial dose for FFF beams and to the slight shift of d_{max} closer to the surface. Vassiliev et al [23] and later Kragl et al [24] explain the shifts of d_{max} as a result of two competitive effects: beam hardening for flattened beams (shifts d_{max} downstream) and larger head scatter contribution for flattened beams with increasing field size (shifts d_{max} upstream). This is supported by our data, where the difference in d_{max} diminishes with increasing field size and both FFF beams eventually have d_{max} for the largest field size located deeper than flattened beams. The non-flatness of FFF profiles increases with energy as the probability of photon scattering into lateral directions decreases with the increasing energy of incident photons. The non-flatness characteristic of X6 and X6FFF (table 2) is comparable to the one reported by Vassiliev et al for a Clinac 21EX FFF prototype (measured at SSD 100 cm) [23]. The largest difference is observed for the smallest field size, TrueBeam's non-flatness parameter for X6 and X6FFF being approximately 2 % lower than for the 21EX. Smaller variations of FFF profiles with depth may be attributed to more uniform mean energy in a radial direction [57]. The mean energy of flattened beams is subject to larger changes due to the variable beam hardening effect of the non-uniformly thick flattening filter.

3.4.2 Penumbras

The sharper penumbra of FFF beams at shallow depths can be attributed to their lower mean energy, hence shorter range of secondary electrons. However, less energetic FFF beams are more prone to scattering, therefore at sufficient depth they will eventually form a wider penumbra than flattened beams. Increase widening of penumbra of FFF beams as a function of field size may be due to the profile normalization method. Kragl et al [24] report non significant differences in penumbra for flattened and FFF beams of

prototype Elekta linacs. Pönish [53] reports 0.5 mm penumbra reduction for X6FFF of Clinac 2100 prototype for a field 10x10 cm^2 and 10 cm depth.

3.4.3 Out-of-field dose

Out-of-field dose evaluation for the Clinac 2100 FFF prototype, based on Monte Carlo simulation, was recently published [58]. Our measurements for TrueBeam concur qualitatively with the simulation. The ratio of dose profiles outside a field is a result of two competing effects: decrease of collimator scatter and head leakage, and increase of phantom scatter resulting from lower mean energy of FFF beams [58]. Increased phantom scatter constrains the dose reduction potential of FFF beams.

The comparison of FFF and flattened profiles partially depends on the method used for their normalization, especially for larger field sizes and higher nominal energy where a difference in shape between FFF and flattened profile is more accentuated. In our opinion, the normalization to penumbra represents an extreme option that maximizes the difference in primary dose deposited in a phantom for a FFF and flattened beam. The additional contribution of primary dose proportionally creates additional scatter; hence, the comparison of profiles normalized to penumbra can be understood as the worst case scenario of dose reduction for FFF beams.

In clinical situations, dose outside of the target will be influenced by many parameters such as size, location, and shape of the target as well as the degree of modulation and delivery technique used (IMRT or VMAT) and their interplay with beam characteristics (energy and shape of a profile). As is obvious from the measured data (figure 3.3), the best possible dose reduction outside a field will be in general achieved for small field sizes and higher energy FFF beams.

3.4.4 Changes in the output

The observed increase in the dose delivery efficiency resulting from the flattening filter removal is consistent with data published in Vassiliev et al [23] (2.3 for X6FFF and 5.5 for X18FFF). Less dependence of the output on field size and reduced collimator exchange effect for FFF beams related to the reduction of head scatter is comparable with other reports [23, 24, 53].

3.4.5 HDMLC transmission and dosimetric leaf gap

Lower transmission and its smaller off-axis variation are related to the lower and more uniform mean energy of FFF beams [57]. Larger variation of transmission with depth for low energetic beams may be attributed to more pronounced MLC beam hardening effect.

3.4.6 Modeling in Eclipse

Eclipse modeling of the four beams is generally accurate. The selected criteria - 1 % DD and 1 mm DTA - seem to be reasonable and is achieved in the majority of the investigated points for symmetric as well as asymmetric fields. The worst gamma score result (87 %) was observed for the group of asymmetric profiles of the X10 bundle. The value of gamma is always below 2, meaning if the criteria of 2 mm DTA and 2 % DD were selected, these values would always be attained.

Omitting the outliers in the gamma histograms, there is lower occurrence of higher gamma values for both FFF bundles (table 5) and one could therefore anticipate that the modeling of FFF bundles is easier. AAA uses only a single source model for FFF beams. The second (virtual) source, which model dose contribution from the extra-focal radiation in flattened beams, is left out for FFF beams as the majority of extra-focal photons originate from a missing flattening filter. This approach appears to ensure a good performance also for asymmetric fields where the model agreement is slightly better for FFF beams as well (table 5).

The agreement with the measurement is not only influenced by the quality of the beam model, but also by imperfections in the measured dataset. To reduce these imperfections, all profiles were aligned and normalized prior to the evaluation. Influences of the discrete character and noise in the measured profiles are partially suppressed by the used algorithm for 1D gamma analysis [27]. There was not any measure taken to symmetrize beams, which influenced the agreement evaluation for the X10FFF bundle where a slight (clinically acceptable) asymmetry of the beam is the cause of several points with higher gamma values in the high dose region of a profile. X10FFF is the only bundle that exhibits higher gamma values in this region.

3.5 Conclusion

Basic dosimetric properties were summarized for four photon beams of the first clinically used TrueBeam STx linear accelerator. All bundles were successfully modeled by the analytical anisotropic algorithm with an acceptable level of agreement with measured data.

Chapter 4

Ion-recombination correction for different ionization chambers in high dose rate flattening filter free photon beams[1]

4.1 Introduction

Recently, there has been an increased interest in flattening-filter-free (FFF) linear accelerators [23–25, 42]. Removal of the filter results in available dose rates up to 14 and 24 Gy min^{-1} for nominal energies of 6 and 10 MV (in depth of maximum dose (d_{max}), a source-surface distance (SSD) of 100 cm and a field size of 10 x 10 cm^2), respectively. To guarantee accurate relative and reference dosimetry for such FFF beams, we investigated the charge collection efficiency of multiple air-vented and one liquid ionization chamber for dose rates up to 31.9 Gy min^{-1}.

The two main processes leading to ion recombination are "initial recombination" and "general recombination". Initial recombination is caused by the recombination of two particles originating from the same particle track. It has been previously shown by several authors that within air-vented ionization chambers this contribution is minimal and

[1]This chapter has been published as a manuscript [29]: S. Lang, J. Hrbacek, A. Leong, and S. Klöck, "Ion-recombination correction for different ionization chambers in high dose rate flattening-filter-free photon beams," Physics in Medicine and Biology, vol. 57, no. 9, p. 2819, 2012.

independent of dose rate [59,60]. General recombination occurs when particles originating from different particle tracks recombine. Boag [61] developed a theoretical method to account for the general recombination in both pulsed and continuous beams. He proposed the two-voltage method [62] to determine the correction for incomplete collection of ions at sufficiently high applied voltages. Since then numerous investigations regarding the ion-collection efficiency of different chambers used for reference dosimetry under a range of conditions have been published [59,60,63–65]. Recently, Bruggmoser et al [65] determined saturation coefficients for a selection of plane parallel and cylindrical chambers in pulsed photon and electron beams up to 42 mGy pulse^{-1}.

For liquid ionization chambers, the two-voltage method cannot be applied because the effect of initial recombination cannot be neglected due to the high ionization density in the particle track and the short mean free path of ions in liquid [66–68]. Moreover, initial recombination is affected by the applied voltage and thus leads to a dependence of the general recombination efficiency upon the applied voltage. Pardo-Montero et al [69] developed and verified a three-voltage method as well as a modified two-voltage method to determine charge-collection efficiency in parallel plate liquid ionization chambers.

In this chapter, we contribute to these investigations a detailed analysis of recombination effects in several air-vented ionization chambers as well as one liquid ionization chamber using pulsed high dose rate photon beams without a flattening filter. This chapter is the first systematic study of the performance of ionization chambers with an FFF accelerator commissioned for clinical use. Earlier investigations have been limited to high dose per pulse (DPP) electron beams [65]. While the clinical use of the FFF is rapidly increasing [70] detailed studies regarding the behaviour of commonly used detectors in conjunction with these beams are lacking.

The beam pulse pattern of both FFF and flattened beams were analysed to show the influence of dose rate, DPP and pulse repetition frequency (PRF) on collection efficiency. Detectors used for reference as well as relative dosimetry were investigated to ensure that the depth-dose curves and profiles were not distorted due to insufficient charge collection within high dose rate regions.

4.2 Material and methods

4.2.1 Linear accelerator and beam characteristics

Experimental data were collected using a Varian TrueBeam linear accelerator (Varian Medical Systems, Paulo Alto) at nominal energies of 6 and 10 MV with and without a flattening filter in the beam path (X6, X10 and X6FFF, X10FFF, respectively). The characteristics of the four beams have been previously described in detail by Hrbacek et al [42]. For X6 and X10 beams, dose rates between 1 and 6 Gy min^{-1} (d_{max}, SSD = 100 cm, 10 x 10 cm^2) are clinically available. By comparison, X6FFF allows dose rates between 4 and 14 Gy min^{-1}, while X10FFF allows dose rates between 4 and 24 Gy min^{-1} (d_{max}, SSD = 100 cm, 10 x 10 cm^2).

Table 4.1 summarizes the parameters regarding the beam pulse pattern of the four energies at respective minimum and maximum dose rates. The DPP and PRF were measured with the Delta^4 phantom (ScandiDos, Uppsala). At the maximum dose rate, the PRF was equal for all beams. The increased dose rate of FFF beams is due to the increased DPP relative to flattened beams. Reduction of the dose rate is achieved within the TrueBeam system by changing the PRF, whilst maintaining the same DPP. For X6 and X10, pulses are generated at regular intervals (every 2.8 ms at the maximum dose rate). For X6FFF and X10FFF, however, every fourth to fifth pulse is omitted. Therefore, for X6 and X10 DR, the DPP and PRF can be related but not for the FFF beams.

4.2.2 Detectors under investigation

The general ion-collection efficiency at different DPP and PRF was determined for the following six ionization chambers in total:

- PTW 34 001 Roos chamber,
- PTW 34 045 Advanced Markus Chamber,
- PTW 31 010 Semiflex chamber,
- PTW 31 016 PinPoint chamber,

TABLE 4.1: Basic characteristics of the beam pulse pattern for the four beams available on TrueBeam inear accelerator. Dose rate ranges (DRR)(measured at the depth of maximum dose (d_{max}), SSD = 100 cm, field size of 10 x 10 cm^2 and measured for the d_{max}, SSD = 90 cm, field size 40 x 40 cm^2), time between two pulses and DPP (d_{max}, 40 x 40 cm^2, SSD = 90 cm) were measured using Delta^4 phantom (ScandiDos, Sweden). For X6 and X10 beams, pulses are generated at regular intervals (every 2.78 ms at the maximum dose rate); however, for X6FFF and X10FFF every fourth to fifth pulse is omitted.

Beam	Dose rate range (10x10) Gy min^{-1}	Dose rate range (40x40) Gy min^{-1}	Time between pulses ms	DPP in d_{max} mGy
X10FFF	4.0-24.0	5.3-31.9	16.7-2.8	1.7
X6FFF	4.0-14.0	5.6-21.6	9.7-2.8	1.1
X6	1.0-6.0	1.4-8.6	16.7-2.8	0.4
X10	1.0-6.0	1.4-8.4	16.7-2.8	0.4

TABLE 4.2: Basic specifications of the chambers (PTW, Freiburg) investigated: four different thimble (t) chambers and two plane-parallel (pp) chambers. Chambers differed in terms of active volume, applied voltage and geometry. The microLion chamber is filled with liquid isooctane. All other chambers are vented and respectively filled with air.

Beam	DRR (10x10) Gy min^{-1}	DRR (40x40) Gy min^{-1}	Time between pulses ms	DPP in d_{max} mGy
31 010 Semiflex	t	0.125	+400	0.100
31 016 Pinpoint	t	0.016	+400	0.060
34 001 Roos	pp	0.350	+200	0.125
34 045 AdvMarkus	pp	0.020	+300	0.022
30 013 Farmer	t	0.600	+400	0.140
31 018 microLion	t/liquid	0.002	+800	5.300

- PTW 30 013 Farmer chamber,
- PTW 31 018 microLion chamber, liquid ionization chamber.

Details on the chambers, provided in the manuals of the vendor (PTW, Freiburg), are summarized in table 4.2.

4.2.3 Ion-collection efficiency for gas-filled chambers

According to Boag [61], the ion-collection efficiency of an air-vented ionization chamber in pulsed beams can be expressed as follows:

$$f = u^{-1} ln(1 + u), \tag{4.1}$$

where

$$u = \mu\rho\frac{d^2}{V}. \tag{4.2}$$

μ is a constant involving the ion-recombination coefficient and mobilities, ρ is the pulse charge density, d is the equivalent electrode spacing and V is the polarizing voltage. For small charge densities, this formula can be expanded up to the first-order term, which leads to a description of the saturation correction:

$$k_S = \frac{1}{f} = 1 + \frac{\mu}{2}\rho\frac{d^2}{V}. \tag{4.3}$$

For chambers that follow this relation, the saturation coefficient k_S can be determined using Boag's two-voltage method [62]:

$$k_S = \frac{\frac{V_1}{V_2} - 1}{\frac{V_1}{V_2} - \frac{Q_1}{Q_2}}. \tag{4.4}$$

V_1 is the operating voltage and V_2 is an arbitrary voltage (smaller than the operating voltage), and Q_1 and Q_2 are the collected charges at these voltages. We determined the correction factors for all air-vented filled ionization chambers according to this formula. The operating voltages V_2 for the chambers can be found in table 4.2. V_2 was chosen to be half of V_1, as recommended by Almond [51].
All measurements were performed for a geometry, which maximizes the dose rate, i.e. shortest SSD within commissioning relevant limits (90 cm), largest field size 40 x 40 cm^2), and at the depth of maximum dose. The dose corresponding to 100 MU was

- 1.40 Gy at depth of 1.21cm for X6FFF,
- 1.33 Gy at depth of 2.10 cm for X10FFF,
- 1.46 Gy at depth of 1.43 cm for X6,
- 1.40 Gy at depth of 2.23 cm for X10.

This resulted in a DPP of 1.1 mGy for X6FFF, 1.7 mGy for X10FFF, 0.4 mGy for X6 and 0.4 mGy for X10. The dependence of ion-collection efficiency upon PRF, DPP and beam energy was studied

4.2.4 Ion-collection efficiency for liquid ionization chambers

In liquid ionization chambers, the influence of initial recombination cannot be neglected. The charge released within the chamber is dependent upon the applied voltage. If the DPP is low and the time between pulses is longer than the ion-collection time of the chamber, the collected charge Q will relate linearly to the applied voltage V [69]:

$$Q = Q_0(1 + cV). \tag{4.5}$$

We determined the coefficients c and Q_0 at the PRF less than 100 Hz and a DPP of 0.03 mGy (SSD = 120 cm, depth = 25 cm, X6 and X10). According to the modified two-voltage method of Pardo-Montero et al [69], which is valid so long as the ion-collection time is small relative to the time between two consecutive pulses, the ion-collection efficiency can be determined as follows:

$$f = \frac{(1 + cV_2)^2 V_1 Q_1 - (1 + cV_1)(1 + cV_2)V_2 Q_1}{(1 + cV_2)^2 V_1 Q_1 - (1 + cV_1)^2 V_2 Q_2}. \tag{4.6}$$

According to this method, we determined the collection efficiency of the liquid ionization chamber for all four beams at the lowest available PRF (time between two pulses >ion-collection time of 5.3 ms). For a higher PRF, the relative collection efficiency compared to the Markus chamber was determined. The ratio of reading between the liquid-filled chamber and the Markus chamber was compared for different doses per pulse. DPP was changed by varying the measurement depth (2-30 cm) as well as the SSD (SSD = 90 cm and SSD = 120 cm). The collection efficiency of the Markus chamber was above 0.994 (shown in the first part of the results) and therefore neglected for the relative comparison to the liquid ionization chamber. For the lowest DPP (SSD = 120 cm, depth = 30 cm), the ratio was set to 1, as it is known that the collection efficiency is high (above 0.995) for a DPP below 0.3 mGy [71].

4.2.5 Propagation of uncertainty

Q_1 and Q_2 were measured multiple times and mean values and standard deviations of the mean u_{Q1} and u_{Q2} were calculated. Using uncertainty propagation, the standard

deviation for the ion-collection efficiency u_f was calculated according to

$$f = \sqrt{\left(\frac{\delta f}{\delta Q_1} u_{Q1}\right)^2 + \left(\frac{\delta f}{\delta Q_2} u_{Q2}\right)^2}. \tag{4.7}$$

4.3 Results

4.3.1 Ion-collection efficiency for air-vented chambers

Table 4.3 summarizes the ion-collection efficiency factors of all investigated air-vented chambers for all four beams. The collection efficiency was above 0.985 ($2u_f = 0.002$) in all cases. The Markus chamber demonstrated the largest collection efficiency 0.994 ($2u_f = 0.002$) for X10FFF; 0.997 ($2u_f = 0.001$) for X6 and X10). The collection efficiency was independent of the PRF (figure 4.1), implying that for a given beam with a specific DPP the collection efficiency does not change with the dose rate. Figure 4.1 illustrates the dependence of the Farmer chamber upon the PRF. The Farmer chamber demonstrated the longest collection time of all the air-vented chambers (table 4.1), whereas, all other chambers showed a deduced dependency on the PRF.

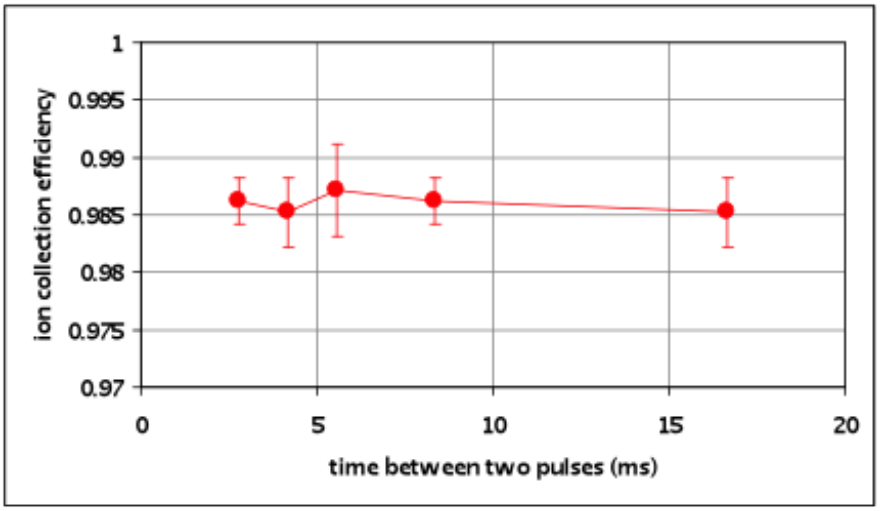

FIGURE 4.1: Dependence of collection efficiency on the PRF when using the Farmer chamber (PTW, Freiburg). According to table 4.2, the Farmer chamber has the longest ion-collection time (air-vented chambers), so all other chambers depend less on the PRF. By altering the time between pulses, the dose rate was varied. For the X10FFF beam, dose rates of 2400 and 400 MU min^{-1} correspond to a time between pulses $dt = 2.78$ ms and $dt = 16.67$ ms, respectively.

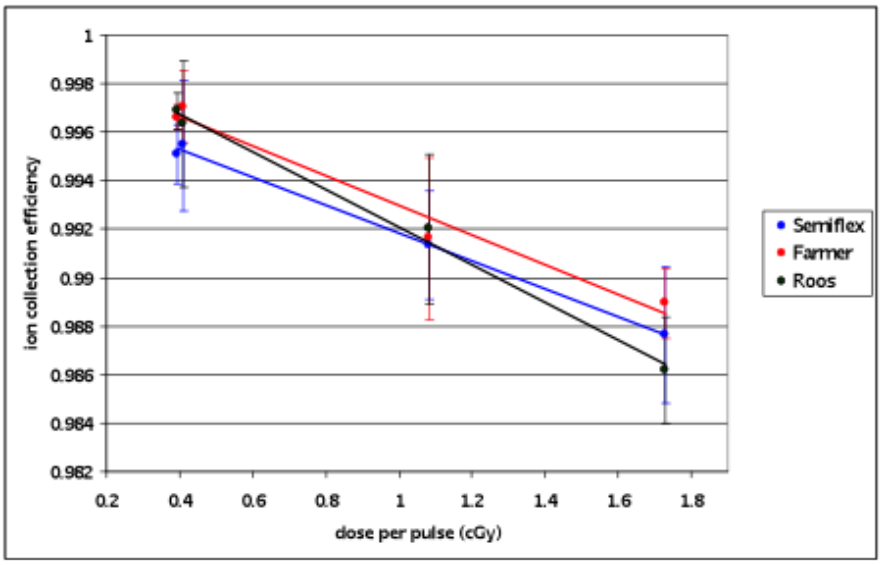

FIGURE 4.2: Ion-collection efficiency decreases linearly with increasing DPP for the Farmer chamber, SemiFlex chamber and Roos chamber (all PTW, Freiburg). (X10FFF: DPP = 1.73 mGy, X6FFF: 1.08 mGy, X6: 0.4 mGy and X10: 0.39 mGy).

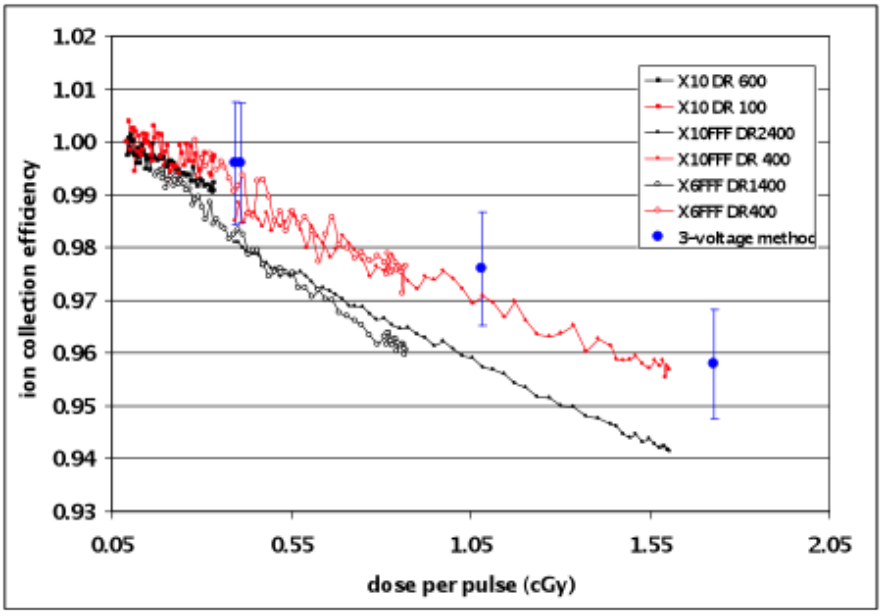

FIGURE 4.3: Relative ion-collection efficiency of the microLion chamber (PTW, Freiburg) for the four beams at the minimum and maximum PRF decreases with increasing DPP. The results obtained using the modified two-voltage method (absolute collection efficiencies) agree well with the relative measurements (compared with the advanced Markus chamber, PTW). The collection efficiency was dependent upon the DPP and the time between two pulses dt. The collection time of the microLion chamber was 5.3 ms.

TABLE 4.3: Ion-collection efficiencies of the five air-vented ionization chambers (PTW, Freiburg) at the depth of maximum dose, field size 40 x 40 cm^2 and SSD = 90 cm. The two standard deviations are given in parentheses.

Chamber	X6 (DPP = 0.4 mGy)	X10 (DPP = 0.4 mGy)	X6FFF (DPP = 1.1 mGy)	X10FFF (DPP = 1.7 mGy)
Semiflex	0.995 (0.003)	0.995 (0.001)	0.991 (0.001)	0.988 (0.001)
Pinpoint	0.991 (0.001)	0.999 (0.001)	0.990 (0.002)	0.990 (0.003)
Farmer	0.997 (0.001)	0.997 (0.002)	0.992 (0.001)	0.989 (0.002)
AdvMarkus	0.999 (0.001)	0.999 (0.001)	0.998 (0.001)	0.994 (0.002)
Roos	0.997 (0.001)	0.996 (0.001)	0.992 (0.001)	0.986 (0.002)

The collection efficiency corrections for 6 and 10 MV beams did not significantly differ. Figure 4.2 illustrates the relationship between ion-collection efficiency and DPP; the collection of charge became less efficient with increasing DPP (table 4.1 shows the DPP for all four beams). Extrapolating the linear fit of the data to zero shows the initial recombination of all chambers below 0.2 % ($2u_f$ = 0.1 %), except for the PinPoint chamber that generated an initial recombination of 0.87 % ($2u_f$ = 0.2 %).

4.3.2 Ion-collection efficiency for liquid-filled chambers

The coefficient c that describes the relationship between produced charge and applied voltage equation 4.5 was determined to be 0.001123 V^{-1} (u = 3.30 x 10^{-5}5 V^{-1}). Figure 4.3 shows the relationship between DPP and collection efficiency for both methods. The collection efficiency was seen to decrease with increasing DPP and PRF. Both methods show comparable results. The collection efficiency for flattened beams was above 0.99. With increasing DPP, the collection efficiency decreases to approximately 0.96 for the X10FFF at a low PRF and 0.94 at a high PRF (both DPP = 1.7 mGy).

4.4 Discussion

4.4.1 Ion-collection efficiency for air-vented chambers

Our results confirm that air-vented chambers can be used for relative dosimetry of FFF beams without correction for collection efficiency. When applied for the reference dosimetry, a collection efficiency of 0.991 (for X10FFF) and 0.998 (for X6) was found for the Farmer chamber at the reference geometry (SSD = 100 cm, depth = 10 cm, field size 10 x 10 cm^2).

For the PinPoint chamber, a low ion-collection coefficient for all four beams was found

as well as a very high initial-recombination factor. Agostinelli et al [72] reported for the PinPoint chamber (PTW 31014) that the saturation curve was not linear above 150 V. Therefore, the two-voltage method leads to an underestimation of the collection efficiency by approximately 0.5 % (for an applied voltage of 400 V). The design of the two PinPoint chambers PTW 31 014 and PTW 31 016 is very similar. It is therefore likely that the PTW 31 016 chamber operated at 400 V was also within the nonlinear region and the collection efficiency using the two-voltage method was underestimated.

Results obtained for the collection efficiency of the Roos and Farmer chamber are in a good agreement with those published by Bruggmoser et al [65]. Their calculated collection efficiency of 0.985 % in pulsed electron beams (for a DPP of 1.7 mGy) corresponds with our measurement of the X10FFF beam. The collection efficiency for doses per pulse of 1.1, 0.41 and 0.39 mGy were determined to be 0.990, 0.996 and 0.9965, respectively. Similarly, we found 0.992 % (X6FFF, DPP = 1.1 mGy), 0.996 % (X6, DPP = 0.4 mGy) and 0.9965 % (X10, DPP = 0.4 mGy)). Using the Farmer chamber, Bruggmoser et al [65] published slightly lower collection efficiencies (0.981 at DPP = 1.7 mGy, 0.989 at DPP = 1.1 mGy and 0.9955 at 0.41 mGy). However, a different polarizing voltage was applied (300 V rather than 400 V).

4.4.2 Ion-collection efficiency for liquid-filled chambers

The microLion chamber had an ion-collection efficiency of 0.94 when exposed to the X10FFF beam at the maximum dose rate. An ion-collection efficiency correction should therefore be applied for both reference and relative dosimetry. Lowering of the dose rate increased the ion-collection efficiency because the time between pulses became long enough for the pulses to be fully collected. Measuring the depth-dose curves of a 10 x 10 cm^2 field (X10FFF, DR 24 Gy min^{-1}), the collection efficiency varied from 0.941 at the depth of maximum dose to 0.977 at 30 cm depth. Normalizing the beam to the dose maximum, as is a common practice, leads to an overestimation of dose in the tail region of the depth-dose curve. This discrepancy increased with depth.

Most liquid-filled ionization chambers described in the literature have a larger active volume [73, 74] or use a different liquid [75] than the microLion chamber. A similar chamber design was evaluated by [71]. For a 6 MV beam with dose rate of 1 Gy min^{-1} and DPP of 0.36 mGy, a collection efficiency of 0.995 was determined. This is in agreement with our result (0.996 (u = 0.005)). Wickman et al [76] reported a collection

efficiency of 0.9945 for pulsed radiation at a PRF of 100 Hz, which reduced to 0.992 when the PRF was increased to 200 Hz. In our study, a similar reduction was observed when the PRF was increased to 330 Hz.

4.5 Conclusion

Five commonly used air-vented ionization chambers were investigated to determine their collection efficiency in the high dose rate and high DPP FFF photon beams. For all chambers, the collection efficiency was above 0.986 and can therefore be used reliably for relative dosimetry. The Markus chamber demonstrated the largest ion-collection efficiency (0.994 at DPP = 1.7 mGy, X10FFF beam). The order of correction for reference dosimetry is given within the manuscript.

Additionally, the performance of the iso-octane-filled microLion chamber was tested. The ion-collection efficiency for flattened beams was above 0.99 for both investigated beams at all dose rates. However, we observed a relatively low collection efficiency of 0.960 for the X10FFF beam at a dose rate of 5.32 Gy min^{-1}. Increasing the dose rate to 31.9 Gy min^{-1} further decreased the collection efficiency to 0.940. It is therefore not advisable to use this chamber for FFF depth-dose curve measurements.

Chapter 5

Effect of high dose per pulse flattening filter-free beams on cancer cell survival [1]

5.1 Introduction

The question to what extent treatment delivery time or dose rate impact tumour cell survival has a long history in radiation therapy. While there is increasing evidence in the recent literature that extended delivery time might impact cancer cell survival, there is a paucity of studies investigating the potential effect of modified dose rate on cancer cells [77–81].

New technologies have revolutionized radiation oncology within the last decade. Applying the treatment dose to the patients using innovative techniques such as intensity-modulated radiation therapy (IMRT) or volumetric-modulated arc therapy (VMAT), dose conformity to the tumour is increased while sparing of healthy tissue is optimized. This advantage is achieved through radiation fields which are highly spatially and temporally regulated by modifying dose rate as well as beam shape. Furthermore, technical achievements within recent years (VMAT, flattening filter-free beam = FFF) allow us to deliver significantly faster radiation treatment to the patient compared with standard

[1] This chapter has been published as a manuscript [30]: I. Lohse, S. Lang, J. Hrbacek, S. Scheidegger, S. Bodis, N. S. Macedo, J. Feng, U. M. Lütolf, and K. Zaugg, "Effect of high dose per pulse flattening filter-free beams on cancer cell survival," Radiotherapy and Oncology, vol. 101, no. 1, pp. 226-232, 2011.

radiation techniques. Based on recent literature, there is increasing evidence that modulation of delivery time and/or dose rate can effect tumour cell survival. The clinical significance of this observation, as well as the underlying molecular mechanisms, remains unclear.

Data from Shibamoto et al. suggested that beam interruptions greater than 8min, and treatment delivery times exceeding 20 min, require dose escalation to compensate for greater sublethal damage repair [82]. Using a theoretical approach and in vitro studies, Keall et al. demonstrated that extended treatment time is a dominant factor which influences cell survival [83]. Furthermore, Moiseenko et al. showed an increased clonogenic survival for a 5 min IMRT head-and-neck treatment compared to a 1 min acute radiation delivery [84]; data which are supported by the findings of Mu et al. [85]. Using dosimetric studies, Murphy et al. theoretically demonstrated that different tumour locations within an IMRT plan experience highly differentiated dose-rate histories [86]. Bewes et al. found a significant trend to increased survival as the average dose rate was decreased, while keeping the total dose constant. In addition, their in vitro studies showed that extended delivery times can substantially increase cell survival [87]. These preliminary data suggest that modulating delivery time, and to a lesser extent, dose rate when treating cancer patients with ionizing radiation might have a profound impact on tumour cell survival. Due to recent technical improvements in radiation therapy, (e.g. IMRT, VMAT, flattening filter-free (FFF) technology etc.), there is an urgent need to further elucidate the biological response of modulating dose rate or delivery time on tumour cells and to better understand the molecular mechanism underlying the spatiotemporal modulation of ionizing radiation, and specifically, its clinical significance.

On March 16 2009, the TrueBeam STx linear accelerator (Varian Medical Systems, Palo Alto, CA, USA) was released for clinical use at the University Hospital of Zurich, Switzerland. This new generation of linear accelerators enables us to apply a wide spectrum of clinically relevant treatment regimens, including those with an extremely high dose rate (from stereotactic single high dose to classic fractionated treatment regimens). Using the so-called FFF technique allows the radiation dose to be delivered up to four times faster than with current modalities. While this is of clinical advantage (shorter treatment time significantly correlates with higher precision of radiation fields due to reduction of organ movement or patient's displacement), no radiobiological studies have established whether such a high dose-rate translates into a differential stress response and cell survival pattern in tumour versus normal cells.

As previously published by our group and others, FFF beams show a lower mean energy, an increased dose per pulse (instantaneous dose rate), a lower pulse repetition frequency, as well as a different beam profile compared to a beam of the same average dose with the flattening-filter in place [24, 42]. Undertaking in vitro experiments at the same linear accelerator using two beams with the same average dose rate but with and without flattening filter allows us, for the first time, the possibility to maintain treatment conditions as identical as possible. The goal of this study is to investigate if this difference in beam characteristic, especially the increase in dose per pulse, translates into a different radiobiological response in tumour cells. In addition, we examine the effect of changing the dose rate from 400 to 2400 cGy/min on cancer cell survival while keeping the dose per pulse constant.

5.2 Material and methods

5.2.1 Cell culture

The human glioblastoma cell lines T98G (expressing mutated p53), and U87-MG (expressing functional p53) were purchased from the American Type Culture Collection (ATCC). The cells were maintained in monolayer culture in Dulbecco's Modified Eagle Medium (DMEM) supplemented with 10% FBS, 1% L-Glutamine and 1% Penicillin/Streptomycin. All cells were grown in a humidified atmosphere of 5% CO_2 at 37 °C.

5.2.2 Irradiation

Using the TrueBeam STx linear accelerator (Varian Medical Systems, Palo Alto, CA, USA) a pulsed photon beam of the nominal energy of 10 MV was generated with flattening filter (X10) and compared to the beam of the same nominal energy without flattening filter (X10FFF). Each beam can be produced at different dose rates (DR), which are achieved by modifying the pulse repetition frequency (PRF). The change of DR does not influence the dose per pulse (DPP). Table 5.1 summarizes the quality index (QI), which is an indicator for mean energy, DPP, and PRF for beams and DR used in our experiments.

Table 5.1: Beam characteristics

energy	QI	DPP (cGy/pulse)	DR (cGy/min)	PRF (Hz)	time to deliver 5 Gy (s)
X10 FFF	0.691	0.13	2400	360	12.5
X10 FFF	0.691	0.13	400	60	75
X10	0.735	0.028	600	360	50
X10	0.735	0.028	400	240	75
X10	0.735	0.028	20	12	1500

Irradiation of samples was performed at source-to-surface distance of 100 cm, field size 10x10 cm^2 and at the depth of maximum dose. The samples were placed on 5 cm of water equivalent RW3 plates (PTW). The build-up for every beam was provided by RW3 plates of appropriate thickness placed on top of the samples. In the reference conditions, 100 monitor units (MU) corresponded to 100 cGy, hence dose per pulse expressed in the units of MU/pulse or cGy/pulse was the same.

In our study we investigated the effect of four different combinations of DPP and PRF on cancer cell survival: X10 20 cGy/min, X10 400 cGy/min, X10FFF 400 cGy/min, and X10FFF 2400 cGy/min. As the control experiment, X10FFF was compared to X10 in the conditions of identical DPP, PRF, and dose. To achieve the same DPP for X10 and X10FFF beam, additional layer of attenuation material ensuring 4-fold DPP reduction was introduced in the experimental setup for X10FFF beam (in total 30.5 cm of RW3 plates). To irradiate with the same PRF, a DR of 400 MU/min and 1600 MU/min was used for X10 and X10FFF beam, respectively. To deliver the same dose the number of MUs was increased by a factor of four.

To deliver a homogenous dose to all samples, we used Petri dishes of 3cm diameter. Three samples were irradiated at the same time when treating with the flattened beams and only one sample when treated with the flattening filter free beams due to the differences in dose profiles. An analysis of the dose beam profiles of corresponding beams shows that the dose rate within the samples did not vary more than ± 2 %.

5.2.3 Dose verification

For both energies, verification of the applied dose was performed using gafchromic film (EBT2, ISP), placed above and under the Petri dishes, performed in duplicates on four different days. In a third separate experiment, film was placed within the dishes on top of the medium. Films were scanned using Epson 10,000XL Scanner and an individual

five-step calibration in solid water was done to convert density to dose.
Measurements of absolute dose in the equivalent depths of water (2.2 cm for X10, 2.1 and 30.5 cm for X10FFF) were performed using a pinpoint chamber (results not shown). The output of the linear accelerator was checked prior to each experiment using the LinaCheck device (PTW, Freiburg).

5.2.4 Clonogenic assay

Exponentially growing cells were plated into 3 cm Petri dishes. Cells were exposed to 5 or 10 Gy of irradiation. Following irradiation, cells were incubated for 10-14 days at 37 °C in a humidified atmosphere of 5% CO_2 for colony formation. Colonies were fixed with methanol, stained with 1% crystal violet and counted. Colony plating efficiency was calculated as previously described [88].

5.2.5 Statistical analysis

All data are presented as means ± standard deviation (SD). The data was analysed using the statistical programme SPSS version 16.0 (SPSS Inc., Chicago, IL). Differences among the groups were compared by one-way analysis in combination with post hoc Scheffe test. Two-tailed values of $p < 0.05$ were considered significant.

5.2.6 Bio-mathematical model

For fitting the experimental data, the Γ-LQ-model [89] was used. The kinetic model consists of a part describing killing of tumour cells (tumour cell number N = N(t)) and a part to include cellular repair mechanisms by a dose equivalent Γ = Γ(t). The equations describing the model are the following:

$$\begin{aligned} \frac{d\Gamma}{dt} &= R - \gamma\Gamma^2 \\ \frac{dN}{dt} &= (\alpha - 2\beta\Gamma)RN \end{aligned} \tag{5.1}$$

Here, R = R(t) is the dose rate, which can be an arbitrary function of time. In the following, two different dose rate functions are used: a constant dose rate (20, 400 and 2400 cGy/min) and a pulsed dose rate function according to the beam characteristics in table 5.1. The coefficient γ describes the effectiveness of repair, with units of Gy^{-1} min^{-1}. For including cellular repair, a second order kinetic is assumed. In figure 5.1 the time dependent course of $\Gamma(t)$ is illustrated for pulsed dose application: $\Gamma(t)$ is accumulated during a pulse and is faded away for $\gamma \neq 0$ Gy^{-1} min^{-1} between two pulses due to the repair of sublethal entities. The value $\gamma = 0$ Gy^{-1} min^{-1} leads to the classical LQ-formalism. It has been demonstrated previously [89], that the use of a dose rate dependent value of γ is in good agreement to the LPL-model of Curtis [90] when using second order repair kinetics. The parameters α and β are coefficients for radio-sensitivity.

Equation 5.1 have been implemented in a computer programme and were solved numerically by the Runge-Kutta integration.

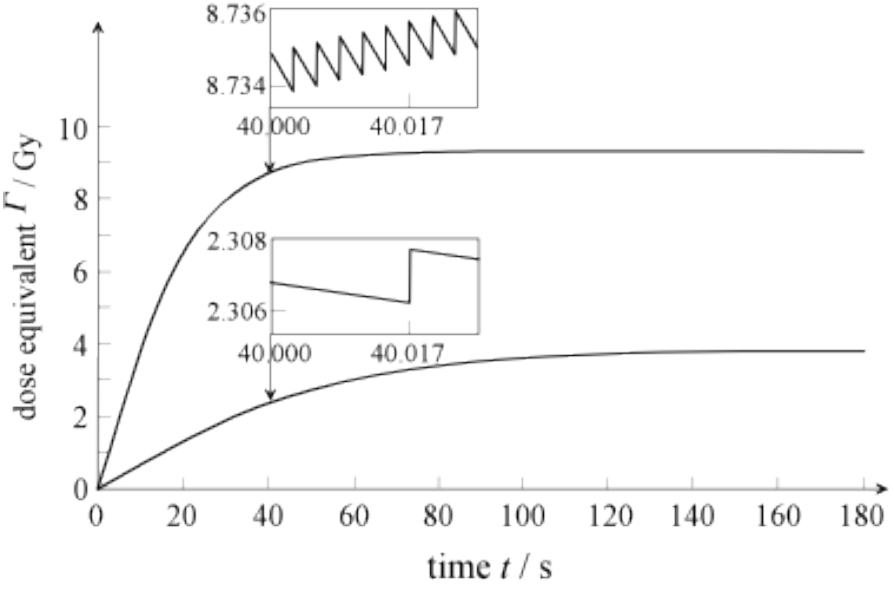

FIGURE 5.1: Time dependent course of the dose equivalent $\Gamma(t)$ for pulsed dose application, according beam characteristics. Upper curve: R = 2400 cGy/min, PRF = 360 Hz. Lower curve: R = 400 cGy/min, PRF = 60 Hz.

5.3 Results

5.3.1 Increased treatment time increases tumour cell survival

For our study we used flattened as well as FFF beams generated by the TrueBeam STx linear accelerator. Since these two beams differ in their beam profile, we first performed experiments to verify the accuracy of dose application to our in vitro model system as well as the standard deviations within treatments. Two established glioblastoma cell lines, T98G and U87-MG, were irradiated with either 5 or 10 Gy at 10 MV using different dose rates: 20, 400, or 2400 cGy/min. Due to technical limitations of the TrueBeam STx linear accelerator, irradiation using dose rates of 20 and 400 cGy/ min was performed using the flattened X10 beam, while the dose rate of 2400 cGy/min was applied using the flattening filter-free X10FFF beam. The first two dose rates (20 and 400 cGy/min) differ in PRF with constant DPP, while 400 and 2400 cGy/min differ in DPP as well as PRF. For all three treatments, delivery time and mean dose are altered (figure 5.2 A). Gafchromic films were placed underneath the samples to verify the applied dose. The X10 FFF beam delivered 4.92 Gy (±0.11 Gy)/9.79 Gy (±0.16 Gy) and X10 beam 4.92 Gy (±0.12 Gy)/9.82 Gy (±0.17 Gy). Gafchromic films inside the PetriDishes measured a dose of 4.82 Gy (X10FFF) and 4.86 Gy (X10). Day to day variation of the output of the linear accelerator was within 1% for both energies. The analysis of the clonogenic assays revealed that cells irradiated with a dose of 5 Gy showed a reduction in clonogenic survival in a dose rate-dependent fashion, but the reduction of cell survival was only statistically significant in cells irradiated with 2400 cGy/min if compared to cells irradiated with 400 cGy/min (figure 5.2 B). In contrast, clonogenic survival was markedly reduced upon irradiation with a total dose of 10 Gy and increasing dose rates (figure 5.2 C) in both cell lines (*$p \leq 0.05$; **$p \leq 0.001$).

These data show that increasing dose rates and decreasing delivery time lead to a reduction of clonogenic survival in T98G and U87-MG and that this effect is more pronounced when treating the cells with the higher dose of 10 Gy compared to 5 Gy and using the FFF technique. This observation might be due to an overload of the DNA damage repair machinery due to the higher dose and number of pulses per minute or to other so far unknown molecular mechanisms triggered by high radiation doses. During this

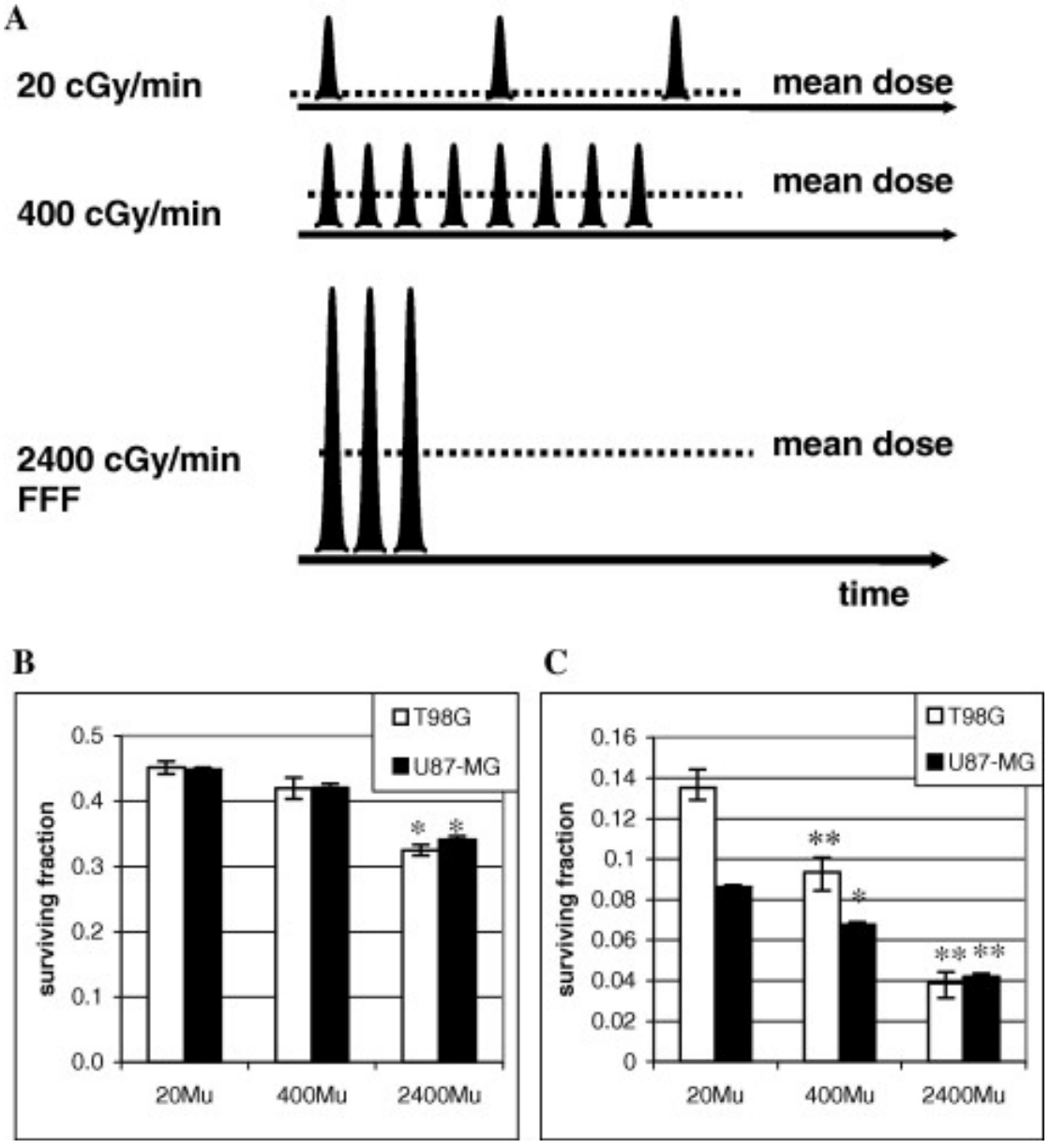

FIGURE 5.2: IR efficacy is increased with increasing dose rates. (A) Beam characteristics of the treatment as indicated. (B, C) T98G (empty bars) and U87-MG (filled bars) cells were irradiated with (B) 5 Gy (C) 10 Gy with dose rates of 20, 400 and 2400 cGy/min. Clonogenic survival was accessed as a measure for irradiation efficiency. Experiments were done in triplicates and repeated at least four times. $^{*}p \leqslant 0.05$; $^{**}p \leqslant 0.001$

experiment, we changed delivery time as well as dose per pulse at the same time, therefore we performed two additional experiments where we changed PRF or DPP separately.

5.3.2 The use of the flattening filter-free beam more efficiently decreases tumour cell survival

Recent publications state that delivery time is one of the most prominent factors influencing cancer cell survival during radiation therapy [77,82,83]. Until recently, technical challenges made it difficult to perform experiments to distinguish whether an effect on cancer cell survival was caused by delivery time or dose per pulse.
In order to examine if the above observation on cancer cell survival is caused by the different beam profile of the flattened versus FFF beam, we modified in our next experiment DPP as well as PRF while keeping the mean dose as well as the delivery time the same (figure 5.3 A). This experiment was performed at a DR of 400 cGy/min since it is the only dose rate available for both beams. Again, T98G and U87-MG cells were irradiated with either X10 or X10 FFF with 5 or 10 Gy using a dose rate of 400 cGy/min.

Colony formation assays revealed reduced survival rates after irradiation with the X10FFF beam compared to the cells irradiated with the X10 beam (figure 5.3 B and C), which was statistically significant when treating with 10 Gy. The reduction in cell survival after irradiation with 10 Gy, although still significant, was lower in the U87-MG cells.
This result prompted us to investigate whether this phenomenon is dose dependent, meaning the higher the single dose, the more pronounced the cancer cell survival diverges within the two beams. We irradiated U87-MG cells using either X10 or X10FFF with 400 cGy/min (figure 5.3 D). Interestingly, the data revealed that when escalating the single dose while keeping the mean dose and delivery time identical between the two beams, irradiation with the X10FFF beam showed a statistically significant reduction of clonogenic survival compared to the treatment with the X10 beam at a dose of 10 Gy and above and this effect was more distinct the higher the single dose. While we do not see any difference in cell killing at a dose level of 5 Gy, which is a commonly used dose in clinical palliative treatment schedules, we see a striking difference in our in vitro model comparing X10 and X10FFF using high single doses as frequently used in stereotactic

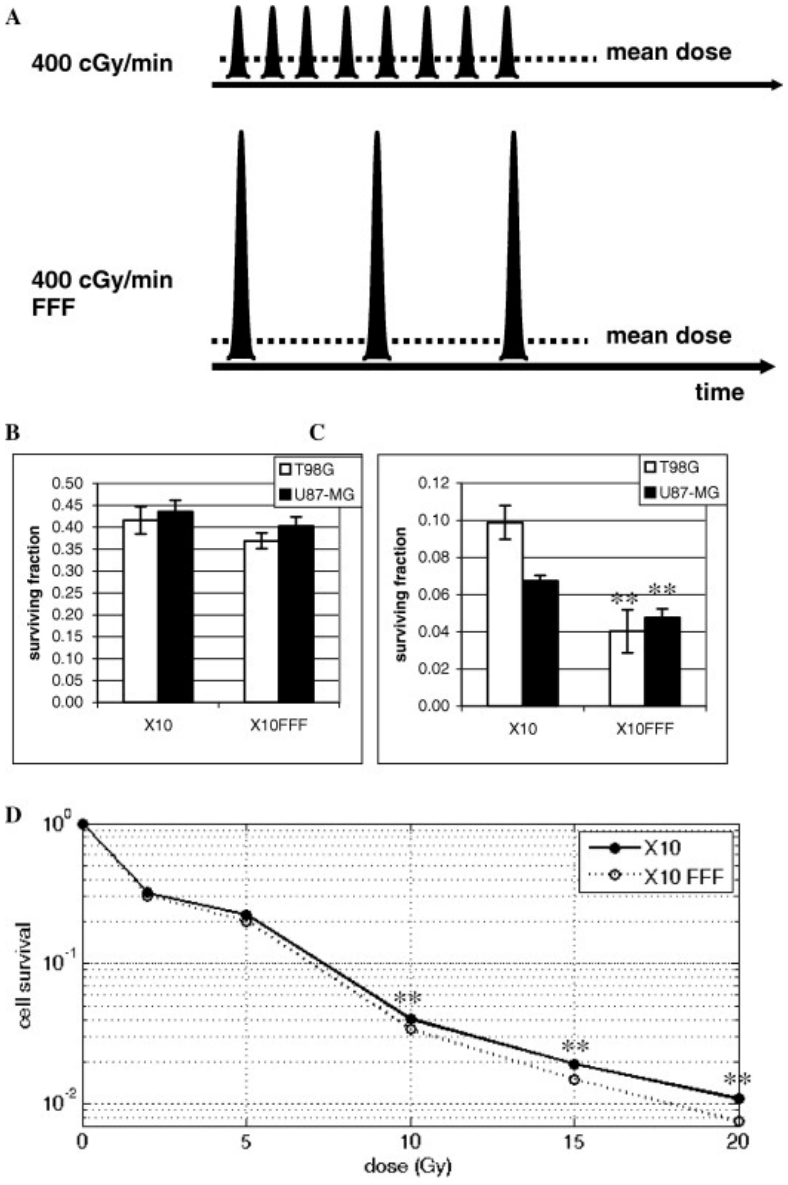

FIGURE 5.3: Flattening filter-induced reduction in cell death after irradiation. (A) Treatment schedule with same mean dose and delivery time, but changes in PRF and DPP. (B, C) T98G (empty bars) and U87-MG (filled bars) cells were irradiated with (B) 5 Gy or (C) 10 Gy with a dose rates of 400 cGy/min with either the X10 or the X10FFF beam and survival measured by colony survival assay. Experiments were done in triplicates and repeated seven times. (D) Dose-response curve of U87-MG cells irradiated with either the X10 (full circles) or X10FFF (empty circles) beam. Clonogenic survival was accessed as a measure for irradiation efficiency. $^*p \leqslant 0.05$; $^{**}p \leqslant 0.001$

treatment regimens such as 10, 15 and 20 Gy.

5.3.3 Increased dose per pulse reduces clonogenic survival

As previously described, removal of the flattening filter leads to a decrease of the mean energy of the FFF beam [42]. The flattening filter contributes to a partial absorption of low energy photons irradiation and therefore to a hardening of the beam. Consequently, removing the flattening filter leads to a reduction in the mean energy. The effective energy of the X10 FFF is approximately comparable to a flattened 8 MV beam. The data described may therefore be an effect of the different beam characteristics of FFF and flattened beam. To test this hypothesis, we irradiated T98G (figure 5.4 B) and U87-MG (figure 5.4 C) cells with 5 and 10 Gy using the X10 and the X10FFF beams in a setup where we reduced the dose per pulse of the X10FFF beam to the level of the X10 beam using additional attenuation material (see Material and methods) and the dose was delivered with the same number of pulses per minute (figure 5.4 A). As shown in figure 5.4 B and C, we did not find any statistical significance between these two treatment schedules. Cells irradiated with the X10FFF beam in the dose-reduction setup showed the same clonogenic survival as cells irradiated with the X10 beam.

5.3.4 Influence of PRF on cancer cell survival

This raises the question whether treating the cell lines using the same DPP but different PRF influences colony cell formation. We therefore treated the two cell lines with the X10 FFF beam either with 400 or 2400 cGy/min (figure 5.4 D). There was only a slight statistical significance when treating the U87-MG cells with 5 Gy using 400 cGy/min compared to 2400 cGy/min, but no significance in the T98G cells treated with 5 or 10 Gy nor in the U87-MG cells treated with 10 Gy (figure 5.4 E and F). These data suggest that changing PRF does not seem to impact cancer cell survival in radiation therapy.

5.3.5 Comparison with the Γ-LQ model

For both cell lines, T98G and U87-MG, the Γ-LQ model in principle is able to fit the clonogenic survival at 5 and 10 Gy. For the T98G cell line, the following parameters are

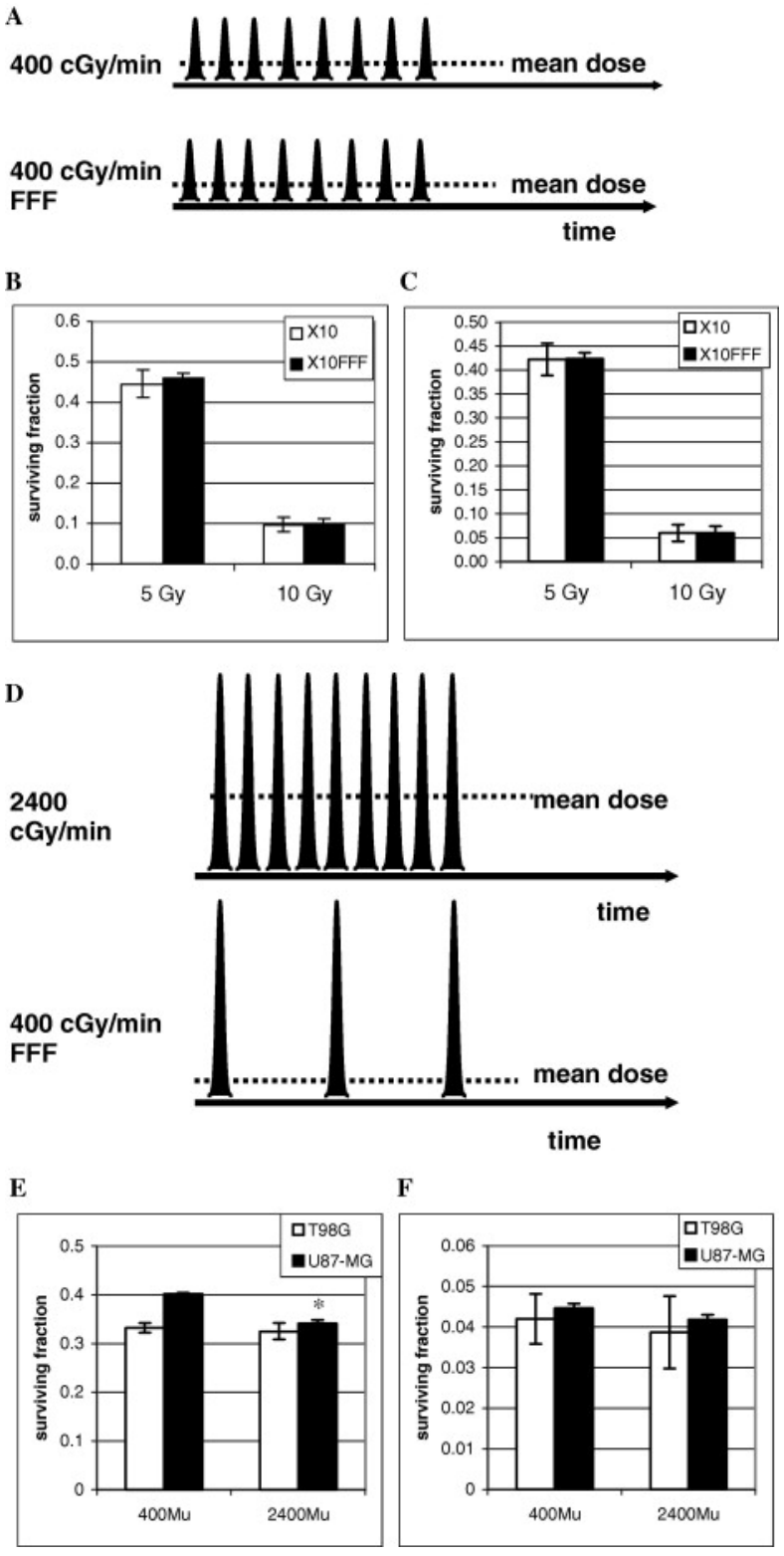

FIGURE 5.4: Flattening filter-induced reduction in cell death depends on the dose per pulse, but not on dose rates. (A) Beam characteristics used in experiment B and C. (B, C) T98G(A) and U87-MG (B) cells were irradiated with 5 and 10 Gy with either the X10 (empty bars) or the X10FFF beam including reduced dose per pulse (filled bars). Clonogenic survival was accessed as a measure for irradiation efficiency. (D) Beam characteristics used in experiment E and F. (E, F) T98G (empty bars) and U87-MG (filled bars) cells were irradiated with (E) 5 Gy or (F) 10 Gy with dose rates of 400 and 2400 cGy/min using the FFF beam. Clonogenic survival was accessed as a measure for irradiation efficiency. $^*p \leqslant 0.05$

used for fitting (figure 5.5): $\alpha = 0.03$ Gy^{-1}, $\beta = 0.04$ Gy^{-2}) and $\gamma = 0.556$ min^{-1} for a constant dose rate R = 2400 cGy/min and $\gamma = 0.361$ min^{-1} for R = 400 cGy/min. For a constant dose rate R = 20 cGy/min, γ has to be adapted to a value of 0.0313 min^{-1}. The use of a pulsed delivery according to the beam characteristics in table 5.1 leads to the same clonogenic survival. In contrast to the experimental findings in figures 5.3 and 5.4, the computer simulation reveals no difference in the cell survival curve between the two different pulse patterns at 400 cGy/min. A similar behaviour can be observed for the U87-MG cell line (with $\alpha = 0.018$ Gy^{-1}, $\beta = 0.04$ Gy^{-2}). At a dose rate of 2400 cGy/min, a good fit is reached with $\gamma = 0.486$ min^{-1} for both, constant dose rate and pulsed dose application. If the dose rate is reduced to 400 cGy/min by adapting the PRF to 60 Hz or by the continuous dose rate, γ has to be adapted to 0.208 min^{-1}.

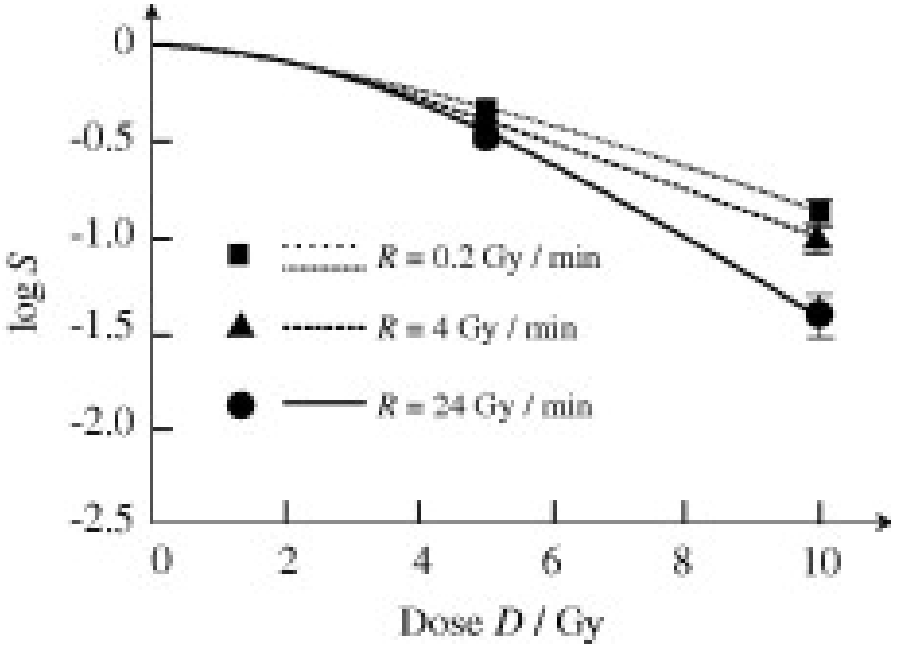

FIGURE 5.5: Surviving fraction of T98G-glioblastoma cells at different dose rates. For 24Gy/min, the Γ-LQ-model can fit the experimental data with α=0.03Gy^{-1}, $\beta = 0.04$ Gy^{-2} and $\gamma = 0.556$ min^{-1}; for 4 Gy/min, γ has to be adapted to 0.361 min^{-1} and for R = 0.2 Gy/min, a good fit can only be achieved by adapting the kinetic constant to $\gamma = 0.0313$ min^{-1}.

5.4 Discussion

The results presented here show that clonogenic survival is statistically reduced if the total dose is delivered with a higher dose per pulse. Indeed, cells irradiated using either the X10 or X10FFF beam show a difference in clonogenic survival which can be

explained by the higher dose per pulse delivered by the X10FFF.

Radiation-induced double-strand breaks (DSB) are the most harmful lesions that arise after irradiation because of their impact on genome stability and cell survival [91]. The delivery of higher doses per pulse might reduce cell survival by an increase in DNA damage induction, especially an increase in DSB [92,93]. Recent publications suggest that a higher dose per pulse might lead to so far unknown changes in proteins and fatty acids, as well as organelles which have been found to play an important role in the induction of cell death induced by irradiation [94–96]. Investigating the role of the unfolded protein response in the endoplasmic reticulum or cytoplasm might therefore give further insights on the potential mechanism of action of high doses per pulse. Of special interest is how normal tissue as well as in vivo tumour models are impacted by modulating the dose per pulse to further elucidate the clinical relevance of the observation described in this paper. In addition it would be of interest how dose per pulse differs depending on the molecular background of the normal as well as the tumour tissue and if it plays a role in low-dose ionizing radiation [97–100].

In contrast to the experimental observations, the Γ-LQ model reveals no difference for both, cell lines between pulsed and continuous dose application. This is an indication, that the use of second order kinetics is a simplistic approximation for a limited range of dose rate. There are possibly different repair mechanisms at different time scales leading to a dose rate and PRF dependent cell killing. Especially very fast repair processes or components of the repair system (typically with kinetic constants above 103 min^{-1}) could be responsible for the sensitivity of the cellular system to the pulse pattern, as demonstrated in figures 5.3 and 5.4. Pulsed beam characteristics should be included in bio-mathematical models. Therefore, the use of kinetic models such as the Γ-LQ model is recommended to include the correct time dependent course of dose delivery.

More data is needed to better understand the effect of modified dose rates on tumour as well as on normal tissue, and to develop refined bio-mathematical models for clonogenic cell survival.

Chapter 6

Dosimetric comparison of flattened and unflattened beams for stereotactic ablative radiotherapy of stage I non-small cell lung cancer[1]

6.1 Introduction

Stereotactic body radiotherapy (SBRT) has become a standard for treatment of inoperable early stage non-small cell lung cancer (NSCLC) [101]. This is based on numerous phase I/II clinical studies demonstrating high local control rates and good tolerability for this novel treatment strategy. Less obvious is the question, which of the several available SBRT techniques is most advantageous. Key parameters to evaluate SBRT planning and delivery are conformity of dose distribution, organ sparing and treatment time. The latter is of great importance, since prolonged treatment sessions have been associated with intrafractional shifts in patient and tumor positioning [102, 103]. Substantially shortened SBRT delivery with at the same time improved conformity has been

[1]This chapter has been accepted for publication in *Medical physics* [31]: J. Hrbacek, S. Lang, S. Graydon, S. Klöck and O. Riesterer, "Comparison of flattened and unflattened beams for stereotactic ablative radiotherapy of stage I non-small cell lung cancer." (The exact citation is not yet known.)

demonstrated for RapidArc SBRT (Varian Medical Systems, Palo Alto, USA) in comparison to conventional static field SBRT [104,105]. RapidArc is a volumetric modulated arc technique (VMAT) that allows for fast planning and treatment delivery [106].

More recently, linear accelerators with flattening filter free (FFF) beams were introduced into clinical operation. FFF beams are characterized by high dose rates and their combination with advanced delivery techniques such as VMAT allows further improvement of treatment delivery efficiency. FFF beams are most frequently utilized for treatments where higher fraction doses need to be delivered, including hypofractionated SBRT of stage I-II non-small cell lung cancer (NSCLC), metastases of lung and liver, and other abdominal tumors [42, 107–112].

In parallel to the planning studies, there is also the first data appearing on acute toxicities experienced by patients treated with FFF beams. There is an acceptable degree of early toxicities, not significantly different from treatment with conventional beams, reported for treatment in thorax and liver [70] or SBRT of lung malignancies [113]. This evidence is supported by radiobiological studies [30, 114–116] that report comparable cell survival between conventional and high dose rate FFF beams for various cell lines.

Though most studies focus primarily on the enhancement in delivery efficiency, changes in the dosimetric outcome attributed to FFF beams remain an interesting topic. In comparison to conventional beams of the same nominal energy, FFF beams exhibit non-uniform profile, lower mean energy, reduced head scatter and leakage, less energy variation in lateral direction, and differences in penumbra. In addition, there is an interplay effect between a beam's dose rate, fraction dose, and machine parameters such as speed of MLC leaf motion and gantry rotation, in case FFF beams are combined with advanced techniques, such as IMRT or VMAT. For these reasons, beam comparison is not a trivial task and may depend on an interaction of machine/beam characteristic and various site specific parameters, such as size and location of treatment target, presence of inhomogeneities, organ motion, etc.

Here we present a planning comparison of VMAT versus FFF VMAT SBRT for treatment of early stage lung cancer. We performed the comparison in rigorous fashion to assess exclusively the contribution coming from the interchange of treatment beam.

6.2 Material and Methods

In total 11 patients with stage I (T1-T2 N0 M0) non small cell lung cancer were enrolled into the study prospectively as they were registered for treatment in our clinic. There is relatively wide variation in volume and location of PTV across the group of patients, however, a rigid stratification of patients is not ensured. Motion encompassing tumour volumes (internal target volume, ITV) and normal tissues were contoured on 4-dimensional computed tomography images and the ITV was expanded by 5 mm to create a planning target volume (PTV). The PTV size ranged from 10.1 cm^3 to 144.5 cm^3 (median of 34 cm^3).

For each case, three VMAT plans were prepared utilizing a 6 MV flattened photon beam (X6FF) and two non-flattened beams of nominal energy 6 MV and 10 MV (X6FFF, X10FFF) for a TrueBeam STx linear accelerator (Varian Medical Systems).

VMAT is delivered in two coplanar 360° arcs with 90° angular separation of the collimator. An avoidance sector was used to spare the contralateral lung. Using the beams eye view, the avoidance sector was defined, when the PTV passes entirely behind the contralateral lung. Treatment plans were generated using Eclipse treatment planning system (Varian Medical Systems) using the Progressive Resolution Optimizer and Analytical Anisotropic Algorithm (PRO & AAA, version 8.9, Varian Medical Systems). For each beam the maximum available dose rate was used, i.e. 600 MU/min, 1400 MU/min, and 2400 MU/min for X6FF, X6FFF, and X10FFF, respectively. Basic characteristics of the beams and the accuracy of their modeling using the AAA under physics conditions have been described in [42]. Optimization constraints were set to produce dose distributions that meet the criteria of the RTOG-0915 protocol [117]. Optimization started from the common setting, however, the constraints were progressively enhanced for each plan individually. The radiation schedule used for plan comparison in all patients was 50 Gy in 5 fractions. According to the RTOG protocol at least 95 % of the PTV should obtain the prescription dose and 99 % receive at least 90 % of the prescription dose (45 Gy). Target inhomogenity was partially controlled by setting a weak constraint on the maximum dose to the PTV, however, the priority was to generate a steep dose gradient outside of the PTV. The dose fall-off was controlled by a supporting margin structure, a 20 mm thick envelope around PTV with a 3 mm separation from PTV. A single constraint limiting the maximum dose to the structure was applied. The maximum dose to the margin structure was gradually reduced during the optimization until the point it

would affect the PTV coverage.

Further, organ specific dose constraints have been defined: spinal cord <30.0 Gy, oesophagus <32.5 Gy, heart <35 Gy, lung V_{20Gy} <10 %, lung $V_{12.5Gy}$ <15 %, and contralateral lung V_{5Gy} <25 %.

For each patient, plans utilizing X6FF, X6FFF and X10FFF beams were prepared. The dose calculation grid of AAA was 2.5 mm. Plans were normalised to the maximum dose within a PTV. The relative reference isodose (%RX) that ensures sufficient PTV coverage was determined. The following parameters were used to quantify the resultant dose distributions:

- number of monitor units (MU)
- mean dose rate (DR)
- minimum, mean, and maximum dose to ITV
- relative reference isodose (%RX)
- dose to healthy tissue (D_{HT} = body - PTV)
- conformity indexex ($CI_{100\%}$, $CI_{80\%}$, $CI_{60\%}$, $CI_{50\%}$): ratio of the volume enclosed by the 50Gy, 40Gy, 30Gy, and 25Gy isodose and V_{PTV}, respectively
- ratio of the volume enclosed by 25 Gy isodose and V_{PTV} (V_{25Gy}/ V_{PTV})
- maximum dose at any point 2 cm or further away from the PTV (D_{2cm})
- gradient measure (GM): mean distance between the 50 Gy and the 25 Gy isodose
- V_{20Gy} and $V_{12.5Gy}$ for both lungs
- V_{5Gy} for the contralateral lung
- Dose[2] to spinal cord, oesophagus, brachial plexus, heart, great vessels, trachea, large bronchus, and rib

Values of the investigated parameters obtained for X6FFF and X10FFF plans were related to the corresponding X6FF plans. The ratios are denoted as X6FFF/X6FF

[2]For OARs, maximum dose to an organ (Dmax) and also dose received by 1% of organ's volume ($D_{1\%}$) have been determined in order to obtain a more robust estimate of the highest doses within an OAR.

and X10FFF/X6FF. The Kolmogorov-Smirnov test was used to check if the parameters are normally distributed. This hypothesis was rejected for all parameter sets; therefore the non-parametric two-sided paired Wilcoxon signed-rank test was applied to compare parameters obtained for FFF beams with the ones of the flattened beam.
All plans were subject to the routine pre-treatment verification process using the Delta^4 unit (Scandidos, Uppsala, Sweden). Reference dose distribution for the pre-treatment verification was calculated with a 1.2 mm grid. Gamma agreement Scores (GS) for a dose difference of 3% and a distance to agreement of 2 mm were determined. In order to check the dose distribution calculation in more clinically relevant conditions, i.e. in the presence of low density tissue, selected plans were also subject to a verification using absolutely calibrated gafchromic films (EBT2, ISP, Wayne, USA) in a thorax phantom (CIRS, Norfolk, USA).

6.3 Results

All plans have a qualitatively comparable outcome. There are only minor differences observed in achieved dose distributions and corresponding dose volume histograms when comparing the three plans (X6FF, X6FFF, and X10FFF) related to the same patient (figure 6.1).

In 9 out of 11 patients, all criteria specified by the RTOG protocol were met. In 2 patients, the rib dose was exceeded due to these being part of, or adjacent to, the PTV. Obtained dose distributions are conformal ($CI_{100\%}$ <1.17) and exhibit steep dose fall-off outside of the PTV (mean GM of 11.74 mm). A summary of dosimetric analysis averaged over the group of plans utilizing the same beam is provided in table 6.2.
RX% ranged between 70 % and 80 %, having the largest spread for X10FFF plans. The maximum difference in the inhomogeneity among the three plans corresponding to one patient (X6, X6FFF, and X10FFF) was between 0.5 % and 6.5 %. It was not observed that the inhomogeneity within a target would be influenced by the beam selection in a systematic fashion. Similarly, ITV coverage does not change significantly with the beam selection. The point of maximum dose appears within ITV for all plans, despite the fact it was not controlled by any constraint. The ratio of monitor units for FFF versus FF plans in our study ranges from 0.95 to 1.21 and from 0.93 to 1.25 for X6FFF/X6FF

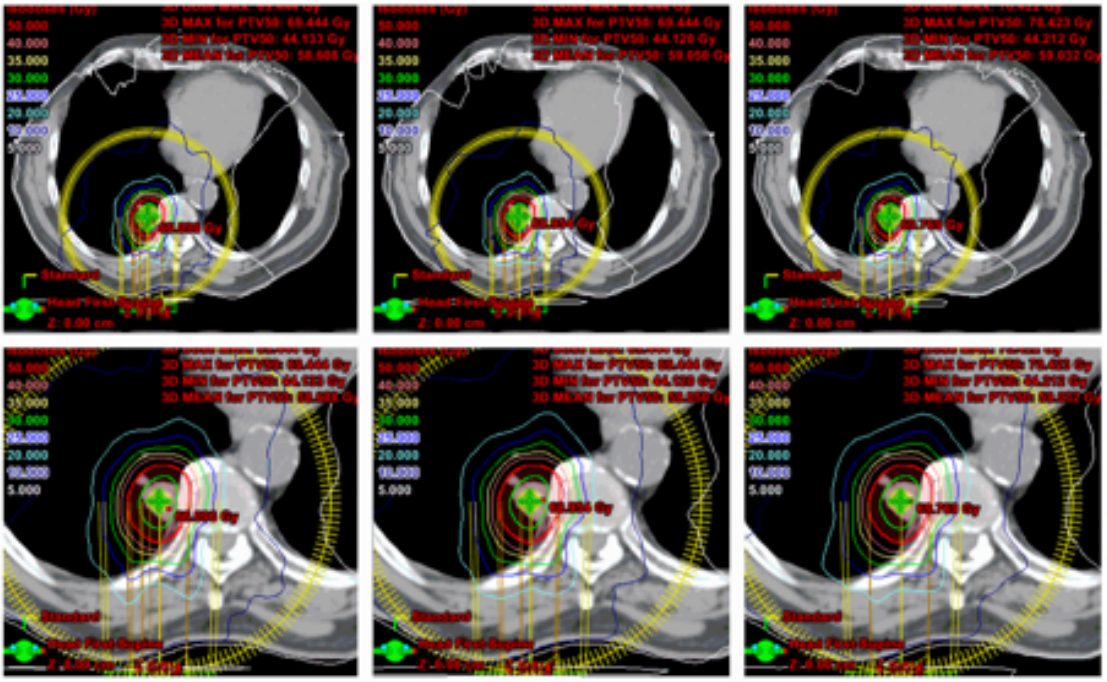

FIGURE 6.1: Comparison of dose distribution for X6FFF (left), X6FF (middle), X10FFF (right) plan in one transverse slice (upper row) and detail of high dose region (lower row).

and X10FFF/X6FF comparisons, respectively. The ratio systematically increases with increasing size of the PTV (up to +25 % for 150 cm^3 PTV). Yet the D_{HT} does not follow this trend (figure 6.2).

Comparison of cumulative dose volume histograms for a patient's body shows that X6FFF plans exhibit improved conformity and reduce the volume of tissue that receives more than 50% of the prescription dose. Parameters related to dose gradient show statistically significant improvement (table 6.1, figure 6.3). $CI_{50\%}$, $CI_{60\%}$, $CI_{80\%}$, and $CI_{100\%}$ are on average reduced by 4.6 % ($p < 0.001$), 4.6 % ($p = 0.002$), 3.1 % ($p = 0.002$), and 1.2 % ($p = 0.039$), respectively. Gradient measure is on average reduced by 4.2 % ($p < 0.001$). Due to dose reduction in the surrounding lung tissue, the V_{20Gy} and $V_{12.5Gy}$ are reduced by 5.5 % ($p = 0.002$) and 4.5 % ($p < 0.001$). These dosimetric improvements in the fall-off were not observed for the X10FFF plans. Differences in sparing of normal tissues were not found to be statistically significant for either of the two FFF beams.

Delivery of X6FFF and X10FFF plans exhibits reduced treatment time. Whereas mean beam-on time was 111 s ± 11 s) for X10FFF, 128 s ± 19 s for X6FFF, and X6FF plans require on average 269 s ± 71 s. While the mean dose rate was 1555 ± 264 MU/min,

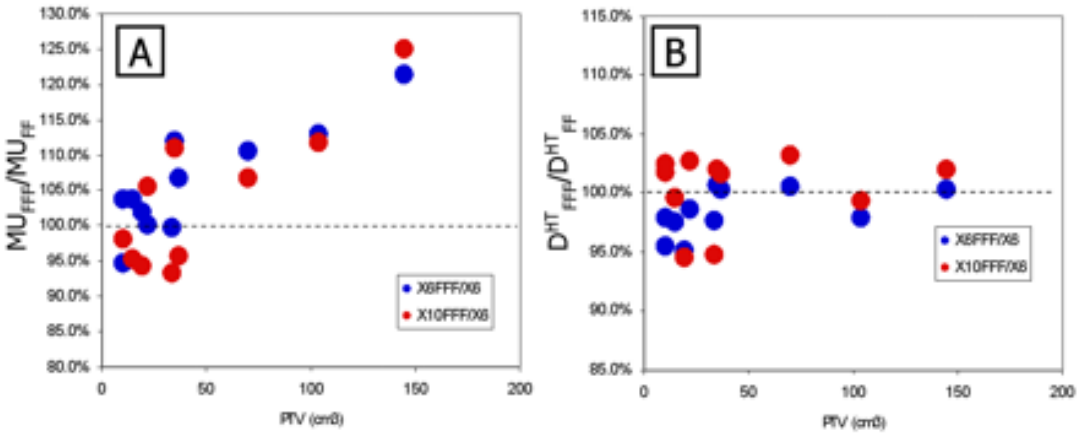

FIGURE 6.2: Comparison of a) number of MU and b) dose to healthy tissue for X6FFF/X6FF and X10FFF/X6FF. The X6FF beam represents the reference.

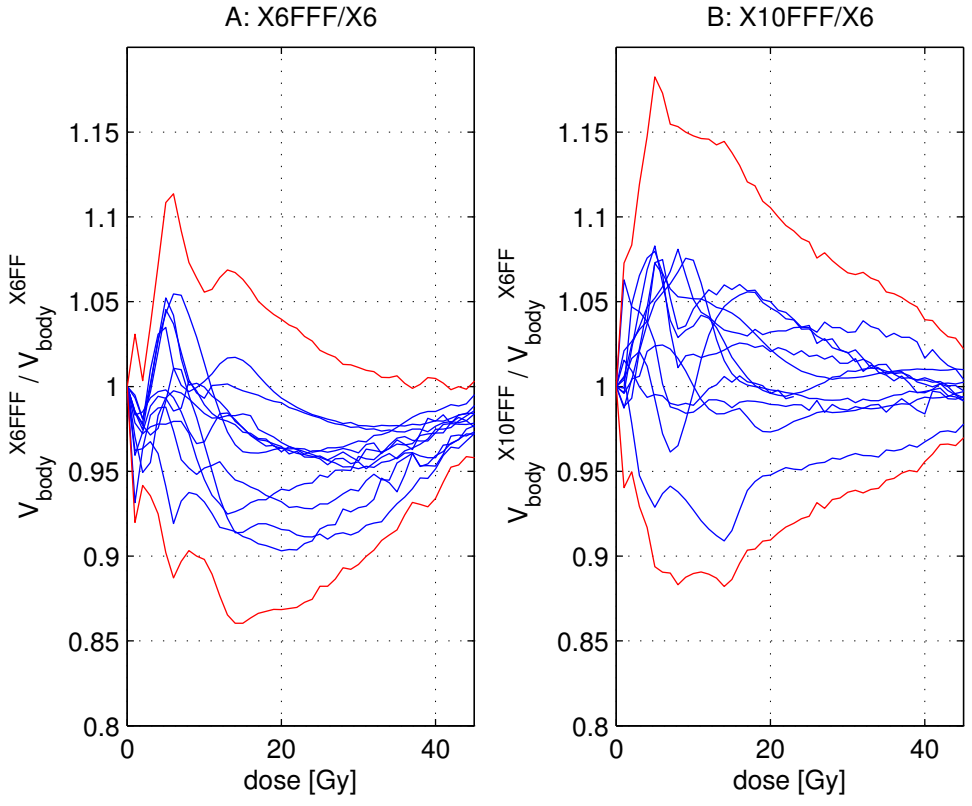

FIGURE 6.3: Comparison of the cumulative dose volume histrograms for the body structure of 11 patients for X6FFF/X6FF (A) and X10FFF/X6FF (B). Comparison of volume receiving less than 10 Gy is not displayed due to limited calculation accuracy of TPS in this region. Red lines correspond to ±3 SD.

TABLE 6.1: Overview of statistically significant dosimetric parameters for the plan comparison between the three energies (mean ± 2SD [min - max]

Parameter		mean ratio	p
$CI_{50\%}$	X6FFF/X6FF	0.954 ± 0.050 [0.914 - 0.994]	<0.001
lung $V_{12.5Gy}$	X6FFF/X6FF	0.955 ± 0.039 [0.920 - 0.986]	<0.001
$CI_{60\%}$	X6FFF/X6FF	0.954 ± 0.040 [0.920 - 0.977]	0.002
$CI_{80\%}$	X6FFF/X6FF	0.969 ± 0.027 [0.950 - 0.989]	0.002
lung V_{20Gy}	X6FFF/X6FF	0.945 ± 0-051 [0.917 - 1.000]	0.002
GM	X6FFF/X6FF	0.958 ± 0.036 [0.930 - 0.983]	0.004
MU	X6FFF/X6FF	1.061 ± 0.151 [0.946 - 1.214]	0.024
D_{2cm}	X6FFF/X6FF	0.980 ± 0.041 [0.947 - 1.008]	0.024
$CI_{100\%}$	X6FFF/X6FF	0.988 ± 0.023 [0.971 - 1.010]	0.039

1368 ± 63 MU/min, for X10FFF and X6FFF, plans using the conventional X6FF were delivered with the constant maximum dose rate of 600 MU/min.

Verification of all plans showed acceptable and comparable results for all plans in homogeneous as well as heterogeneous phantoms. Mean GS (3 %, 2mm) using the Delta^4 phantom were 98.9 % (2SD = 3.2 %), 99.2 % (2SD = 2.3 %), and 99.2 % (2SD = 2.3 %) for X6FFF, X6FF and X10FFF modalities respectively. Verification using a thorax phantom showed GS >98 % in all cases.

6.4 Discussion

To our knowledge, the first reported study on utilizing FFF beams for NSCLC comes from Vassiliev et al [42]. This study was carried out with a FFF prototype obtained by modifying a Clinac 21EX. The dose calculation used was a pencil beam algorithm with Batho power law inhomogeneity correction. The authors reported that the utilization of a FFF beam yields a comparable dose distribution and reduces treatment time. However, due to the rather experimental setup and limited accuracy of the used algorithm, this early study can be understood as a proof of principle rather than a clinically relevant comparison. Ong et al [107] performed a study with 10 stage I NSCLC patients. Clinical plans were delivered with a 6 MV beam from a Novalis TX with HDMLC (Varian Medical Systems, Palo Alto, USA). Re-planning utilised a 10 MV FFF beam from a TrueBeam accelerator with Millenium MLC (Varian Medical Systems, Palo Alto, USA), hence combining different machines as well as MLCs with different leaf thickness. Apart from increased number of monitor units and decreased treatment time, there was not a significant difference observed between the obtained dose distributions. The 6 MV FFF

beam was not utilized arguing by increased skin dose. Navaria et al [108] compared clinical outcomes for 10 MV FFF VMAT and 6 MV FF 3D-CRT for stage I NSCLC patients. This study demonstrated reduced dose to the ipsilateral lung and follow up data (median of 16 months) showed comparable radiological response.

In addition to the studies above, we extend the comparison by the X6FFF beam, use a single treatment technique, and keep other machine parameters, which are not associated directly with treatment beam, unchanged. This paper extends our previous work that focused mainly on the efficiency of treatment delivery [109].

Results of this study suggest that the X6FFF beam has the potential advantage of generating more conformal dose distributions than the ones achieved with X6FF and X10FFF beams. Due to the stochastic character of the optimization, there can be large local differences in dose to healthy tissue adjacent to the PTV. However, dose deposited outside this volume has a smooth character and is determined by beam penumbra and scattered dose. Our previous measurements of beam penumbra and dose outside a field [28], showed that X6FFF has a slightly sharper penumbra than X6FF or X10FFF at shallow depths and for small fields, presumably due to the shorter range of less energetic secondary particles. At the same time, X6FFF is more prone to scattering due to lower mean energy and therefore its penumbra may exceed that of X6FF or X10FFF, if depth and field size are sufficiently large. From this perspective, we assume that X6FFF plans benefit from the combination of utilizing the least energetic beam and the shallow water equivalent depths encountered for NSCLC patient group due to the presence of lung tissue. In agreement with Ong et al [107], other than reduction of delivery time, we did not observe any statistically significant change of the evaluated dosimetric parameters of X10FFF plans in comparison with X6FF plans.

Early studies showed a reduction of monitor units when using FFF beams. Vassiliev et al [118] reported an average reduction of monitor units by a factor 2.0 for a 6 MV prostate IMRT on a Clinac 21 EX (Varian Medical Systems) FFF prototype. Similarly, Stathakis et al [119] reported an example of a 6 MV IMRT on a Clinac 23 EX (Varian Medical Systems) for lung and prostate, where monitor units for FFF plans were reduced by a factor 2.6. This effect originated from a different approach to the calibration of beams. In these studies, the removal of the flattening filter was not followed by a re-calibration, therefore the dose contribution of 1 MU increased proportionally with the increase of beam output.

TABLE 6.2: Results of the dosimetric analysis of the treatment plans with the three different beams used (X6FFF, X6FF and X10FFF): mean ± 2SD and obtained minimal and maximal value

	X6FFF	X6FF	X10FFF
MU	2781 ± 546 [2334 - 3210]	2638 ± 723 [2086 - 3146]	2696 ± 470 [2314 - 2949]
Mean DR [MU/min]	1368 ± 63 [1312 - 1400]	600 ± 0	1555 ± 264 [1370 - 1745]
%RX	74% ± 5% [72% - 75%]	74% ± 5% [71% - 78%]	75% ± 7% [70% - 80%]
ITV mean dose [Gy]	62.2 ± 3.5 [59.6 - 65.6]	62.5 ± 3.9 [60.4 - 66.5]	62.3 ± 3.5 [59.5 - 64.9]
ITV max dose [Gy]	67.6 ± 3.9 [65.4 - 70.0]	67.6 ± 4.4 [64.4 - 70.4]	67.2 ± 5.1 [62.5 - 70.4]
ITV min dose [Gy]	55.8 ± 4.7 [52.6 - 60.4]	55.9 ± 5.8 [51.6 - 61.6]	56.7 ± 6.8 [51.1 - 62.9]
D_{HT} [Gy]	1.5 ± 2.2 [0.3 - 3.9]	1.5 ± 2.1 [0.3 - 3.9]	1.5 ± 2.2 [0.3 - 4.0]
$CI_{100\%}$	1.03 ± 0.10 [0.99 - 1.15]	1.04 ± 0.09 [1.00 - 1.15]	1.04 ± 0.11 [0.99 - 1.17]
$CI_{80\%}$	1.60 ± 0.22 [1.45 - 1.74]	1.66 ± 0.25 [1.48 - 1.82]	1.65 ± 0.25 [1.49 - 1.85]
$CI_{60\%}$	2.76 ± 0.56 [2.33 - 3.06]	2.89 ± 0.69 [2.39 - 3.30]	2.90 ± 0.68 [2.41 - 3.29]
$CI_{50\%}$	3.95 ± 0.95 [3.20 - 4.57]	4.15 ± 1.20 [3.22 - 5.00]	4.17 ± 1.17 [3.22 - 4.84]
GM [mm]	11.6 ± 6.4 [8.4 - 16.8]	12.1 ± 6.6 [8.8 - 17.4]	12.1 ± 6.2 [9.1 - 17.2]
D_{2cm} [Gy]	20.8 ± 6.7 [17 - 26.8]	21.2 ± 6.9 [17.2 - 26.6]	21.3 ± 6.2 [18 - 26.2]
Lung $V_{20.0Gy}$ [cm^3]	3.5 ± 4.8 [1.0 - 8.3]	3.7 ± 5.2 [1.0 - 8.8]	3.7 ± 5 [1.0 - 8.8]
Lung $V_{12.5Gy}$ [cm^3]	6.9 ± 7.9 [2.1 - 14.4]	7.2 ± 8.2 [2.1 - 14.8]	7.2 ± 8 [2.3 - 14.7]
Contralateral lung V_{5Gy} [cm^3]	2.8 ± 7.1 [0.0 - 11.2]	2.6 ± 6.6 [0.0 - 9.8]	3.4 ± 8.8 [0.0 - 13.7]
Spinal cord [Gy]	13.6 ± 9.3 [4.7 - 21.8]	13.3 ± 9.8 [4.8 - 21.9]	14.4 ± 9.2 [5.3 - 22.0]
Oesophagus [Gy]	9.6 ± 8.7 [2.4 - 16.0]	9.7 ± 9.4 [2.5 - 17.4]	9.8 ± 8.9 [2.4 - 16.9]
Heart/pericardum [Gy]	7.2 ± 6.8 [0.3 - 10.9]	7.1 ± 6.8 [0.3 - 11.0]	7.8 ± 7.2 [0.3 - 11.0]
Great vessels [Gy]	15.1 ± 17.0 [7.2 - 30.9]	15.2 ± 17.8 [7.7 - 31.5]	15.4 ± 17.6 [7.2 - 31.8]
Trachea/large bronchus [Gy]	12.9 ± 19.4 [1.5 - 25.1]	13.2 ± 20.3 [1.4 - 26.1]	13.4 ± 20.5 [1.3 - 25.5]
Ribs [Gy]	47.8 ± 28.8 [28.9 - 60.0]	48.2 ± 27.9 [29.6 - 59.1]	49.1 ± 29.1 [30.1 - 62.0]

TrueBeam requires individual calibration of each bundle. Our beams are calibrated to deliver 1 cGy/MU to the reference point under the reference conditions (SSD 90 cm, depth 10 cm, field size 10x10 cm^2), therefore the inequality in the MU "strength" is eliminated (at least in respect to the dose delivered to the reference point) and the number of MU for all plans is comparable. The increase of MU for FFF plans for larger PTVs is associated with the conical profile of FFF beams. With increasing field size, dose needs to be deposited at larger distances from the beam's central axis where FFF fields deliver less dose per MU than FF fields and this effect needs to be compensated by increasing the number of MU.

Our previous measurements showed that FFF beams increase dose to skin by up to 10 % depending on energy, depth, and field size [28]. Increased surface dose of FFF beams, in accordance with our findings, was reported in [120], with author's stating that the increase in the surface dose is unlikely to be clinically significant. Our current clinical results support this statement as we do not observe a higher degree of skin reaction in patients treated with the X6FFF beam.

It should be noted that treatment planning systems in general are known to perform with limited accuracy in the low dose region. Howell et al [121] demonstrate approximately 30 % dose underestimation for one specific plan at the distance of 3 cm from the edge of a treatment field using one of the preceding versions of AAA. This corresponds with the analysis of our commissioning data where we observe up to 20 % in local dose in the tails of measured and TPS modeled profiles (measured up to 5 cm beyond a field's edge). The differences vary with energy, field size, and depth of measurement. For these reasons, regions receiving less than 10 Gy (20 % of the prescription dose) was removed from our comparison.

An assessment of changes in peripheral doses is not trivial and is typically determined experimentally or by Monte Carlo simulation. While in the proximity of a treatment field edge, peripheral dose is mainly determined by scattered photons, at larger distances, it depends primarily on radiation leakage of an accelerator's head. Kragl et al [122] reported a 23% and a 31% reduction in peripheral dose when the flattening filter is removed for 6 MV and 10 MV lung SBRT plans, respectively. However, a substantial clinical benefit from reduction of low dose exposure by use of FFF beams in terms of less radiation induced secondary cancers is unlikely in the case of lung cancer.

Results of the pre-treatment verification are comparable for both flattened and unflattened beams, and in agreement with previously published results [123].

The reduction of treatment delivery time remains the most obvious benefit of FFF beams. In this study, the maximum dose rate of 1400 MU/min of the X6FFF beam appears to be sufficient for the delivery of 10 Gy/fx distributed over two 360-degree arcs. The optimizer does not make use of the additional dose rate range available for the X10FFF beam (up to 2400 MU/min). The mean dose rate of X10FFF plans is only 14 % higher than the one of X6FFF plans and the average delivery time gets shorter on average by 17 seconds. The situation could be potentially different for higher fraction dose or in case the speed of gantry rotation would increase. Another option could be utilizing partial arcs, hence delivering the same fraction dose over a shorter arc length. However, such plans could potentially be more prone to motion interplay effects. It was demonstrated [124, 125] that increasing of arc length (using a double-arc instead of a single-arc) improves the robustness of a plan to intrafractional motion.

Generally, high dose rate beams need to be utilized with a caution when applied for the treatment of moving targets. The ability of FFF beams to deliver treatment more efficiently in the end means that substantial dose can be delivered to a wrong place in a short time, if motion management is not carried out properly. It was demonstrated that even short duration intrafractional shifts can cause significant dosimetric deviations during vertebral SBRT [126]. On the other hand, faster treatment time may be an important contribution in an attempt to reduce tumor position uncertainty related to intrafractional motion [109] and may allow for relatively easy implementation of treatment during a few consecutive breath holds [127].

6.5 Conclusion

The use of FFF beams for stereotactic radiation therapy of NSCLC patients yields dose distributions qualitatively comparable to flattened beams and significantly reduces treatment delivery time. Utilizing the X6FFF beam improves conformity of dose distribution. On the other hand, X10FFF beam offers a slight improvement in treatment efficiency, and lower skin and peripheral dose. All effects are relatively small.

Chapter 7

The use of photon beams of a flattening filter-free linear accelerator for hypofractionated volumetric modulated arc therapy in localized prostate cancer[1]

7.1 Introduction

The possibility of a low α/β-ratio for prostate cancer provides a radiobiological advantage for hypofractionated radiotherapy (RT) with excellent local control and low toxicity [128]. Intensity modulated RT (IMRT) and volumetric-modulated arc therapy (VMAT) are used to reduce doses to bladder and rectum while maintaining optimized dose coverage and conformity of the planning target volume (PTV) [129]. Compared with three-dimensional conformal RT (3D-CRT), these highly conformal treatments require more monitor units (MU) and increased treatment time. There is also increased leakage and scatter dose from the linear accelerator (LINAC) multileaf collimator (MLC)

[1]This chapter has been published as a manuscript [32]: D. R. Zwahlen, S. Lang, J. Hrbacek, C. Glanzmann, S. Kloeck, Y. Najafi, T. Streller, G. Studer, K. Zaugg, and U. M. Luetolf, "The use of photon beams of a flattening filter-free linear accelerator for hypofractionated volumetric modulated arc therapy in localized prostate cancer," International Journal of Radiation Oncology* Biology* Physics, vol. 83, no. 5, pp. 1655-1660, 2012.

outside the treatment volume resulting in a higher whole-body dose [130]. Increasing head shielding and removing the flattening filter reduces head leakage and scatter. In particular, removal of the flattening filter reduces number of photon interactions within the gantry and increases dose delivery efficiency [20].

TrueBeam STx (Varian Medical Systems, Paolo Alto, CA) is a new platform of LINAC designed to deliver flattened, as well as flattening filter-free (FFF), beams [28]. Historically, the flattening filter provided a relatively flat beam profile over the entire treatment field and dose distributions were calculated in a simplified way. With beam intensity-modulated techniques, including IMRT and VMAT, the MLC is used to modify the fluence distribution producing optimal fluence maps for FFF beams similar to those with a flattening filter [20, 23]. Interest in FFF technology is resulting from the expectation that it will allow faster treatment delivery with dose rates up to 24 Gy/min [26]. Several studies summarized the properties of FFF beams of various LINACs based on Monte Carlo simulations or dosimetric measurements [23,24,28,57,119,131]. Few studies however have investigated the feasibility of using FFF beams for IMRT treatment planning [42,118,119,131]. The studies were performed for prototype LINAC and treatment planning systems with preclinical release and showed comparable IMRT dosimetric plan quality for FFF compared with flattened beams.

This is the first treatment planning study investigating hypo-fractionated VMAT with 6 MV and 10 MV FFF photon beams in a clinically released setting for patients with localized prostate cancer.

7.2 Materials and methods

7.2.1 Patient selection and contouring

This planning study included the computed tomographies of 7 patients with localized prostate cancer. After ethics approval, men were treated in the CHHiP trial (Conventional or Hypofractionated High Dose Intensity Modulated Radiotherapy for Prostate Cancer, The Institute of Cancer Research, Sutton, Surrey, UK) at the University Hospital Zurich. Patients were randomized between conventional radiation therapy (74 Gy in 37 fractions) and the experimental groups of 60 Gy in 20 fractions and 57 Gy in 19 fractions (treating 5 days per week) [132]. All patients were treated with RapidArc plans

TABLE 7.1: Volumes for planning target volumes, organs at risk, and dose constraints,

Volume (ccm)	Mean (± 1 SD)	Range	Dose constraints
PTV 1	202.5 (± 29.0)	149.0 - 238.2	V99% ≥ 76% of PD, mean (PTV1-PTV2) ≥ 80% of PD
PTV 2	136.1 (± 31.5)	101.3 - 198.3	V99% ≥ 91% of PD, mean (PTV1-PTV2) ≥ 96% of PD
PTV 3	75.3 (± 16.1)	56.3 - 104.1	V99% ≥ 95% of PD, V99% ¡ 105% of PD
Rectum	129.9 (± 31.3)	134.7 - 334.0	V68% ≤ 60%, V81% ≤ 50%, V95% ≤ 15%, V100% ≤ 3%
Bladder	253.6 (± 68.8)	107.9 - 198.9	V68% ≤ 50%, V81% ≤ 25%, V100% ≤ 5%
Urethral bulb			V68% ≤ 50%, V81% ≤ 10%
Femoral heads			V68% ≤ 50%
Bowel			V68% ≤ 17 ml

Abbreviations: ccm = cubic centimeter; PD = prescribed dose; PTV = planning target volume.

and 6MV flattened beams in 2010.

Contouring of target volumes and organs at risk (OAR) was performed using the CHHiP protocol, version 8 [132]. Gross tumour volume (GTV) included the prostate only, whilst the clinical target volume (CTV) 1 included the prostate and base of seminal vesicles proximal 2 cm) with 5-mm margin or prostate and seminal vesicles with 5-mm margin for patients with risk of seminal vesicle involvement. CTV 2 encompassed the prostate only with a 5-mm margin, whilst CTV 3 included the prostate only. For all CTV's, 5-mm margins were used to generate PTV's 1-3, with PTV's 2 and 3 having a 0-mm, there was 0-mm margin posteriorly or posterior inferiorly. OARs outlined included bladder, rectum, bowel, femoral heads, urethral bulb, and skin. All generated PTV and OAR volumes are summarized in table 7.1.

7.2.2 Photon beams

Treatment planning was performed using four photon beams of TrueBeam STx LINAC. Beams with nominal energies of 6 MV and 10 MV with flattening filter in the beam path (X6 and X10) and FFF beams (X6FFF, X10FFF) were investigated. A detailed description of these beam characteristics is reported elsewhere [31]. The removal of the flattening filter had several implications on the beam properties including a non-flat beam profile, an increase in maximal dose rate of up to 14 Gy/min for X6FFF and 24 Gy/min for X10FFF as well as a decrease in mean radial energy (TPR20/10: X6 0.667, X6FFF 0.631, X10 0.738, X10FFF 0.692) because there was no beam hardening. As a measure of beam energy, the beam quality index TPR20/10 (ratio of the tissue phantom ratio at 20 cm and 10 cm) was used.

7.2.3 Treatment planning

The prescribed dose in all cases was 19 x 3 = 57 Gy. Four VMAT plans (RapidArc) were calculated for each patient using the Eclipse External Beam Planning System (PRO 8.9, AAA 8.9, Varian Medical Systems). The plans were normalized such that PTV3 received a mean dose of 100% of the prescribed dose. Dose constraints were specified in the CHHiP trial protocol [132] and are reported in table 7.1. One 360 ° arc (n = 3) was used to fullfil the constraints with maximum dose rate of 600 MU/min for flattened beams and 1,200 MU/min for unflattened beams. A second arc (n = 4) was added in case constraints could not be met. For single arc plans, the collimator angle was 45°, whereas for the two arcs plans, the collimator angle was 90°. Objectives for OAR were interactively lowered during optimization for X6 beams without compromising target coverage. After achieving a satisfactory set of constraints, plans for all four energies were optimized using these constraints. The final dose calculation was performed with Eclipse AAA 8.9 algorithm and a calculation grid size of 2.5 mm.

7.2.4 Plan evaluation and statistical methods

Plan evaluation was performed according to the CHHiP trial protocol [132]. MU, mean body dose, surface dose (cumulative dose in the first 2 mm of the body), mean doses to rectum and bladder, conformity index (volume enclosed by the prescription isodose/target volume) of PTV 1, ratio of volume receiving 50% of dose to PTV 1, and treatment time were recorded.

Plans using X6FFF, X10FFF, and X10 beams were compared with the X6 base plan and ratios of acquired dosimetric parameters recorded. Statistical analysis was performed with MATLAB, version 7.6, software (MathWorks, Natick, MA). Mean values and standard deviation of the mean (SD) were collected. Relative dosimetric changes were compared applying the nonparametric Wilcoxon signed-rank test. A two-sided p value 0.05 was considered statistically significant. Confidence intervals (CI) included 95% of the measured data. Box-whisker plots were created for selected data, showing ratios of X6FFF, X10FFF, and X10 beams to X6 beam.

TABLE 7.2: MU, dose parameters, and beam-on time (mean ±1 SD)

	X6	X6FFF	X10	X10FFF
Number of MUs	897 (± 202)	951 (± 141)	718 (± 88)	896 (± 133)
Mean body dose (Gy)	8.52 (± 2.40)	8.83 (± 2.46)	8.06 (± 2.36)	8.27 (± 2.32)
Mean dose to rectum (Gy)	55.6 (± 3.6)	55.7 (± 3.2)	57.0 (± 3.8)	55.6 (± 4.11)
Mean dose to bladder (Gy)	36.2 (± 7.7)	36.7 (± 8.0)	36.0 (± 8.3)	35.5 (± 8.0)
Conformity PTV 1	1.38 (± 0.11)	1.39 (± 0.12)	1.38 (± 0.12)	1.38 (± 0.13)
Inhomogeneity PTV 3	7.1 (± 0.99)	7.9 (± 0.85)	6.9 (± 0.78)	7.6 (± 1.51)
Beam-on time (min)*	1 min, 47 sec	1 min, 34 sec	1 min, 43 sec	1 min, 34 sec

Abbreviations: FFF = flattening filter-free; MU = monitor units; PTV = planning target volume
Includes patients treated with one and two arcs, mean values are calculated for all patients.

7.3 Results

7.3.1 Dose distribution and PTV coverage

For all treatment plans, there were only minor differences in dose distributions using X6FFF, X10FFF, X10, and X6 beams. No difference was detected between the four beam qualities with respect to PTV coverage and conformity (figure 7.1). Target inhomogeneity was increased by 1% for X6FFF and X10FFF beams compared with flattened beams (figure 7.2), and below the expected specification of 10% (table 7.2).

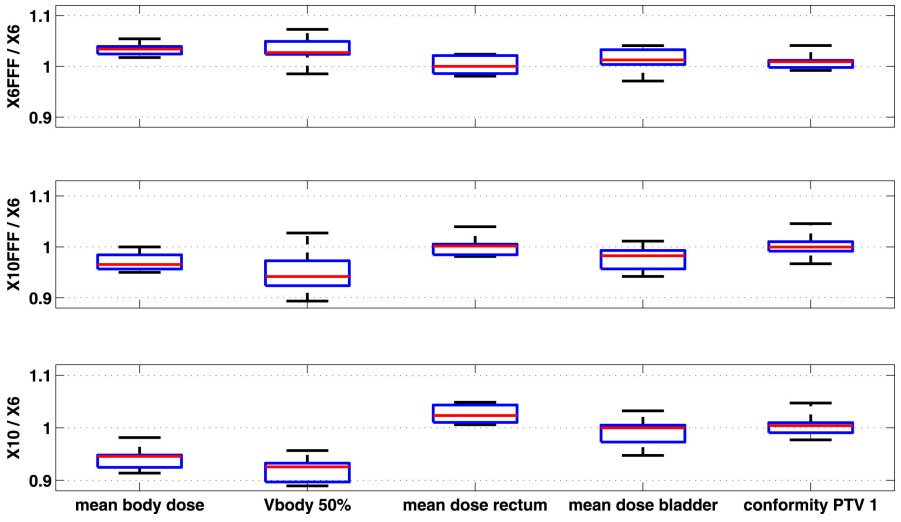

FIGURE 7.1: Box-whisker plots for different dose parameters. Ratio of X6 flattening filter-free (FFF) (top), X10FFF (middle), and X10 (bottom) with X6. The red line represents the median value, the blue box the interquartile range, and the whiskers minimum and maximum. PTV = planning target volume.

7.3.2 MU and mean body dose

The mean body dose decreased significantly with increasing mean energy of the beam (r^2 = 0.8275, p <0.01; figure 7.3). Using X6FFF beam delivered 3.6% more dose compared

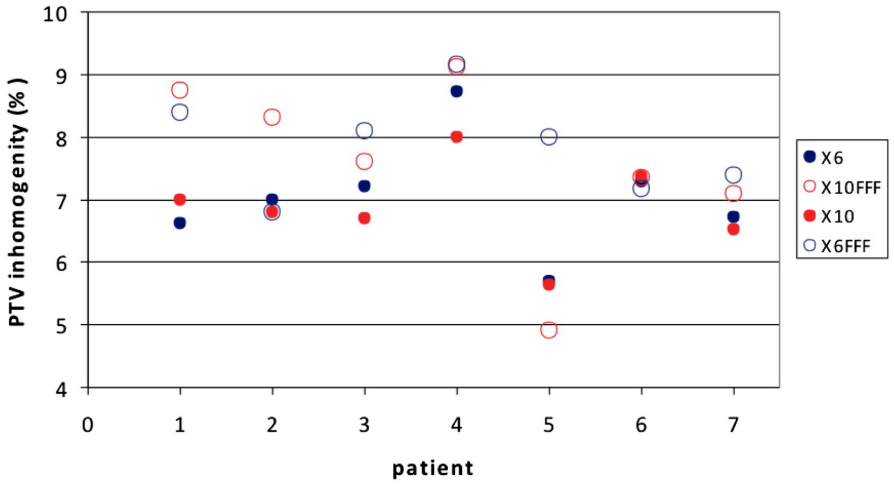

FIGURE 7.2: Planning target volume (PTV) inhomogeneity (defined as Dmax - Dmin in PTV 3) for the four different energies. Inhomogeneity is increased for flattening filter-free (FFF) beams.

with the X6 beam (p <0.01, 95% CI = 2.2 to 4.9%), whereas the X10FFF beam delivered 3.0% less dose (p <0.01, 95% CI = -2.3% to 4.7%) and the X10 beam 5.8% less dose (p <0.01, 95% CI = -3.8% to -7.8%). The volume receiving 50% of the prescribed dose to PTV 1 decreased significantly with increasing mean energy (figure 7.1).

MU significantly increased for X6FFF by 7.7% (p <0.02, 95% CI = 0.8% to 16.5%), and for X10FFF by 1.2% (p = 0.7, 95% CI = 8.2% to 9.8%); however, this increase was not significant. A significant decrease of 18.8% (p <0.02, 95% CI = 4.7% to 30.9%) in MU for X10 was detected because of the higher mean energy (table 7.2).

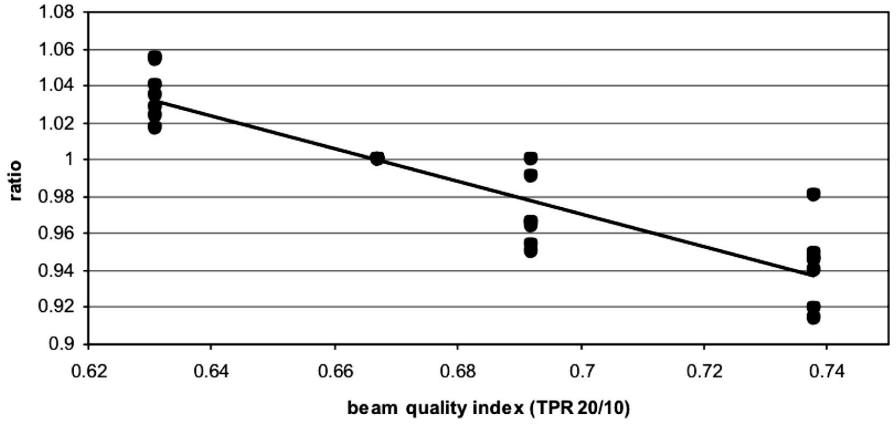

FIGURE 7.3: Mean body-dose dependence on the beam quality. Body dose was normalized to mean body dose of X6 beam.

7.3.3 Dose to skin and organs at risk

Compared with X6 beams, the mean skin dose significantly increased by 8.2% (p <0.01, CI = 5.9e11.3%) for X6FFF beams and decreased significantly by 9.1% (p <0.01, CI = 7.8% to 11.7%) and 12.9% (p <0.01, CI = 9.9% to 14.1%) for X10FFF and X10 beams. There was no difference in mean dose to the rectum and dose parameters V68%, V81%, V95%, and V100% were not statistically different for X6, X6FFF, and X10FFF beams (figure 7.1). A significant increase in mean dose of 2.6% (p <0.01, 95%CI = 0.6 - 4.2%) to the rectum was measured for X10 compared with X6 beam energy. The mean dose to the bladder was increased significantly by 1.3% for X6FFF (p <0.02, 95%CI = 0.1% to 2.2%) and decreased significantly by 2.3% (p <0.02, 95%CI = 0.2% to 3.7%) for X10FFF; no significant changes were detected for X10 (table 7.2). For the urethral bulb, there was no difference for V68% and V81% with respect to the four beams, and V68% for bowel and femoral heads were within the required constraints for all patients and beam energies.

7.3.4 Treatment time

For plans using a single arc, treatment time was significantly reduced to 1 min when using X6FFF and 10XFFF beams. The mean treatment time for single arc X6 and X10 plans were 1 min, 30 s, and 1 min, 25 s (table 7.2). The higher maximum dose rates for FFF beams allowed the gantry to run at maximum speed during the full arc. For flattened beams the gantry had to slow down in order to deliver the necessary MU. There was no difference in treatment time if two arcs were used.

7.4 Discussion

The results of this planning study demonstrated that with hypo-fractionated VMAT, dose distribution, conformity, and homogeneity within the PTVs were similar using either flattened or unflattened 6 and 10 MV photon beams. We showed that the mean body dose was a function of beam energy and decreased with increasing mean energy. Absence of the flattening filter resulted in a 3.6% higher mean body dose for X6FFF compared with X6 beams. X10FFF decreased the mean body dose by 3% compared with

the X6 beam; however, it increased the mean body dose by 2.8% compared with X10. For the rectum, the mean organ dose increased for the 10 MV unflattened photon beam compared with the 6 MV beams. Interestingly, usage of X10FFF decreased mean bladder dose compared with the other three beam qualities. Finally, using FFF technology, treatment time for a single arc was significantly reduced because of increased dose rate and faster delivery time.

Ensuring high-quality 3D-CRT, homogeneous photon fluence across the treatment field is of high priority to achieve optimal PTV coverage and a flattening filter was needed to ensure homogeneous target coverage. However, with the introduction of MLC's, changing leaf positions across the field modulates photon fluence to achieve optimal fluence maps [23, 119]. Thus, a uniform beam is no longer necessary as comparable treatment planning results for either flattened or unflattened beams have been reported [26], in particular for smaller treatment fields used in extracranial stereotactic RT for lung cancer [42]. Vassiliev et al. reported in their planning study, that using 6 and 18 MV IMRT with and without flattening filter resulted in similar treatment plans regarding PTV coverage for prostate cancer. Depending on the beam energy, X6FFF produced superior IMRT plans than X6. X18FFF resulted in inferior plans compared with X18 because of larger differences between optimal and deliverable fluence maps when compared with 6 MV [118]. However, plans and treatment delivery parameters were not fully optimized for FFF beams and the authors state that improvement of PTV coverage for either plan might have been possible with different user-specific cost functions for either the PTV or organs at risk. Similarly, Stathakis et al. observed negligible differences in PTV coverage between flattened and FFF 6 and 18 MV IMRT prostate plans. As expected, our data confirmed the authors finding that superficial dose was decreasing with increasing mean energy [119]. Compared with our study, both groups [118, 119] implemented IMRT techniques with FFF beams on a nonclinical prototype LINAC. Using VMAT technique, we found similar results: PTV coverage was unchanged using flattened or unflattened beam. However, we could detect a small difference of 1% in PTV inhomogeneity for FFF beams (figure 7.2). At this stage, it is unknown if the measured target inhomogeneity has any clinical relevance for treatment outcome of future patients with localized prostate cancer. Applying tighter objectives in the planning optimization process may reduce target inhomogeneities. However, we designed our study keeping all treatment planning objectives constant for all four beam energies.

For flattened beam-intensity modulation treatments, including IMRT and VMAT, the number of MU needed is an indicator for the mean body dose [133]. We found that a higher number of MU for FFF beams compared with flattened beams did not necessarily lead to an increased mean body dose. Because of the non-flat profile of the FFF beam, the integral dose of open fields in a water phantom is smaller than for a flattened beam in relation to 100 MU (figure 7.4). This finding was more pronounced with increasing field size. Therefore, compared with X6 an increase in MU for FFF beams was expected. Indeed, the planning study showed that the number of MU increased for X6FFF and X10FFF by 7.7% and 1.2%. In contrary, Vassiliev et al. [118] as well as Stathakis et al. [119] found a significant decrease in the number of MU for their FFF treatment plans. The reason was that our FFF beams were calibrated in order that 100 MU corresponded to 1 Gy at the depth of maximum dose, as this was common for flattened beams [51]. However, for all prototype LINACs with FFF capabilities used by other groups, only the flattened beams were calibrated. This resulted in a higher dose per 100 MU for the unflattened beams. Therefore they report a decrease in number of MU that we could not confirm in our study. Our data demonstrated that the mean body dose slightly decreased with the mean energy of the beam, despite the increase in number of MU that did not affect the mean body dose.

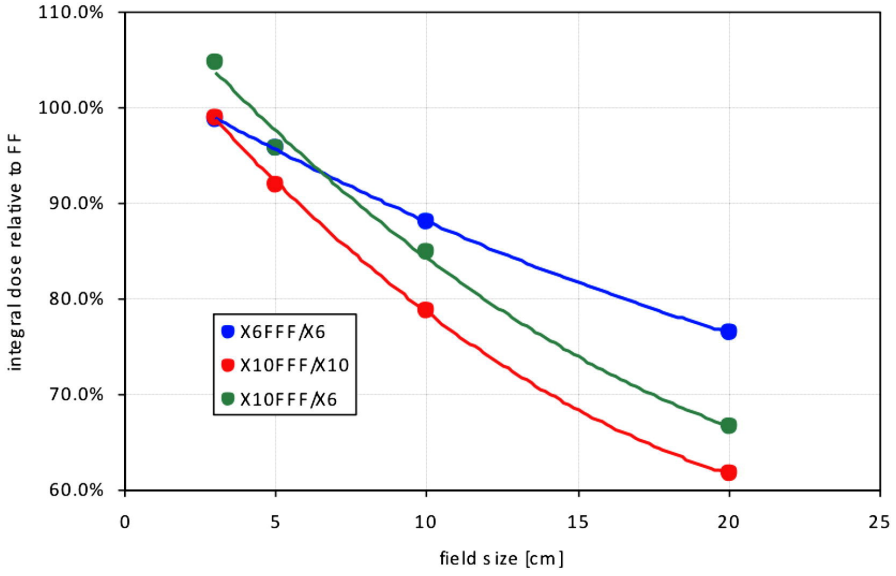

FIGURE 7.4: Integral dose of open fields in a water phantom relative to X6 beam corresponding to 100 MU for different field sizes.

Use of beam-modulating techniques exposes the whole body to a larger amount of scattered low-dose radiation as significant parts of treatment fields are being blocked by

the MLC increasing MU and scatter dose [130]. Prostate cancer patients treated with IMRT might be exposed to a twofold increased risk of developing secondary malignancies compared with 3D-CRT [130]. It is expected that FFF beams compared with flattened beams deposit less dose outside the target volume because of the missing scatter from the flattening filter and the reduced head scatter [58, 118, 122, 131].

Kragl et al. demonstrated that using FFF beams for IMRT prostate treatments resulted in a reduction of treatment head leakage by 52% and 65% for 6 and 10 MV, respectively [122]. Similarly, Cashmore et al. found in their study that IMRT using FFF beams removed unwanted and unnecessary scatter dose from the treatment head and lowered peripheral dose by up to 70% [131].

When applying hypofractionated treatment regimens for localized prostate cancer, treatment delivery time is important. With flattened beams and a limited output of MU/min higher doses per fraction leads to longer beam-on time and organ motion becomes relevant [134]. We found a time advantage for both FFF beams compared with X6 beam if one arc was used for planning. If the gantry was running at maximum speed, the time needed for one arc was 1 min. Flattened beams can deliver in 1 min 600 MU, X6FFF 1400 MU, and X10FFF 2400 MU. Therefore, whenever more than 600 MU per arc are needed, FFF beams reduce treatment time compared with flattened beams. The number of MU needed for the 7 patients ranged between 564 MU and 803 MU (for X10) and 803 MU to 1283 MU (for X6). For FFF beams, the number of MU was slightly increased. Therefore there is a time advantage for both FFF beams compared to X6 beam if one arc is used for planning. Fu et al. found a time advantage for FFF IMRT treatments of 46% depending on the dose per fraction. The time advantage increased when using higher dose per fraction, but was insignificant for standard fractionation of 2 Gy [26]. For sliding window IMRT the potential benefit of high dose rate is limited by the speed of the MLC. For treatments with RapidArc gantry speed is the limiting factor.

Finally, this study has several limitations. Our findings were based on a planning, rather than a clinical study. It is known that treatment planning systems do not correctly model the low-dose region [135]. Therefore the expected advantage of FFF beams to reduce the dose outside the target volume is not shown in our planning study. At this time, our results may be interpreted as having theoretical value rather than showing a clinical benefit for patients. However, this study revealed that non-inferior VMAT plans could be generated to deliver fast and high-quality hypofractionated RT. We acknowledge the

relevance and importance of image-guidance for modern prostate cancer RT when combining hypofractionated VMAT, high dose rate, and fast delivery time because of organ motion; however, this was beyond the scope of this article. Finally, as we carefully analyzed the differences and their impact on treatment planning and delivery, we believe our study contributes to a better understanding of the differences between flattened and unflattened beams in future clinical use.

7.5 Conclusion

For treatment plans with RapidArc, FFF beams resulted in dose distributions similar to flattened beams. We showed that X10FFF photon beams showed advantages in sparing rectum and bladder as well as keeping whole-body dose low. This could positively affect the treatment's toxicity profile using hypofractionated RT and may help to reduce the risk of second malignancies. Importantly, the use of FFF beams reduced treatment time, when gantry speed was a limiting factor for faster delivery of VMAT treatment. With increasing dose per fraction, higher dose rate might be used to reduce treatment time ever further. The described advantages of hypofractionated VMAT combined with unflattened photon beams should be tested in a clinical trial demonstrating the benefits for patients with localized prostate cancer.

Chapter 8

General conclusions

Flattening filter free (FFF) beams represent a new treatment modality of C-arm linear accelerators. In the scope of this thesis, several specific areas have been investigated in order to asses the contribution of FFF beams to clinical radiation therapy.

Measurements of the dosimetric characteristics of FFF beams are summarized and discussed in Chapter 3. This work may be considered as the reference overview of FFF and conventional beam properties of TrueBeam linear accelerator (Varian Medical Systems). The corresponding manuscript [28] has been in the meantime frequently cited[1] by various research groups. The same chapter also deals with the accuracy of beam modeling. Despite the fact that the Analytical Anisotropic Algorithm (Varian Medical Systems) has been simplified for FFF beams, it was shown that FFF beams are modelled with an accuracy comparable to the one known for conventional beams. These findings confirm the previous premise that the absence of flattening filter could make modeling of FFF beams more straightforward (less changes in the energy spectrum, reduction of extra-focal photons, etc.) Quantitative assessment of dose profile and depth dose curve modeling accuracy was possible owing to the modified 1D γ-concept (Chapter 2). This method was originally developed to identify small discrepancies between modeled and measured dose profiles of conventional beams, but it was successfully applied to FFF beams as well thanks to its universal character.

Commissioning measurements required a revision of dosimetric characteristics of ionization chambers with respect to the high dose rates of FFF beams (Chapter 4). The

[1] There are 36 citations reported by Scopus, abstract and citation database of peer-reviewed literature, in February 2014.

collection efficiency of all examined air-vented chambers was found to be sufficiently high to allow reliable assessment of relative dosimetry and correction factors for absolute dosimetry were less than 1 % in all cases. However, ion-collection efficiency was found to be insufficient for an iso-octane-filled ionization chamber when utilized for FFF beams and this chamber cannot be recommended for relative dosimetry of these beams.

Radiobiological effects associated with FFF beams have been studied on two human glioblastoma cell lines (Chapter 5). It was found that clonogenic survival was significantly reduced, if the total dose is delivered with a higher dose per pulse while keeping the mean dose rate constant. It was further demonstrated that X10FFF and X10 with the same dose per pulse do not exhibit differences in survival, hence the difference in the killing efficiency cannot be contributed to changes in energy spectrum. Pulse repetition frequency did not influence the survival.

Treatment planning studies assessing the contribution of FFF beams to stereotactic ablative radiotherapy of stage I non-small cell lung cancer (Chapter 6) and to localized prostate radiation therapy (Chapter 7) have also been carried out. Both studies showed that conventional and FFF beams yield quantitatively comparable dose distributions and only minor dosimetric differences were found. However, significant improvement in treatment delivery efficiency was observed for FFF plans in both studies.

In the case of the lung study, plans utilizing X6FFF beams showed a minor advantage in the steepness of dose gradient on the boundary between PTV and surrounding healthy tissue, which resulted in slightly improved sparing of ipsilateral lung tissue. In the case of the prostate study, plans utilizing X10FFF beams showed advantages in sparing rectum and bladder as well as keeping whole-body dose low. It was also demonstrated that both sets of beams exhibit comparable accuracy of treatment delivery.

Radiation therapy with flattening filter free (FFF) beams is gradually expanding. An increasing number of studies shows that FFF based radiation therapy is moving in routine clinical operation. FFF beams are most frequently utilized for treatments where high fraction doses need to be delivered, especially hypofractionated stereotactic radiotherapy (SRT) of stage I-II non-small cell lung cancer (NSCLC), lung and liver metastases, and other abdominal tumors [108–112]. In addition, FFF beams have been utilized

for the treatment of breast and chest wall [136, 137], esophageal cancer [138], localized prostate cancer [32], spinal radio surgery [139], brain lesions [140], nasopharyngeal carcinoma [141], etc.

Neglecting some site specific differences, it is possible to state, based on the available evidence, that the utilization of FFF beams provides dose distributions that are comparable to the ones achieved with conventional (flattened) beams, but with the advantage of significantly reduced time of treatment delivery. Shorter delivery times are surely increasing patient's comfort during treatment and can favorably reduce uncertainties in the patient positioning, or allow easier handling of tumor motion during treatment delivery (intrafractional motion). Indeed, it has been demonstrated on an 8-field FFF IMRT technique for lung and liver that faster delivery time makes it feasible to treat high doses per fraction delivering each field during a *single* breath-hold [127].

However, high dose rate beams need to be utilised with a caution when applied for the treatment of moving targets. The ability of FFF beams to deliver treatment more efficiently in the end means that substantial dose can be delivered to a wrong place in a short time, if motion management is not carried out properly. It was demonstrated that even short duration intrafractional shifts can cause significant dosimetric deviations during vertebral SBRT [126].

For treatments in the abdomen, the lower dose rates of conventional beams allow statistical "smearing" of motion interplay effects over many breathing cycles. One possible solution for high dose rate FFF beams is to distribute the treatment over multiple parts (in the inter- as well as intra-fractional sense). It has been shown that, although a single VMAT arc delivered at 2400 MU/min is susceptible to motion interplay, using two arcs and at least two fractions reduces the effect to a level that appears unlikely to be clinically significant [124, 125].

This examples illustrate that the application of FFF beams for a specific treatment site needs to be considered in the context of the rest of the radiotherapeutic chain and their mutual interplay.

In parallel to the planning studies, there is also the first data appearing on acute toxicities experienced by patients treated with FFF beams. There is an acceptable degree of

early toxicities, not significantly different from treatment with conventional beams, reported for treatment in thorax and liver [70], SBRT of lung malignancies [113], intensity modulated radio surgery of brain metastases [142], and prostate [143]. This evidence is supported by radiobiological studies [114–116, 144] that report comparable cell survival between conventional and high dose rate FFF beams for various cell lines.

These studies did not confirm our previous findings that an increase in dose per pulse (instantaneous dose rate) decreases cell survival [30]. One of the possible explanations could be a difference in used cell lines, especially when considering that the dependence of survival on dose per pulse varied even between the two cell lines used within our experiment. With the exception of T98G used in [114], all above mentioned studies used different cell lines for their experiments. Karan et al [116] add differences in cell cycle synchronisation as another possible explanation. However, from the overview of these studies, it seems that applied fraction dose could play an important role. Our study showed statistical difference only for single doses of 10 Gy or higher. The maximum fraction dose was 8 Gy in [115], 10 Gy in [116] and [144], and 12 Gy in [114]. Depending on selected cell line, survival at higher doses is relatively low (units of % or less) and could be biased by poor statistics and/or a presence of sterile cells in the experiment, impurities, etc. For the lower doses, where the surviving fraction allowed robust statistic, survival also did not differ in our study.

Despite the fact our study confirmed statistically significant difference in survival, this difference was unlikely to be clinically important, especially when taking into account standard dose per fraction and the fact that radiation therapy is delivered in a fractionated regime and not as a single fraction dose.

Despite the recent move towards more clinical studies, various aspects of the physical characteristics of FFF beams are continuing to be investigated. Georg et al [145] provided a comprehensive summary of the status of FFF related research in 2011. In addition, centers that first began to use FFF beams with TrueBeam linear accelerator presented a joint study on the results of patient specific QA [123], demonstrating that treatment delivery with FFF beams is as accurate as those for conventional beams.

A reduction of out-of-field (peripheral) doses associated with the reduction of head scatter and leakage has been evaluated [122] in clinically relevant conditions (lung SBRT, prostate and head&neck IMRT). At about 20 cm from the field edge, the dose was

reduced by more than 20 %. The relative difference increases with the nominal beam energy.

The dose calculation accuracy of FFF beams has been found to be comparable to the ones known for conventional beams [146]. A study focussing on the accuracy of modeling of FFF beams in a heterogeneous lung/tissue phantom [147] found an overestimation of penumbral width for very small fields incident on tissue equivalent material located within lung [147]. It was demonstrated that FFF beams exhibit rather small off-axis variations in energy, potentially allowing to ignore these changes in a treatment planning system [57]. Slightly increased surface dose of FFF beams was reported [120], in accordance with our findings, with the author's stating that the increase in the surface dose is unlikely to be clinically significant.

Various detectors have also been compared to alanine detector for the dosimetry of small fields of FFF beams [148]. The determined output factors were found to agree within the measurement uncertainty or only a small correction was required. Another study on ion-recombination of specific ionization chambers in FFF beams was published [149] and further improvements in Monte Carlo simulations, such as adapting the virtual source model to mimic a FFF beam production [150], have been achieved.

The concept of a direction-selective flattening filter - a small conical filter in the proximity of a target - has also been proposed [151]. The authors claim it represents a solution midway between classical and FFF beams, taking advantage of increased dose rate and reduced leakage while preserving a flat beam profile for field sizes up to 15 cm diameter.

In summary, the current clinical evidence appears to fulfill the expectations based on the previous theoretical assumptions and experiments done with FFF prototype linacs. The main advantages of FFF beams are improved efficiency of treatment delivery and the reduction of unwanted scatter dose. Available data suggests that there is not a necessity to apply any radio-biological corrections. With ongoing clinical experience, further optimization of the treatment modality is expected. While FFF beams have expanded the dose rate range, other components utilized in modulated radiation therapy, such as speed of a multi-leaf collimator and rotational speed of a gantry, have remained the same. It is the author's opinion that further enhancements of treatment planning optimization algorithms or hardware changes that will exploit higher dose rates, may

contribute to further improve the outcome of FFF radiation therapy. However, these improvements are likely to be marginal.

Bibliography

[1] C. W. Miller, "An 8-MeV linear accelerator for X-ray therapy," *Proceedings of the IEE-Part I: General*, vol. 101, no. 130, pp. 207–221, 1954.

[2] G. R. Newbery and D. K. Bewley, "The performance of the medical research council 8 mev linear accelerator," *Br J Radiol*, vol. 28, pp. 241–51, May 1955.

[3] "WHO Regional Office for Europe: European Health for All database [online database]."

[4] J. Ferlay, E. Steliarova-Foucher, J. Lortet-Tieulent, S. Rosso, J. W. W. Coebergh, H. Comber, D. Forman, and F. Bray, "Cancer incidence and mortality patterns in europe: estimates for 40 countries in 2012," *Eur J Cancer*, vol. 49, pp. 1374–403, Apr 2013.

[5] G. Delaney, S. Jacob, C. Featherstone, and M. Barton, "The role of radiotherapy in cancer treatment," *Cancer*, vol. 104, no. 6, pp. 1129–1137, 2005.

[6] J. Van Dyk *et al.*, *The modern technology of radiation oncology.* Medical Physics Publ., 1999.

[7] American Medical Association Survey & Data Resources, *Physician characteristics and Distribution in the US.* Survey & Data Resources, American Medical Association, 2010.

[8] F. M. Khan, *The physics of radiation therapy*, vol. 3. Lippincott Williams & Wilkins Philadelphia, 2003.

[9] P. F. O'Brien, B. A. Gillies, M. Schwartz, C. Young, and P. Davey, "Radiosurgery with unflattened 6-mv photon beams," *Med Phys*, vol. 18, no. 3, pp. 519–21, 1991.

[10] T. R. Mackie, T. Holmes, S. Swerdloff, P. Reckwerdt, J. O. Deasy, J. Yang, B. Paliwal, and T. Kinsella, "Tomotherapy: a new concept for the delivery of dynamic conformal radiotherapy," *Medical physics*, vol. 20, p. 1709, 1993.

[11] P. L. Petti, M. S. Goodman, T. A. Gabriel, and R. Mohan, "Investigation of buildup dose from electron contamination of clinical photon beams," *Med Phys*, vol. 10, no. 1, pp. 18–24, 1983.

[12] T. C. Zhu and B. E. Bjärngard, "The fraction of photons undergoing head scatter in x-ray beams," *Phys Med Biol*, vol. 40, pp. 1127–34, Jun 1995.

[13] P. C. Lee, "Monte carlo simulations of the differential beam hardening effect of a flattening filter on a therapeutic x-ray beam," *Med Phys*, vol. 24, pp. 1485–9, Sep 1997.

[14] B. Nilsson, "Electron contamination from different materials in high energy photon beams," *Phys Med Biol*, vol. 30, pp. 139–51, Feb 1985.

[15] A. R. Hounsell and J. M. Wilkinson, "Electron contamination and build-up doses in conformal radiotherapy fields," *Phys Med Biol*, vol. 44, pp. 43–55, Jan 1999.

[16] E. E. Klein, J. Esthappan, and Z. Li, "Surface and buildup dose characteristics for 6, 10, and 18 mv photons from an elekta precise linear accelerator," *J Appl Clin Med Phys*, vol. 4, no. 1, pp. 1–7, 2003.

[17] R. Jeraj, T. R. Mackie, J. Balog, G. Olivera, D. Pearson, J. Kapatoes, K. Ruchala, and P. Reckwerdt, "Radiation characteristics of helical tomotherapy," *Med Phys*, vol. 31, pp. 396–404, Feb 2004.

[18] J. L. Robar, S. A. Riccio, and M. A. Martin, "Tumour dose enhancement using modified megavoltage photon beams and contrast media," *Phys Med Biol*, vol. 47, pp. 2433–49, Jul 2002.

[19] U. Titt, O. Vassiliev, F. Pönisch, L. Dong, H. Liu, and R. Mohan, "A flattening filter free photon treatment concept evaluation with monte carlo," *Medical physics*, vol. 33, p. 1595, 2006.

[20] O. N. Vassiliev, U. Titt, S. F. Kry, F. Pönisch, M. T. Gillin, and R. Mohan, "Monte carlo study of photon fields from a flattening filter-free clinical accelerator," *Medical physics*, vol. 33, p. 820, 2006.

[21] E. Ishmael Parsai, D. Pearson, and T. Kvale, "Consequences of removing the flattening filter from linear accelerators in generating high dose rate photon beams for clinical applications: A monte carlo study verified by measurement," *Nuclear Instruments and Methods in Physics Research Section B: Beam Interactions with Materials and Atoms*, vol. 261, no. 1, pp. 755–759, 2007.

[22] S. Zefkili, C. Kappas, and J. C. Rosenwald, "On-axis and off-axis primary dose component in high energy photon beams," *Med Phys*, vol. 21, pp. 799–808, Jun 1994.

[23] O. N. Vassiliev, U. Titt, F. Pönisch, S. F. Kry, R. Mohan, and M. T. Gillin, "Dosimetric properties of photon beams from a flattening filter free clinical accelerator," *Physics in medicine and biology*, vol. 51, no. 7, p. 1907, 2006.

[24] G. Kragl, S. af Wetterstedt, B. Knäusl, M. Lind, P. McCavana, T. Knöös, B. McClean, and D. Georg, "Dosimetric characteristics of 6 and 10mv unflattened photon beams," *Radiotherapy and Oncology*, vol. 93, no. 1, pp. 141–146, 2009.

[25] J. Cashmore, "The characterization of unflattened photon beams from a 6 mv linear accelerator," *Physics in medicine and biology*, vol. 53, no. 7, p. 1933, 2008.

[26] W. Fu, J. Dai, Y. Hu, D. Han, and Y. Song, "Delivery time comparison for intensity-modulated radiation therapy with/without flattening filter: a planning study," *Phys Med Biol*, vol. 49, pp. 1535–47, Apr 2004.

[27] J. Hrbacek, T. Depuydt, A. Nulens, A. Swinnen, and F. Van den Heuvel, "Quantitative evaluation of a beam-matching procedure using one-dimensional gamma analysis," *Medical physics*, vol. 34, p. 2917, 2007.

[28] J. Hrbacek, S. Lang, and S. Klöck, "Commissioning of photon beams of a flattening filter-free linear accelerator and the accuracy of beam modeling using an anisotropic analytical algorithm," *International Journal of Radiation Oncology* Biology* Physics*, vol. 80, no. 4, pp. 1228–1237, 2011.

[29] S. Lang, J. Hrbacek, A. Leong, and S. Klöck, "Ion-recombination correction for different ionization chambers in high dose rate flattening-filter-free photon beams," *Physics in Medicine and Biology*, vol. 57, no. 9, p. 2819, 2012.

[30] I. Lohse, S. Lang, J. Hrbacek, S. Scheidegger, S. Bodis, N. S. Macedo, J. Feng, U. M. Lütolf, and K. Zaugg, "Effect of high dose per pulse flattening filter-free beams on cancer cell survival," *Radiotherapy and Oncology*, vol. 101, no. 1, pp. 226–232, 2011.

[31] J. Hrbacek, S. Lang, S. Graydon, S. Kloeck, and O. Riesterer, "Dosimetric comparison of flattened and unflattened beams for stereotactic ablative radiotherapy of stage i non-small cell lung cancer," *Medical Physics*, 2014.

[32] D. R. Zwahlen, S. Lang, J. Hrbacek, C. Glanzmann, S. Kloeck, Y. Najafi, T. Streller, G. Studer, K. Zaugg, and U. M. Luetolf, "The use of photon beams of a flattening filter-free linear accelerator for hypofractionated volumetric modulated arc therapy in localized prostate cancer," *International Journal of Radiation Oncology* Biology* Physics*, vol. 83, no. 5, pp. 1655–1660, 2012.

[33] D. Fontenla, J. Napoli, and C. Chui, "Beam characteristics of a new model of 6-mv linear accelerator," *Medical physics*, vol. 19, p. 343, 1992.

[34] M. G. Marshall, "Matching the 6-mv photon beam characteristics of two dissimilar linear accelerators," *Medical physics*, vol. 20, p. 1743, 1993.

[35] N. A. of Clinical Physics (NACP), "Procedures in external radiation therapy dosimetry with electron and photon beams with maximum energies between 1 and 50 mev," *Acta radiol. Oncology*, vol. 19, p. 55, 1980.

[36] S. Thomas and K. Foster, "Radiotherapy treatment planning with dynamic wedges-an algorithm for generating wedge factors and beam data," *Physics in medicine and biology*, vol. 40, no. 9, p. 1421, 1995.

[37] J. Cygler, G. Daskalov, G. Chan, and G. Ding, "Evaluation of the first commercial monte carlo dose calculation engine for electron beam treatment planning," *Medical physics*, vol. 31, p. 142, 2004.

[38] G. X. Ding, D. M. Duggan, C. W. Coffey, P. Shokrani, and J. E. Cygler, "First macro monte carlo based commercial dose calculation module for electron beam treatment planning - new issues for clinical consideration," *Physics in medicine and biology*, vol. 51, no. 11, p. 2781, 2006.

[39] T. Depuydt, B. Vanstraelen, J. Verstraete, and J. Van den Heuvel, "WE-D-224A-06: Comparison of Film Based IMRT Verification with EPID Based Fluence Verification," *Medical Physics*, vol. 33, p. 2248, 2006.

[40] D. A. Low, W. B. Harms, S. Mutic, and J. A. Purdy, "A technique for the quantitative evaluation of dose distributions," *Medical physics*, vol. 25, p. 656, 1998.

[41] D. A. Low and J. F. Dempsey, "Evaluation of the gamma dose distribution comparison method," *Medical Physics*, vol. 30, p. 2455, 2003.

[42] O. N. Vassiliev, S. F. Kry, J. Y. Chang, P. A. Balter, U. Titt, and R. Mohan, "Stereotactic radiotherapy for lung cancer using a flattening filter free clinac," *Journal of Applied Clinical Medical Physics*, vol. 10, no. 1, 2009.

[43] J. Balog, G. Olivera, and J. Kapatoes, "Clinical helical tomotherapy commissioning dosimetry," *Medical physics*, vol. 30, p. 3097, 2003.

[44] W. Ulmer, J. Pyyry, and W. Kaissl, "A 3d photon superposition/convolution algorithm and its foundation on results of monte carlo calculations," *Physics in medicine and biology*, vol. 50, no. 8, p. 1767, 2005.

[45] J. Sievinen, W. Ulmer, and W. Kaissl, "Aaa photon dose calculation model in eclipse," *Palo Alto (CA): Varian Medical Systems*, vol. 118, 2005.

[46] A. Fogliata, G. Nicolini, E. Vanetti, A. Clivio, and L. Cozzi, "Dosimetric validation of the anisotropic analytical algorithm for photon dose calculation: fundamental characterization in water," *Physics in medicine and biology*, vol. 51, no. 6, p. 1421, 2006.

[47] A. Van Esch, L. Tillikainen, J. Pyykkonen, M. Tenhunen, H. Helminen, S. Siljamäki, J. Alakuijala, M. Paiusco, M. Iori, and D. P. Huyskens, "Testing of the analytical anisotropic algorithm for photon dose calculation," *Medical physics*, vol. 33, p. 4130, 2006.

[48] C. M. Bragg and J. Conway, "Dosimetric verification of the anisotropic analytical algorithm for radiotherapy treatment planning," *Radiotherapy and oncology*, vol. 81, no. 3, pp. 315–323, 2006.

[49] K. Breitman, S. Rathee, C. Newcomb, B. Murray, D. Robinson, C. Field, H. Warkentin, S. Connors, M. Mackenzie, P. Dunscombe, *et al.*, "Experimental validation of the eclipse aaa algorithm," *Journal of Applied Clinical Medical Physics*, vol. 8, no. 2, 2007.

[50] G. X. Ding, D. M. Duggan, B. Lu, D. E. Hallahan, A. Cmelak, A. Malcolm, J. Newton, M. Deeley, and C. W. Coffey, "Impact of inhomogeneity corrections on dose coverage in the treatment of lung cancer using stereotactic body radiation therapy," *Medical physics*, vol. 34, p. 2985, 2007.

[51] P. R. Almond, P. J. Biggs, B. Coursey, W. Hanson, M. S. Huq, R. Nath, and D. Rogers, "Aapm's tg-51 protocol for clinical reference dosimetry of high-energy photon and electron beams," *Medical physics*, vol. 26, p. 1847, 1999.

[52] I. Griessbach, M. Lapp, J. Bohsung, G. Gademann, and D. Harder, "Dosimetric characteristics of a new unshielded silicon diode and its application in clinical photon and electron beams," *Medical physics*, vol. 32, p. 3750, 2005.

[53] F. Pönisch, U. Titt, O. N. Vassiliev, S. F. Kry, and R. Mohan, "Properties of unflattened photon beams shaped by a multileaf collimator," *Medical physics*, vol. 33, p. 1738, 2006.

[54] M. Schwedas, M. Scheithauer, T. Wiezorek, and T. G. Wendt, "Strahlenphysikalische einflussgrössen bei der dosimetrie mit verschiedenen detektortypen," *Zeitschrift für Medizinische Physik*, vol. 17, no. 3, pp. 172 – 179, 2007.

[55] A. Van Esch, J. Bohsung, P. Sorvari, M. Tenhunen, M. Paiusco, M. Iori, D. P. Huyskens, *et al.*, "Acceptance tests and quality control (qc) procedures for the clinical implementation of intensity modulated radiotherapy (imrt) using inverse planning and the sliding window technique: experience from five radiotherapy departments," *Radiotherapy and oncology*, vol. 65, no. 1, pp. 53–70, 2002.

[56] Z. Chang, Z. Wang, Q. J. Wu, H. Yan, J. Bowsher, J. Zhang, and F.-F. Yin, "Dosimetric characteristics of novalis tx system with high definition multileaf collimator," *Medical physics*, vol. 35, p. 4460, 2008.

[57] D. Georg, G. Kragl, S. Af Wetterstedt, P. McCavana, B. McClean, and T. Knöös, "Photon beam quality variations of a flattening filter free linear accelerator," *Medical physics*, vol. 37, p. 49, 2010.

[58] S. F. Kry, O. N. Vassiliev, and R. Mohan, "Out-of-field photon dose following removal of the flattening filter from a medical accelerator," *Physics in medicine and biology*, vol. 55, no. 8, p. 2155, 2010.

[59] J. Burns and K. Rosser, "Saturation correction for the ne 2560/1 dosemeter in photon dosimetry," *Physics in Medicine and Biology*, vol. 35, no. 5, p. 687, 1990.

[60] K. Derikum and M. Roos, "Measurement of saturation correction factors of thimble-type ionization chambers in pulsed photon beams," *Physics in Medicine and Biology*, vol. 38, no. 6, p. 755, 1993.

[61] J. Boag, *Radiation Dosimetry vol 2 (FH Attix and WC Roesch)*. Academic Press, New York, 1966.

[62] J. Boag and J. Currant, "Current collection and ionic recombination in small cylindrical ionization chambers exposed to pulsed radiation," *British Journal of Radiology*, vol. 53, no. 629, pp. 471–478, 1980.

[63] J. Havercroft and S. Klevenhagen, "Ion recombination corrections for plane-parallel and thimble chambers in electron and photon radiation," *Physics in medicine and biology*, vol. 38, no. 1, p. 25, 1993.

[64] F. DeBlois, C. Zankowski, and E. B. Podgorsak, "Saturation current and collection efficiency for ionization chambers in pulsed beams," *Medical physics*, vol. 27, p. 1146, 2000.

[65] G. Bruggmoser, R. Saum, A. Schmachtenberg, F. Schmid, and E. Schüle, "Determination of the recombination correction factor ks for some specific plane-parallel and cylindrical ionization chambers in pulsed photon and electron beams," *Physics in medicine and biology*, vol. 52, no. 2, p. N35, 2007.

[66] A. Mozumder, "Effect of an external electric field on the yield of free ions. iii. electron scavenging at small concentrations," *The Journal of Chemical Physics*, vol. 61, p. 780, 1974.

[67] J. Pardo, L. Franco, F. Gomez, A. Iglesias, R. Lobato, J. Mosquera, A. Pazos, J. Pena, M. Pombar, A. Rodríguez, *et al.*, "Free ion yield observed in liquid isooctane irradiated by γ rays. comparison with the onsager theory," *Physics in medicine and biology*, vol. 49, no. 10, p. 1905, 2004.

[68] H. Tolli, R. Sjogren, and M. Wendelsten, "A two-dose-rate method for general recombination correction for liquid ionization chambers in pulsed beams," *Physics in Medicine and Biology*, vol. 55, no. 15, pp. 4247–4260, 2010.

[69] J. Pardo-Montero and F. Gómez, "Determining charge collection efficiency in parallel-plate liquid ionization chambers," *Physics in medicine and biology*, vol. 54, no. 12, p. 3677, 2009.

[70] M. Scorsetti, F. Alongi, S. Castiglioni, A. Clivio, A. Fogliata, F. Lobefalo, P. Mancosu, P. Navarria, V. Palumbo, C. Pellegrini, *et al.*, "Feasibility and early clinical assessment of flattening filter free (fff) based stereotactic body radiotherapy (sbrt) treatments," *Lung*, vol. 34, p. 48, 2011.

[71] K. Stewart, A. Elliott, and J. Seuntjens, "Development of a guarded liquid ionization chamber for clinical dosimetry," *Physics in medicine and biology*, vol. 52, no. 11, p. 3089, 2007.

[72] S. Agostinelli, S. Garelli, M. Piergentili, and F. Foppiano, "Response to high-energy photons of ptw31014 pinpoint ion chamber with a central aluminum electrode," *Medical physics*, vol. 35, p. 3293, 2008.

[73] B. Johansson and G. Wickman, "General collection efficiency for liquid isooctane and tetramethylsilane used as sensitive media in a parallel-plate ionization chamber," *Physics in medicine and biology*, vol. 42, no. 1, p. 133, 1997.

[74] B. Johansson, G. Wickman, and J. Bahar-Gogani, "General collection efficiency for liquid isooctane and tetramethylsilane in pulsed radiation," *Physics in Medicine and Biology*, vol. 42, no. 10, p. 1929, 1997.

[75] A. Dasu, P.-O. Löfroth, and G. Wickman, "Liquid ionization chamber measurements of dose distributions in small 6 mv photon beams," *Physics in medicine and biology*, vol. 43, no. 1, p. 21, 1998.

[76] G. Wickman and H. Nystrom, "The use of liquids in ionization chambers for high precision radiotherapy dosimetry," *Physics in Medicine and Biology*, vol. 37, no. 9, p. 1789, 1992.

[77] J. F. Fowler, J. S. Welsh, and S. P. Howard, "Loss of biological effect in prolonged fraction delivery," *International Journal of Radiation Oncology* Biology* Physics*, vol. 59, no. 1, pp. 242–249, 2004.

[78] E. J. Hall and A. J. Giaccia, *Radiobiology for the Radiologist*. Wolters Kluwer Health, 2006.

[79] J. Z. Wang, X. A. Li, W. D. D'Souza, and R. D. Stewart, "Impact of prolonged fraction delivery times on tumor control: a note of caution for intensity-modulated radiation therapy (imrt)," *International Journal of Radiation Oncology* Biology* Physics*, vol. 57, no. 2, pp. 543–552, 2003.

[80] J. Z. Wang and X. A. Li, "Impact of tumor repopulation on radiotherapy planning," *International Journal of Radiation Oncology* Biology* Physics*, vol. 61, no. 1, pp. 220–227, 2005.

[81] C. C. Ling, L. E. Gerweck, M. Zaider, and E. Yorke, "Dose-rate effects in external beam radiotherapy redux," *Radiotherapy and Oncology*, vol. 95, no. 3, pp. 261–268, 2010.

[82] Y. Shibamoto, M. Ito, C. Sugie, H. Ogino, and M. Hara, "Recovery from sublethal damage during intermittent exposures in cultured tumor cells: implications for dose modification in radiosurgery and imrt," *International Journal of Radiation Oncology* Biology* Physics*, vol. 59, no. 5, pp. 1484–1490, 2004.

[83] P. J. Keall, M. Chang, S. Benedict, H. Thames, S. S. Vedam, and P.-S. Lin, "Investigating the temporal effects of respiratory-gated and intensity-modulated radiotherapy treatment delivery on in vitro survival: An experimental and theoretical study," *International Journal of Radiation Oncology* Biology* Physics*, vol. 71, no. 5, pp. 1547–1552, 2008.

[84] V. Moiseenko, J. P. Banáth, C. Duzenli, P. L. Olive, *et al.*, "Effect of prolonging radiation delivery time on retention of gammah2ax," *Radiation Oncology*, vol. 3, no. 1, p. 18, 2008.

[85] X. Mu, P.-O. Löfroth, M. Karlsson, and B. Zackrisson, "The effect of fraction time in intensity modulated radiotherapy: theoretical and experimental evaluation of an optimisation problem," *Radiotherapy and oncology*, vol. 68, no. 2, pp. 181–187, 2003.

[86] M. J. Murphy, P.-S. Lin, and C. Ozhasoglu, "Intra-fraction dose delivery timing during stereotactic radiotherapy can influence the radiobiological effect," *Medical physics*, vol. 34, p. 481, 2007.

[87] J. Bewes, N. Suchowerska, M. Jackson, M. Zhang, and D. McKenzie, "The radiobiological effect of intra-fraction dose-rate modulation in intensity modulated radiation therapy (imrt)," *Physics in Medicine and Biology*, vol. 53, no. 13, p. 3567, 2008.

[88] N. A. Franken, H. M. Rodermond, J. Stap, J. Haveman, and C. Van Bree, "Clonogenic assay of cells in vitro," *Nature protocols*, vol. 1, no. 5, pp. 2315–2319, 2006.

[89] S. Scheidegger, G. Lutters, and S. Bodis, "A lq-based kinetic model formulation for exploring dynamics of treatment response of tumours in patients," *Zeitschrift für Medizinische Physik*, vol. 21, no. 3, pp. 164–173, 2011.

[90] S. B. Curtis, "Lethal and potentially lethal lesions induced by radiation—a unified repair model," *Radiation research*, vol. 106, no. 2, pp. 252–270, 1986.

[91] J. E. Haber, "Partners and pathways: repairing a double-strand break," *Trends in Genetics*, vol. 16, no. 6, pp. 259–264, 2000.

[92] G. Gordon Steel, "The estro breur lecture cellular sensitivity to low dose-rate irradiation focuses the problem of tumour radioresistance," *Radiotherapy and Oncology*, vol. 20, no. 2, pp. 71–83, 1991.

[93] G. Gordon Steel, J. D. Down, J. H. Peacock, and T. C. Stephens, "Dose-rate effects and the repair of radiation damage," *Radiotherapy and Oncology*, vol. 5, no. 4, pp. 321–331, 1986.

[94] J. Hamilton and E. J. Bernhard, "Cell signalling and radiation survival: The impact of protein phosphatases," *International journal of radiation biology*, vol. 85, no. 11, pp. 937–942, 2009.

[95] P. Jeggo and M. F. Lavin, "Cellular radiosensitivity: how much better do we understand it?," *International journal of radiation biology*, vol. 85, no. 12, pp. 1061–1081, 2009.

[96] H. Yoshida, "Er stress response, peroxisome proliferation, mitochondrial unfolded protein response and golgi stress response," *IUBMB life*, vol. 61, no. 9, pp. 871–879, 2009.

[97] H. P. Rodemann, "Molecular radiation biology: perspectives for radiation oncology," *Radiotherapy and Oncology*, vol. 92, no. 3, pp. 293–298, 2009.

[98] F. Rödel, B. Frey, G. Capalbo, U. Gaipl, L. Keilholz, R. Voll, G. Hildebrandt, and C. Rödel, "Discontinuous induction of x-linked inhibitor of apoptosis in ea. hy. 926 endothelial cells is linked to nf-κb activation and mediates the anti-inflammatory properties of low-dose ionising-radiation," *Radiotherapy and Oncology*, vol. 97, no. 2, pp. 346–351, 2010.

[99] H. B. Honoré and S. M. Bentzen, "A modelling study of the potential influence of low dose hypersensitivity on radiation treatment planning," *Radiotherapy and oncology*, vol. 79, no. 1, pp. 115–121, 2006.

[100] J. Harney, N. Shah, S. Short, F. Daley, N. Groom, G. D. Wilson, M. C. Joiner, and M. I. Saunders, "The evaluation of low dose hyper-radiosensitivity in normal human skin," *Radiotherapy and oncology*, vol. 70, no. 3, pp. 319–329, 2004.

[101] J. W. Powell, E. Dexter, E. M. Scalzetti, and J. A. Bogart, "Treatment advances for medically inoperable non-small-cell lung cancer: emphasis on prospective trials," *The Lancet Oncology*, vol. 10, no. 9, pp. 885–894, 2009.

[102] T. G. Purdie, J.-P. Bissonnette, K. Franks, A. Bezjak, D. Payne, F. Sie, M. B. Sharpe, and D. A. Jaffray, "Cone-beam computed tomography for on-line image guidance of lung stereotactic radiotherapy: localization, verification, and intrafraction tumor position," *International Journal of Radiation Oncology* Biology* Physics*, vol. 68, no. 1, pp. 243–252, 2007.

[103] M. S. Hoogeman, J. J. Nuyttens, P. C. Levendag, and B. J. Heijmen, "Time dependence of intrafraction patient motion assessed by repeat stereoscopic imaging," *International Journal of Radiation Oncology* Biology* Physics*, vol. 70, no. 2, pp. 609–618, 2008.

[104] W. F. Verbakel, S. Senan, J. P. Cuijpers, B. J. Slotman, and F. J. Lagerwaard, "Rapid delivery of stereotactic radiotherapy for peripheral lung tumors using volumetric intensity-modulated arcs," *Radiotherapy and Oncology*, vol. 93, no. 1, pp. 122–124, 2009.

[105] C. L. Ong, W. F. Verbakel, J. P. Cuijpers, B. J. Slotman, F. J. Lagerwaard, and S. Senan, "Stereotactic radiotherapy for peripheral lung tumors: a comparison of volumetric modulated arc therapy with 3 other delivery techniques," *Radiotherapy and Oncology*, vol. 97, no. 3, pp. 437–442, 2010.

[106] K. Otto, "Volumetric modulated arc therapy: Imrt in a single gantry arc," *Medical physics*, vol. 35, p. 310, 2008.

[107] C. L. Ong, W. F. Verbakel, M. Dahele, J. P. Cuijpers, B. J. Slotman, and S. Senan, "Fast arc delivery for stereotactic body radiotherapy of vertebral and lung tumors," *International Journal of Radiation Oncology* Biology* Physics*, vol. 83, no. 1, pp. e137–e143, 2012.

[108] P. Navarria, A. M. Ascolese, P. Mancosu, F. Alongi, E. Clerici, A. Tozzi, C. Iftode, G. Reggiori, S. Tomatis, M. Infante, *et al.*, "Volumetric modulated arc therapy with flattening filter free (fff) beams for stereotactic body radiation therapy (sbrt) in patients with medically inoperable early stage non small cell lung cancer (nsclc)," *Radiotherapy and Oncology*, 2013.

[109] S. Lang, B. Shrestha, S. Graydon, F. Cavelaars, C. Linsenmeier, J. Hrbacek, S. Klöck, G. Studer, and O. Riesterer, "Clinical application of flattening filter free beams for extracranial stereotactic radiotherapy," *Radiotherapy and Oncology*, 2013.

[110] G. Reggiori, P. Mancosu, S. Castiglioni, F. Alongi, C. Pellegrini, F. Lobefalo, M. Catalano, A. Fogliata, S. Arcangeli, P. Navarria, *et al.*, "Can volumetric modulated arc therapy with flattening filter free beams play a role in stereotactic body radiotherapy for liver lesions? a volume-based analysis," *Medical Physics*, vol. 39, p. 1112, 2012.

[111] P. Mancosu, S. Castiglioni, G. Reggiori, M. Catalano, F. Alongi, C. Pellegrini, S. Arcangeli, A. Tozzi, F. Lobefalo, A. Fogliata, *et al.*, "Stereotactic body radiation

therapy for liver tumours using flattening filter free beam: dosimetric and technical considerations," *Radiat Oncol*, vol. 7, p. 16, 2012.

[112] B. M. Prendergast, J. B. Fiveash, R. A. Popple, G. M. Clark, E. M. Thomas, D. J. Minnich, R. Jacob, S. A. Spencer, J. A. Bonner, and M. C. Dobelbower, "Flattening filter-free linac improves treatment delivery efficiency in stereotactic body radiation therapy," *Journal of Applied Clinical Medical Physics*, vol. 14, no. 3, 2013.

[113] B. M. Prendergast, M. C. Dobelbower, J. A. Bonner, R. A. Popple, C. J. Baden, D. J. Minnich, R. J. Cerfolio, S. A. Spencer, and J. B. Fiveash, "Stereotactic body radiation therapy (sbrt) for lung malignancies: preliminary toxicity results using a flattening filter-free linear accelerator operating at 2400 monitor units per minute," *Radiation Oncology*, vol. 8, no. 1, p. 273, 2013.

[114] W. F. Verbakel, J. van den Berg, B. J. Slotman, and P. Sminia, "Comparable cell survival between high dose rate flattening filter free and conventional dose rate irradiation," *Acta Oncologica*, vol. 52, no. 3, pp. 652–657, 2013.

[115] R. King, W. Hyland, A. Cole, K. Butterworth, S. McMahon, K. Redmond, C. Trainer, K. Prise, C. McGarry, and A. Hounsell, "An in vitro study of the radiobiological effects of flattening filter free radiotherapy treatments," *Physics in medicine and biology*, vol. 58, no. 5, p. N83, 2013.

[116] T. Karan, V. Moiseenko, B. Gill, R. Horwood, A. Kyle, and A. Minchinton, "Radiobiological effects of altering dose rate in filter-free photon beams," *Physics in medicine and biology*, vol. 58, no. 4, p. 1075, 2013.

[117] "RTOG 0915: A randomized phase II study comparing 2 stereotactic body radiation therapy (SBRT) schedules for medically inoperable patients with stage I peripheral non-small cell lung cancer."

[118] O. N. Vassiliev, S. F. Kry, D. A. Kuban, M. Salehpour, R. Mohan, and U. Titt, "Treatment-planning study of prostate cancer intensity-modulated radiotherapy with a varian clinac operated without a flattening filter," *International Journal of Radiation Oncology* Biology* Physics*, vol. 68, no. 5, pp. 1567–1571, 2007.

[119] S. Stathakis, C. Esquivel, A. Gutierrez, C. R. Buckey, and N. Papanikolaou, "Treatment planning and delivery of imrt using 6 and 18mv photon beams without

flattening filter," *Applied Radiation and Isotopes*, vol. 67, no. 9, pp. 1629–1637, 2009.

[120] Y. Wang, M. K. Khan, J. Y. Ting, and S. B. Easterling, "Surface dose investigation of the flattening filter-free photon beams," *International Journal of Radiation Oncology* Biology* Physics*, vol. 83, no. 2, pp. e281–e285, 2012.

[121] R. M. Howell, S. B. Scarboro, S. Kry, and D. Z. Yaldo, "Accuracy of out-of-field dose calculations by a commercial treatment planning system," *Physics in medicine and biology*, vol. 55, no. 23, p. 6999, 2010.

[122] G. Kragl, F. Baier, S. Lutz, D. Albrich, M. Dalaryd, B. Kroupa, T. Wiezorek, T. Knöös, and D. Georg, "Flattening filter free beams in sbrt and imrt: dosimetric assessment of peripheral doses," *Zeitschrift für Medizinische Physik*, vol. 21, no. 2, pp. 91–101, 2011.

[123] S. Lang, G. Reggiori, J. P. Vaqué, C. Calle, J. Hrbacek, S. Klöck, M. Scorsetti, L. Cozzi, and P. Mancosu, "Pretreatment quality assurance of flattening filter free beams on 224 patients for intensity modulated plans: A multicentric study," *Medical physics*, vol. 39, p. 1351, 2012.

[124] W. Verbakel, C. Ong, S. Senan, J. Cuijpers, B. Slotman, and M. Dahele, "Flattening filter-free beams for sbrt: Advantages and risks," *International Journal of Radiation Oncology* Biology* Physics*, vol. 84, no. 3, pp. S826–S827, 2012.

[125] C. L. Ong, M. Dahele, B. J. Slotman, and W. F. Verbakel, "Dosimetric impact of the interplay effect during stereotactic lung radiation therapy delivery using flattening filter-free beams and volumetric modulated arc therapy," *International Journal of Radiation Oncology* Biology* Physics*, vol. 86, no. 4, pp. 743–748, 2013.

[126] C. L. Ong, M. Dahele, J. P. Cuijpers, S. Senan, B. J. Slotman, and W. F. Verbakel, "Dosimetric impact of intrafraction motion during rapidarc stereotactic vertebral radiation therapy using flattened and flattening filter-free beams," *International Journal of Radiation Oncology* Biology* Physics*, 2013.

[127] J. Boda-Heggemann, S. Mai, J. Fleckenstein, K. Siebenlist, A. Simeonova, M. Ehmann, V. Steil, F. Wenz, F. Lohr, and F. Stieler, "Flattening-filter-free

intensity modulated breath-hold image-guided sabr (stereotactic ablative radiotherapy) can be applied in a 15-min treatment slot," *Radiotherapy and Oncology*, 2013.

[128] M. Ritter, J. Forman, P. Kupelian, C. Lawton, and D. Petereit, "Hypofractionation for prostate cancer," *Cancer journal (Sudbury, Mass.)*, vol. 15, no. 1, p. 1, 2009.

[129] R. Shaffer, W. Morris, V. Moiseenko, M. Welsh, C. Crumley, S. Nakano, M. Schmuland, T. Pickles, and K. Otto, "Volumetric modulated arc therapy and conventional intensity-modulated radiotherapy for simultaneous maximal intraprostatic boost: a planning comparison study," *Clinical oncology*, vol. 21, no. 5, pp. 401–407, 2009.

[130] E. J. Hall, "Intensity-modulated radiation therapy, protons, and the risk of second cancers," *International Journal of Radiation Oncology* Biology* Physics*, vol. 65, no. 1, pp. 1–7, 2006.

[131] J. Cashmore, M. Ramtohul, and D. Ford, "Lowering whole-body radiation doses in pediatric intensity-modulated radiotherapy through the use of unflattened photon beams," *International Journal of Radiation Oncology* Biology* Physics*, vol. 80, no. 4, pp. 1220–1227, 2011.

[132] D. Dearnaley, I. Syndikus, G. Sumo, M. Bidmead, D. Bloomfield, C. Clark, A. Gao, S. Hassan, A. Horwich, R. Huddart, *et al.*, "Conventional versus hypofractionated high-dose intensity-modulated radiotherapy for prostate cancer: preliminary safety results from the chhip randomised controlled trial," *The lancet oncology*, vol. 13, no. 1, pp. 43–54, 2012.

[133] D. Followill, P. Geis, and A. Boyer, "Estimates of whole-body dose equivalent produced by beam intensity modulated conformal therapy," *International Journal of Radiation Oncology* Biology* Physics*, vol. 38, no. 3, pp. 667–672, 1997.

[134] S. Hossain, P. Xia, C. Chuang, L. Verhey, A. R. Gottschalk, G. Mu, and L. Ma, "Simulated real time image guided intrafraction tracking-delivery for hypofractionated prostate imrt," *Medical physics*, vol. 35, p. 4041, 2008.

[135] L. Hoffmann, "Implementation and experimental validation of the high dose rate stereotactic treatment mode at varian accelerators.," *Acta Oncologica*, vol. 48, no. 2, pp. 201–208, 2009.

[136] S. Subramaniam, S. Thirumalaiswamy, C. Srinivas, G. Gandhi, M. Kathirvel, K. Kumar, S. Mallik, M. Babaiah, Y. Pawar, A. Clivio, *et al.*, "Chest wall radiotherapy with volumetric modulated arcs and the potential role of flattening filter free photon beams," *Strahlentherapie und Onkologie*, vol. 188, no. 6, pp. 484–491, 2012.

[137] K. H. Spruijt, M. Dahele, J. P. Cuijpers, M. Jeulink, D. Rietveld, B. J. Slotman, and W. F. Verbakel, "Flattening filter free vs flattened beams for breast irradiation," *International Journal of Radiation Oncology* Biology* Physics*, vol. 85, no. 2, pp. 506–513, 2013.

[138] G. Nicolini, S. Ghosh-Laskar, S. K. Shrivastava, S. Banerjee, S. Chaudhary, J. P. Agarwal, A. Munshi, A. Clivio, A. Fogliata, P. Mancosu, *et al.*, "Volumetric modulation arc radiotherapy with flattening filter-free beams compared with static gantry imrt and 3d conformal radiotherapy for advanced esophageal cancer: a feasibility study," *International Journal of Radiation Oncology* Biology* Physics*, vol. 84, no. 2, pp. 553–560, 2012.

[139] K. Chin, N. Wen, Y. Huang, J. Jin, I. Chetty, and S. Ryu, "Mo-f-108-05: Treatment planning study of volumetric arc therapy for spine stereotactic radiosurgery using flattening filter free beams," *Medical Physics*, vol. 40, no. 6, pp. 407–407, 2013.

[140] J.-Z. Wang, R. Rice, A. J. Mundt, A. Sandhu, and K. T. Murphy, "Feasibility and advantages of using flattening filter-free mode for radiosurgery of multiple brain lesions," *Practical Radiation Oncology*, vol. 2, no. 4, pp. e165–e171, 2012.

[141] M. Zhuang, T. Zhang, Z. Chen, Z. Lin, D. Li, X. Peng, Q. Qiu, and R. Wu, "Advanced nasopharyngeal carcinoma radiotherapy with volumetric modulated arcs and the potential role of flattening filter-free beams," *Radiation Oncology*, vol. 8, no. 1, p. 120, 2013.

[142] F. Stieler, J. Fleckenstein, A. Simeonova, F. Wenz, and F. Lohr, "Intensity modulated radiosurgery of brain metastases with flattening filter-free beams," *Radiotherapy and Oncology*, 2013.

[143] F. Alongi, L. Cozzi, S. Arcangeli, C. Iftode, T. Comito, E. Villa, F. Lobefalo, P. Navarria, G. Reggiori, P. Mancosu, *et al.*, "Linac based sbrt for prostate cancer

in 5 fractions with vmat and flattening filter free beams: preliminary report of a phase ii study," *Radiation Oncol*, vol. 8, no. 1, p. 171, 2013.

[144] B. S. Sørensen, A. Vestergaard, J. Overgaard, and L. H. Præstegaard, "Dependence of cell survival on instantaneous dose rate of a linear accelerator," *Radiotherapy and Oncology*, vol. 101, no. 1, pp. 223–225, 2011.

[145] D. Georg, T. Knöös, and B. McClean, "Current status and future perspective of flattening filter free photon beams," *Medical physics*, vol. 38, p. 1280, 2011.

[146] G. Kragl, D. Albrich, and D. Georg, "Radiation therapy with unflattened photon beams: Dosimetric accuracy of advanced dose calculation algorithms," *Radiotherapy and Oncology*, vol. 100, no. 3, pp. 417–423, 2011.

[147] J. Kavanaugh, R. Kashani, and E. Klein, "Evaluation of flattening filter-free lung/tissue heterogeneity dose calculations for 2 commercial planning systems," *International Journal of Radiation Oncology* Biology* Physics*, vol. 84, no. 3, pp. S874–S875, 2012.

[148] W. Lechner, H. Palmans, L. Sölkner, P. Grochowska, and D. Georg, "Detector comparison for small field output factor measurements in flattening filter free photon beams," *Radiotherapy and Oncology*, 2013.

[149] Y. Wang, S. B. Easterling, and J. Y. Ting, "Ion recombination corrections of ionization chambers in flattening filter-free photon radiation," *Journal of Applied Clinical Medical Physics*, vol. 13, no. 5, 2012.

[150] J. Cashmore, S. Golubev, J. L. Dumont, M. Sikora, M. Alber, and M. Ramtohul, "Validation of a virtual source model for monte carlo dose calculations of a flattening filter free linac," *Medical Physics*, vol. 39, p. 3262, 2012.

[151] N. Chofor, D. Harder, K. Willborn, A. Rühmann, and B. Poppe, "A direction-selective flattening filter for clinical photon beams. monte carlo evaluation of a new concept," *Physics in Medicine and Biology*, vol. 56, no. 14, p. 4355, 2011.

Personal data

Surname	HRBACEK
First name	Jan
Date of birth	7th January 1978
Nationality	Czech

Education

2010 - 2014	University of Zürich (CH) Faculty of Sciences PhD Thesis: Assessment of clinical contribution of flattening filter free beams
1997 - 2003	Czech Technical University in Prague (CZ) Faculty of Nuclear Sciences and Physical Engineering MSc thesis: Influence of polymer gel dosimeter composition on its dosimetric properties
1996 - 1997	Masaryk's Gymnasium Vsetin (CZ)
1995 - 1996	Wellsville Central High School (NY, USA)
1992 - 1995	Masaryk's Gymnasium Vsetin (CZ)

Work experience

since 2010	Center for Proton Therapy, Paul Scherrer Institute (CH)
2008 - 2010	Department of Radio-Oncology, University Hospital Zürich (CH)
2005 - 2008	Department of Radiotherapy, University Hospital Gasthuisberg Leuven (B)
2003 - 2005	Department of Radiotherapy and Oncology, University Hospital Motol Prague (CZ)

Rüschlikon 2014 Jan Hrbacek